Master's thesis

NTNU
Norwegian University of Science and Technology
Faculty of Natural Sciences
Department of Biology

Maren Thu

Phytoplankton Spring Bloom Mapping in Coastal Areas Using Autonomous Underwater Vehicle (AUV) and Optical Approaches

Master's thesis in Ocean Resources
Supervisor: Geir Johnsen
Co-supervisor: Nicole Aberle-Malzahn, Glaucia M. Fragoso
May 2022

Maren Thu

Phytoplankton Spring Bloom Mapping in Coastal Areas Using Autonomous Underwater Vehicle (AUV) and Optical Approaches

Master's thesis in Ocean Resources
Supervisor: Geir Johnsen
Co-supervisor: Nicole Aberle-Malzahn, Glaucia M. Fragoso
May 2022

Norwegian University of Science and Technology
Faculty of Natural Sciences
Department of Biology

NTNU
Kunnskap for en bedre verden

Abstract

Phytoplankton form mesoscale blooms ($<37\,000$ km^2), therefore studies covering different temporal and spatial resolutions are necessary. This is possible by combining information from different instruments-carrying platforms, sensors, and data sources forming a multidimensional understanding of the nature and dynamics of algal blooms. Local phenomena can help us understand changes in the global environment, hence, this thesis aimed to combine state-of-the-art and traditional sampling methods to study algal bloom dynamics in Norwegian coastal areas.

The result from this thesis serves as ground-truthing for other instruments-carrying platforms (satellites, aeroplanes, and drones all equipped with hyperspectral imager (HI), unmanned surface vehicle (USV) and autonomous underwater vehicle (AUV)) and provides detailed information about dominating pigment groups. Conventional approaches such as chemotaxonomy, microscopic analysis and in vivo spectral reflectance suggested dominance of diatoms. In vivo reflectance spectra serve as a "validated" phytoplankton bio-optical signature and can be used to verify remote sensing data of algal blooms in surface waters. The main limitation of using satellite and aerial remote sensing technologies is their constraints to observing the upper water column, missing valuable information about plankton distribution in the deeper water layers.

In this study, an AUV was used to collect information about the distribution of Chlorophyll a concentration, [Chl a], in the water column, complementing the spatial coverage of the satellite remote sensing. A sub-surface [Chl a] maximum was found around 15 meters for several of the fieldworks. By combining information from seawater samples and AUV sensors, the results suggest observation of three different bloom phases (pre-bloom, bloom, post-bloom) for the different fieldworks. The difference between in situ and in vitro estimations of [Chl a] may be due to the patchy distribution of phytoplankton biomass, non-photochemical quenching (NPQ) of Chl a fluorescence and the layering of the water masses. The silhouette camera (SilCam) classification failed to detect and correctly classify "diatom chains". Results from the AUV sensors demonstrated a need to investigate best practices for operating the vehicle when environmental sensors are applied. Through previous development and the results of this thesis, optical approaches and multidimensional sampling using autonomous underwater vehicles have proven to provide a large potential for phytoplankton studies. Interdisciplinary research provides valuable knowledge sharing, improving the understanding of limitations and possibilities of conducting algal bloom research. Further development of adaptive sampling, satellites with HI, and artificial intelligence will enhance this area of research.

Sammendrag

Fytoplankton danner oppblomstring over mesoskalaen (ofte <37 000 km^2), og derfor er studier som har forskjelling oppløsning i tid og rom nødvendige. Ved å kombinere informasjon fra flere instrumentbærende plattformer, sensorer og datakilder kan det dannes en flerdimensjonal forståelse av naturen og dynamikken til algeoppblomstringen. Lokale fenomener kan hjelpe oss å forstå endringene som skjer i det globale miljøet, hvilket danner grunnlaget for hovedmålet med oppgaven, som var å kombinere «state-of-the-art» og tradisjonelle prøvetakingsmetoder for å studere algeoppblomstringsdynamikken i kystområder i Norge.

Resultatene fra denne oppgaven fungerer som verifisering for resultatene fra andre instrumentbærende plattformene (satellitt, fly og droner, alle utstyrt med hyperspektralt kamera (HI), ubemannet overflatefartøy (USV) og autonome undervannsfarkoster (AUV)). Vannprøvene gir også mer detaljert informasjon om dominerende pigmentgrupper. Konvensjonelle tilnærminger som kjemotaksonomi, mikroskopiske analyser og in vivo spektral reflektans antydet en dominans av kiselalger. In vivo reflektansspektre fungerer som en "validert" bio-optisk fytoplanktonsignatur, og kan brukes til å verifisere fjernmåling av algeoppblomstring i havoverflaten. Hovedbegrensningen ved bruk av satellitt- og fjernmålingsteknologier er at de kun observerer de øverste vannlagene, og mister verdifull informasjon om planktonfordelingen i de dypere vannlagene.

I denne studien ble en AUV brukt for å samle informasjon om fordelingen av klorofyll a-konsentrasjon, [Chl a], i vannsøylen, noe som komplementerer den romlige dekningen til satellittens fjernmåling. Det ble avdekket maksimale [Chl a] ved rundt 15 m for flere av innsamlingsdagene. Ved å kombinere informasjon fra vannsprøvene og AUV-sensorene, antyder resultatene observasjon av tre ulike oppblomstringsfaser (før oppblomstring, oppblomstring og etter oppblomstring). Forskjellen mellom in situ og in vitro estimater av [Chl a] kan skyldes den ujevne fordelingen av fytoplanktonbiomasse, ikke-fotokjemisk quenching (NPQ) av Chl a-fluorescens og lagdeling av vannmasser. SilCam-klassifiseringen mislyktes i å detektere og korrekt klassifisere "kiselalgerkjeder". Resultatene fra AUV-sensorene viste et behov for å undersøke optimalisering for datainnsamling ved bruk av miljøsensorer på fartøyet. Optiske tilnærminger og flerdimensjonal prøvetaking ved bruk av autonome undervannsfarkoster har gjennom denne oppgaven og tidligere utvikling, vist seg å ha et stort potensial for studier av algeoppblomstring. Tverrfaglig samarbeid fører til verdifull kunnskapsdeling, og forbedrer forståelsen av begrensninger og muligheter for algeoppblomstringsforskning. Videreutvikling av adaptiv prøvetakning, satellitter med HI og kunstig intelligens vil styrke dette forskningsområdet ytterligere.

Acknowledgment

IV

Table of content

List of Figures

List of Tables

Abbreviations

AI	Artificial intelligence
AILARON	Autonomous Imaging and Learning Ai RObot identifying plaNkton taxa in situ
AMOS	Center for autonomous marine observations and systems, NTNU
AUR-Lab	Applied Underwater Robotics Laboratory, NTNU
AUV	Autonomous underwater vehicle
CDH	The critical depth hypothesis
Chl a	Chlorophyll a
Chl b	Chlorophyll b
Chl c	Chlorophyll c
CTH	Critical turbulence hypothesis
DRH	Dilution-recoupling hypothesis
H	Hopavågen fieldwork (04.05.-05.05.21)
HABs	Harmful Algal blooms
HI	Hyperspectral Imager
HPLC	High-precision liquid chromatography
KEV	Key environmental variable
L-AUV	Light autonomous underwater vehicle
LHP	Light-harvesting pigments
lm	Linear model
M1	Mausund first fieldwork (13.04.-14.04.21)
M2	Mausund second fieldwork (20.04.-21.04.21)
ML	Mixed layer
MLD	Mixed layer depth
NAC	North Atlantic Current
NCC	Norwegian Coastal Current
NO_3^-	Nitrate
NO_2^-	Nitrite
NPQ	Non-photochemical quenching of Chl a fluorescence
NTNU	Norwegian University of Science and Technology
OOI	Object of interest
PC	Principal component
PCA	Principal component analysis
PO_4^{3-}	Phosphate
PP	Primary production
PPC	Photo-protective carotenoids
PS	Photosystem
$R(\lambda)$	Spectral reflectance
RGB	Red, green, blue
ROV	Remotely operated vehicle
SilCam	Silhouette camera
TBS	Trondhjem Biological Station, NTNU
UAV	Unmanned aerial vehicle
USV	Unmanned surface vehicle

x

1 Introduction

Phytoplankton are major global primary producers that account for almost 50% of the oxygen (O_2) production in the atmosphere (Cavicchioli et al., 2019; Falkowski, 2012). They are microscopic organisms (1-200 μm) that incorporate CO_2 during photosynthesis, export carbon to deeper water layers and transfer energy to higher trophic levels. As they serve as the principal food sources for micro-and mesozooplankton, phytoplankton are considered the base of the food web in most marine ecosystems (Kaiser et al., 2011; Winder & Sommer, 2012). Temperate waters are characterized by complex seasonal dynamics of light and thermal stratification, resulting in distinctive seasonality in primary productivity causing spring and autumn blooms (Assmy & Smetacek, 2009; Chiswell, 2011; Kaiser et al., 2011). Diatoms are dominating during the spring bloom and dinoflagellates are major contributors to the autumn bloom (Gollop et al., 2007; Klais et al., 2011).

Coastal areas are regions of high economic value, and are at the same time, highly exposed to anthropogenic influence (Dallolio et al., 2021). For instance, the frequency of Harmful Algal blooms (HABs) has increased globally in coastal areas as a result of human activities causing pollution and eutrophication. HABs can be highly toxic to aquatic organisms and can harm marine ecosystems due to oxygen depletion (anoxia) (Dallolio et al., 2021; Silva et al., 2021). Even though there has been a decrease in HABs events in Norway over the last 20 years, two major HAB events occurred in 1991 and 2019 (Karlson et al., 2021). They caused fish mortalities in Northern Norway, resulting in large economic losses for fish farmers. Since phytoplankton are key organisms in coastal ecosystems (Kaiser et al., 2011; Winder & Sommer, 2012), knowledge of their seasonal dynamics, abundance, biomass, biodiversity and function traits are needed for ecosystem management and decision-making.

Climate change and the corresponding shift in phytoplankton dynamics in time and space can affect ecosystem structure and functioning (Kulk et al., 2020; Winder & Sommer, 2012). Their abundance is highly regulated by key environmental variables (KEVs), such as ocean currents, light, temperature, ocean mixing and nutrient availability (Fragoso et al., 2019a; Johnsen et al., 2020; Volent et al., 2011). Since these variables change with latitude, season and ocean depth, long-term surveys and seasonal studies of phytoplankton community structure and fluctuations are crucial. Satellite remote sensing of ocean colour is used to estimate large-scale patterns of Chlorophyll *a* concentration, [Chl *a*]*, (as a proxy for phytoplankton biomass) and primary production (PP) as they form mesoscale blooms ($<37\ 000\ km^2$) (Dierssen & Randolph, 2013; Volent et al., 2011). A new approach to phytoplankton studies is the inclusion of automated and autonomous technologies (Saad et al., 2020). For a reliable quantification and identification of plankton, however, conventional approaches such as seawater and net sampling are still important for data validation (Fragoso et al., 2021). This thesis will mainly focus on combining state-of-the-art and traditional sampling methods to study algal bloom dynamics in coastal areas.

1.1 Phytoplankton spring bloom

Algal blooms are described as an outbreak and rapid growth of phytoplankton cells well above the average concentration for a given region or water body (Assmy & Smetacek, 2009; Jonsson et al., 2009). These blooms appear as peaks in the annual cycle of phytoplankton biomass, often with [Chl *a*] exceeding 5 μg L^-1. The timing of the bloom is
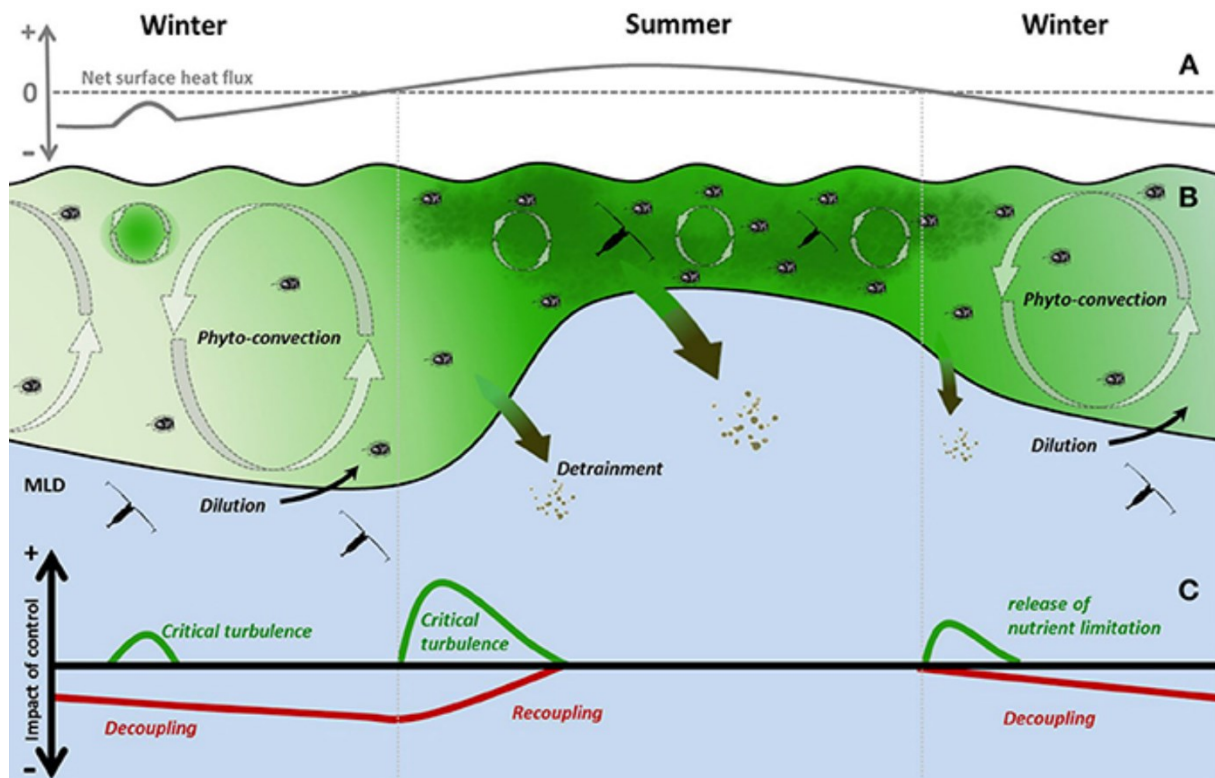
Figure 1.1: The seasonal cycle of phytoplankton in subarctic North Atlantic and the physical and biological controls that impact their abundance. (A) Net surface heat flux. (B) In spring, the light availability due to shallower mixed layer (ML) promotes phytoplankton growth. Stratification results in enhanced growth conditions above the critical depth. Because of increased phytoplankton biomass, there is also an increasing zooplankton grazing. (C) Impact of abiotic (green) and biotic (red) controlling mechanisms on net phytoplankton growth (r) (Lindemann & St. John, 2014).

influenced both by hydrography, nutrient availability and photoperiod (Assmy & Smetacek, 2009). One of the most important seasonal patterns in pelagic food webs is the phytoplankton spring bloom, which provides energy to higher trophic levels after the winter (Lewandowska & Sommer, 2010). Studies have shown that the timing of the spring bloom has been altered because of a changing climate, likely affecting zooplankton recruitment due to mismatch of the seasonal peak of phytoplankton and copepods (Asch et al., 2019; Dezutter et al., 2019; Winder & Sommer, 2012).

The dynamics and composition of the spring bloom vary interannually and among regions, depending on phytoplankton seeding stock, prevailing grazing pressure and weather conditions affecting the mixed layer depth (MLD) (Figure 1.1) (Lindemann & St. John, 2014). When a bloom is initiated, it coincides with prolonged calm, sunny weather, and the shoaling of the MLD creates a layer with more light for phytoplankton to grow (Assmy & Smetacek, 2009; Chiswell et al., 2015). Under these conditions, the bloom will reach its peak within 2–3 weeks. On the other hand, persistent stormy weather can prolong the pre-bloom phase by many weeks, awaiting bloom conditions (Assmy & Smetacek, 2009; Rumyantseva et al., 2019). The Norwegian Sea has been described as an unpredictable environment, where a dynamic weather situation causes a lot of fluctuations in the initiation of the phytoplankton spring bloom (Broms & Melle, 2007; Larsen et al., 2004). According to Sakshaug and Myklestad (1973), the productive season in the Trondheim's fjord starts around March, with a rapidly increasing diatom population reaching its peak during the first week of April. In their study, researchers also observed a second diatom bloom in May-June, which was also observed in recent years at Mausund off the coast of Mid-Norway (Fragoso et al., 2019a; Fragoso et al., 2021).

1.1.1 Major phytoplankton groups

Bloom-forming phytoplankton species differ in size, shape, functional traits and behaviour (Assmy & Smetacek, 2009; Fragoso et al., 2019a; Irigoien et al., 2005). Because they belong to different phylogenetic groups, they also differ in their biochemistry and pigment composition. Due to the large diversity and annual variations, it is not possible to make generalizations about bloom-forming species (Throndsen et al., 2007). However, as a result of high nutrient availability and avoidance from zooplankton grazing, they are usually large (>50 μm) in the spring. Due to of high availability of silicate in early spring, diatoms are major contributors to the spring bloom (Gollop et al., 2007; Klais et al., 2011). Most algal blooms in the oceans are dominated by a broad range of diatom species, whereas many of them form chains (Throndsen et al., 2007). This group is characterized by their silica frustules, where two half-boxes are fit on top of each other. They vary in shape and size, and bloom-forming species are both from pennated and centric families. Typical dominating genera during the spring bloom along coastal Mid-Norway are *Skeletonema*, *Thalassiosira*, *Pseudo-nitzschia* and *Chaetoceros (Assmy et al., 2017; Fragoso et al., 2021; Kraberg et al., 2010; Sakshaug & Myklestad, 1973)*. Another major phytoplankton group is dinoflagellates, which have both auto-, mixo- and heterotrophic modes of nutrition. In the North-East Atlantic, the largest dinoflagellate blooms usually occur in the autumn comprising mainly of the genus *Tripos* (Assmy & Smetacek, 2009; Klais et al., 2011). However, *Tripos* spp. can also be present during the late spring bloom.

1.1.2 Environmental factors

The conditions necessary to trigger phytoplankton spring blooms remain uncertain (Rumyantseva et al., 2019). To date, three main hypotheses have been proposed to describe the bloom onset in temperate and subpolar oceans (Chiswell, 2011; Rumyantseva et al., 2019):

- **The critical depth hypothesis (CDH):** Proposed by Sverdrup (Sverdrup, 1953) saying that algal blooms occur when the surface mixing layer is shallower than the critical depth. The critical depth is defined as the mixing depth where the integrated water column PP equals respiration, assuming that photosynthesis is proportional to light intensity, decreases exponentially with depth and that losses are constant with depth.
- **Critical turbulence hypothesis (CTH):** Suggests that a spring bloom can initiate in a deeper layer due to changes in mixing intensity rather than the mixing depth (Huisman et al., 1999).
- **Dilution-recoupling hypothesis (DRH):** Proposes that the main controlling factor is the decreasing grazing pressure (Rumyantseva et al., 2019). The coupled trophic cycle controls PP, where deep winter mixing dilutes phytoplankton concentrations as a "disturbance". This results in decreased grazing efficiency which allows depth-integrated phytoplankton to grow even when light is limiting. The resulting bloom increases prey-predator interaction described as the "recovery" phase, increasing zooplankton biomass, resulting in increased grazing and phytoplankton biomass decline over time (Behrenfeld, 2010). Further, the loophole hypothesis stress that selective grazing by zooplankton is considered to promote blooms of specific phytoplankton species (Irigoien et al., 2005).

None of these hypotheses describes the full annual cycle of phytoplankton biomass (Chiswell et al., 2015; Silva et al., 2021). To better understand the processes that initiate the spring bloom, an understanding of physical and biological controls that impact their

abundance is important. During spring, the increase in sunlight allows the phytoplankton to grow by taking up the recycled nutrients from winter mixing and river discharges (in the coastal waters) (Silva et al., 2021). At the same time, heat fluxes become positive and the mixed layer (ML) shoals above the critical depth. The degree of stratification, which is mainly determined by freshwater input and warming of the surface water, controls the initiation, maintenance, species composition and succession of algal blooms (Erga et al., 2012). As a result, phytoplankton production exceeds respiration losses, triggering the spring bloom, which increases depth-integrated biomass (Chiswell et al., 2015).

The increased abundance of phytoplankton is commonly known as the start of the annual cycle of seasonal succession in the temperate zone (Greve et al., 2004). Zooplankton takes advantage of increased food availability, resulting in increased grazing. Numerous bioassay experiments have repeatedly demonstrated the relationship between inorganic nitrogen (nitrate (NO_3^-)) concentration and [Chl *a*] (Tilman et al., 1982). According to Falkowski et al. (1998), oceanic phytoplankton productivity is most often limited by nitrate concentration, $[NO_3^-]$. For diatoms and silicoflagellates, silicate ($Si(OH_4)$) is used to build their cell walls (Throndsen et al., 2007). Therefore, low concentrations of this nutrient can also limit their growth. Sometimes also phosphate concentrations, $[PO_4^{3-}]$, and CO_2 have limiting effects on phytoplankton biomass and PP (Klausmeier et al., 2004).

1.2 Light Climate

Light is electromagnetic radiation that is classified into wavelengths, measured in nanometres (nm) (Sakshaug et al., 2009). However, for "light" to have any meaning for biological systems it must be qualified in terms of "light climate" (Cohen et al., 2020). For phytoplankton growth, light climate comprises (Cohen et al., 2020; Sakshaug et al., 2009) of the **intensity** measured as radiance (L) or irradiance (E) in visible light at 400-700 nm (µmol quanta $m^{-2}s^{-1}$), the **spectrum** given by spectral irradiance (W $m^{-2}nm^{-1}$)) and the **duration of light** for a given location (day length (h)) . The spectral irradiance at any point in the ocean depends on the optically active substances of the water, depth and the spectral properties of the incident light (Sakshaug et al., 2009).

1.2.1 Pigments

To utilize different parts of the solar light spectrum attenuated by water, phytoplankton have evolutionary evolved to be able to absorb different wavelengths from varying pigments (chlorophylls, carotenoids and phycobiliproteins) at a given depth (Johnsen & Sakshaug, 2007). The use of high-precision liquid chromatography (HPLC) makes it possible to distinguish between different pigment groups. Phytoplankton groups have different suites of pigments, both light-harvesting and photoprotective (Roy et al., 2011). The light-harvesting pigments (LHP) include pigments such as chlorophylls (*a*, *b*, c_1, c_2 and c_3) absorbing in the blue (400-500nm) and red (600-700 nm) regions, carotenoids (e.g., fucoxanthin) absorbing mostly at 400-530 nm, and phycobiliproteins (e.g., phycoerythrin) with high absorption in the green-orange region (500-570nm) (Cohen et al., 2020; Roy et al., 2011). The photoprotective carotenoids (PPC), on the other hand, affect the colour of phytoplankton cells, and therefore the optical properties of the water (Johnsen & Sakshaug, 2007).

Table 1.1: Chemotaxonomy: functional phytoplankton groups and their pigment composition edited from (Roy et al., 2011). Where x = present and xxx = dominant pigment within the groups.

Groups/Pigments	Chl c_3	Chl c_{2+1}	Perid-inin	Fucoxa-nthin	Diad-ino	Dia-toxanthin	Chl b	Chl a
Chlorophyceae							xxx	xxx
Bacillariophyta (diatoms)		xxx		xxx	xxx	x		xxx
Dinophyta (dinoflagellates)		xxx (c_2)	xxx		xxx	x		xxx
Haptophyte	xxx	xxx		xxx	xxx	x		xxx
Chrysophyceae	xxx	xxx		xxx	xxx	x		xxx
Raphidophyceae		xxx		xxx	xxx	x		xxx
Prasinophyceae							xxx	xxx

The phytoplankton pigments found in a water sample can also indicate the physiological state of the phytoplankton assemblage and be used for chemotaxonomy. If phytoplankton are exposed to high irradiances, they may be high light-acclimated, changing their pigments concentrations and ratios, accordingly, increasing the amount of PPC and reducing the LHP (Rodriquez et al. 2006, Johnsen and Sakshaug et al. 2007). A post-bloom phase is characterized by a larger portion of degraded pigments, such as Chlorophyllide *a*, Phaeophytin *a* and Phaeophorbide *a* (also an indication of grazing) – all of them originating from Chl *a* (Fragoso et al., 2019a; Roy et al., 2011). Since the pigment combination varies for different functional phytoplankton groups they can be used for taxonomic purposes (Table 1.1 presents an overview of the most common pigments and groups) (Roy et al., 2011). An example of this is Peridinin, which only occurs in dinoflagellates, and can therefore be used as an indicator of their presence.

1.2.2 Chlorophyll *a* fluorescence

For a long time, [Chl *a*] has been used as a proxy for phytoplankton biomass, even though the ratio of Chl *a* to carbon varies between organisms and is strongly affected by photo-acclimation (Johnsen & Sakshaug, 2007). Phytoplankton can adjust the amount of Chl *a* pigments in their cells according to the amount of light they are receiving, as well as by regulating their thylakoid stacking (Falkowski & Raven, 2013).

[Chl *a*] is often measured using Chl *a* fluorescence of living organisms. This is the process where a molecule absorbs light at one wavelength and then re-emits light at a longer wavelength (Suggett et al., 2010). First, the absorbed light photon excites an electron in the molecule to a higher energy state which is unstable. Then, the electron returns to a lower energy state, and the excess energy is released as both heat and visible light of a longer wavelength (Suggett et al., 2010; Johnsen et al., 2011). There are several factors affecting in situ/in vivo fluorescence-based measurements of [Chl *a*] (Brunet et al., 2011). At high light, the pH in the thylakoid lumen is lowered due to the splitting of water molecules during photosynthesis, which leads to lower fluorescence emitted from the cells. Another factor that might influence the Chl *a* fluorescence is the effect of non-photochemical quenching (NPQ) (Huot & Babin, 2010; Johnsen et al., 2018; Roesler et al., 2017). This is a mechanism where cells exposed to high light give off excess energy as heat, leading to a reduction in measured [Chl *a*] during daytime hours. One more factor influencing the Chl *a* fluorescence is the ambient light intensity, which needs to be at a high to fully saturate the photosystems (PSI and PSII). However, that may not always be the case, i.e light-limited conditions (Suggett et al., 2010).

1.2.3 In vivo spectral reflectance of phytoplankton

Satellite remote sensing has been used extensively to provide quantitative information about phytoplankton biomass by means of measuring [Chl *a*] (Johnsen & Sakshaug, 2007). The varied optical properties (backscattering and absorption profiles) of different phytoplankton groups can potentially be used to discriminate different pigment groups by use of remote sensing data (Hunter et al., 2008; Volent et al., 2011). An image pixel from a regular digital camera measures light at three wavebands (red, green and blue; RGB) (Johnsen et al., 2013). In contrast, hyperspectral imagers measure continuous light spectra in each image pixel providing a higher spatial and spectral resolution. Hyperspectral data can also be obtained by using a spectrometer, providing hyperspectral data sets such as spectral reflectance (a spectrum from a given point) (Mogstad & Johnsen, 2017). Measuring in vivo spectral reflectance with a spectral resolution of 1 nm provides detailed colour information about the measured object (object of interest; OOI). The signature measured in a laboratory setting serves as a "blueprint answer" to what the optical signatures of different objects actually are (Mogstad & Johnsen, 2017). Important physical parameters affecting the in vivo reflectance spectra $R(\lambda)$ are upwelling- and corresponding downwelling radiance which can be used to obtain reflectance ($R(\lambda)$), defined as the ratio of reflected radiant energy to incident radiant energy at a given reflecting interface (Mogstad et al., 2019; Cohen et al., 2020). Reflectance is a relative and dimensionless unit that can be defined as ($R(\lambda)$, 0-1, where 1 represents 100% reflection). For in vivo spectral reflectance, $R(\lambda)$ can be obtained using the formula given in Equation 1,

$$R(\lambda) = \frac{L_{u\,OOI}(\lambda)}{L_{d\,OOI}(\lambda)}$$

Eq. 1

where $Lu\,OOI(\lambda)$ is the measured spectral upwelling radiance reflected off the OOI, and $Ld\,OOI(\lambda)$ is the spectral downwelling radiance that hits the OOI (Eq. 1). Simplified $R(\lambda)$ is the wavelength-specific fraction of incident light at a given OOI, meaning that $R(\lambda)$ is only dependent on the optical properties of the OOI(s), making it possible to compare any $R(\lambda)$ data set (Mogstad & Johnsen, 2017; Mogstad et al., 2019). $R(\lambda)$ can give information about the absorbance spectra of the algae in the water, as there is an inverse relationship between absorbed and reflected light (Johnsen et al., 1994a). This makes it possible to identify absorbance peaks of different pigments present in the in vivo spectral reflectance measurements (Johnsen et al., 1994a; Roy et al., 2011).

1.3 Autonomous underwater vehicle (AUV)

To improve the capability to study and understand ocean processes influencing phytoplankton distribution, it is necessary to couple sampling with model-derived information (Fehling et al., 2012; Sørensen et al., 2020). In the last decade, mobile robotic platforms, such as autonomous underwater vehicles (AUVs), have become more robust, affordable, and viable for scientific exploration. A common problem when collecting in situ oceanographic data is undersampling. Autonomous sampling using AUVs is an efficient method to collect data with higher spatial and temporal resolution compared to traditional sampling (Fossum et al., 2018). AUVs are untethered, battery-powered torpedo-like underwater instrument carrying platforms and operates supervised or autonomously with limited communication ability (Sørensen et al., 2020). The missions are normally preprogrammed before the operation, where the file will contain information of path,
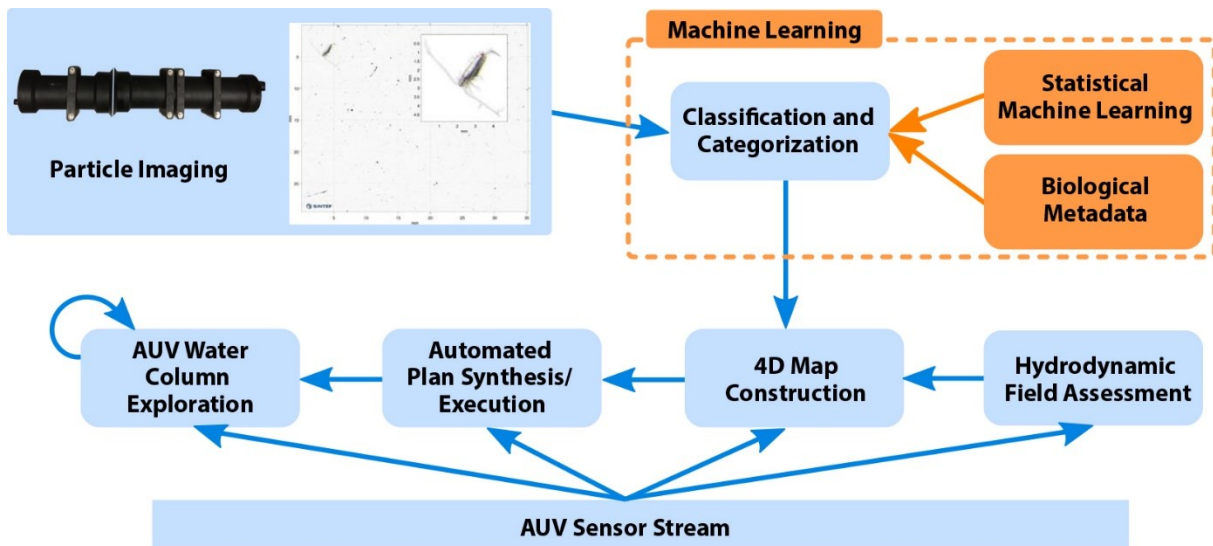
Figure 1.2: The system workflow operation for AILARON, where the orange boxes indicate offline operations (processing steps to generate the classifier) and the blue boxes represent on-board operations (including imaging, classification, sensor evaluation, estimation, and plan execution). The particle imaging is done with a SilCam mounted on an AUV (Saad et al., 2020).

speed, altitude, operational area and when to turn on and off payload sensors. Light AUVs (L-AUVs) can be handled manually and operated from shore or small boats suitable for studies covering the mesoscale (Ludvigsen & Sørensen, 2016).

AUV deployments cover the vertically and horizontally water column, enabling it to detect sub-surface Chl a maximum (Johnsen et al., 2018; Richardson et al., 2000). By applying environmental payload sensors to the platform, measurements of KEVs can be connected to the [Chl a] and provide a better understanding of how they influence the phytoplankton distribution (Sørensen et al., 2020). The advantages of choosing an AUV when studying phytoplankton distribution, is that it has a high payload capacity, can map in 3D, allows operations in areas with limited accessibility and can do on-board intelligent data processing (Saad et al., 2020; Sørensen et al., 2020). On the downside, the vehicle has a limited power supply, there is a risk of loss of data and vehicle, limitation in operations due to traffic and risk of collision, and the possibility of the vehicle getting trapped in water layers (Sørensen et al., 2020).

Technological developments are moving towards adaptive sampling methods (Fossum et al., 2019). Rather than a preprogrammed behaviour, the AUV can use information from payload sensors such as fluorometers measuring [Chl a] for on-board decision making. The payload sensor will then forward its measurements to the mission planning layer and contribute to guidance in the operations control for mission optimization (Fossum et al., 2019; Saad et al., 2020; Sørensen et al., 2020). During the ongoing NFR-project, AILARON (Autonomous Imaging and Learning Ai RObot identifying plaNkton taxa in situ), the aim is to do intelligent on-board sampling using AUVs (Saad et al., 2020). This is an interdisciplinary integrated effort that uses a camera on an AUV to enable characterization of targeted plankton in situ by use of machine learning, artificial intelligence (AI) and robot vision. The AILARON workflow onboard the AUV is explained in Figure 1.2, and can be investigated in more detail in Saad et al. (2020).

1.3.1 Identification and classification using a silhouette camera (SilCam)

Analysing plankton through traditional microscopy is a challenging and time-consuming task where only a limited number of samples can be processed and the temporal resolution is low, due to the small seawater volumes analysed (often <1 L) (Fragoso et al., 2021). A new approach to phytoplankton studies is the inclusion of automated and autonomous technologies such as silhouette cameras (SilCam) (Davies et al. (2017); Saad et al., 2020) for the quantification and identification of plankton. However, conventional approaches are still important for data validation and high-resolution biodiversity assessments (Fragoso et al., 2021). Another great advantage is that these systems collect information on plankton without physically damaging them, since many taxa are fragile and can be destroyed through net sampling and fixation. Images from imaging systems generally have reduced optical resolution, detecting OOIs >150 mm, only sufficient for taxonomic details of OOI larger than the optical resolution of the camera (Benfield et al., 2007; Saad et al., 2020). The SilCam classifier is based on deep learning algorithms, state-of-the-art machine learning for image-based classification, shown to perform better than traditional classification approaches (Krizhevsky et al., 2012; McCulloch & Pitts, 1943), for more details see Nøland (2022).

1.4 Multidimensional ocean observations

The International Ocean Color Coordinating Group (IOCCG) states in their report from 2000 that for phytoplankton studies it is necessary to take a multi-layered approach (IOCCG,
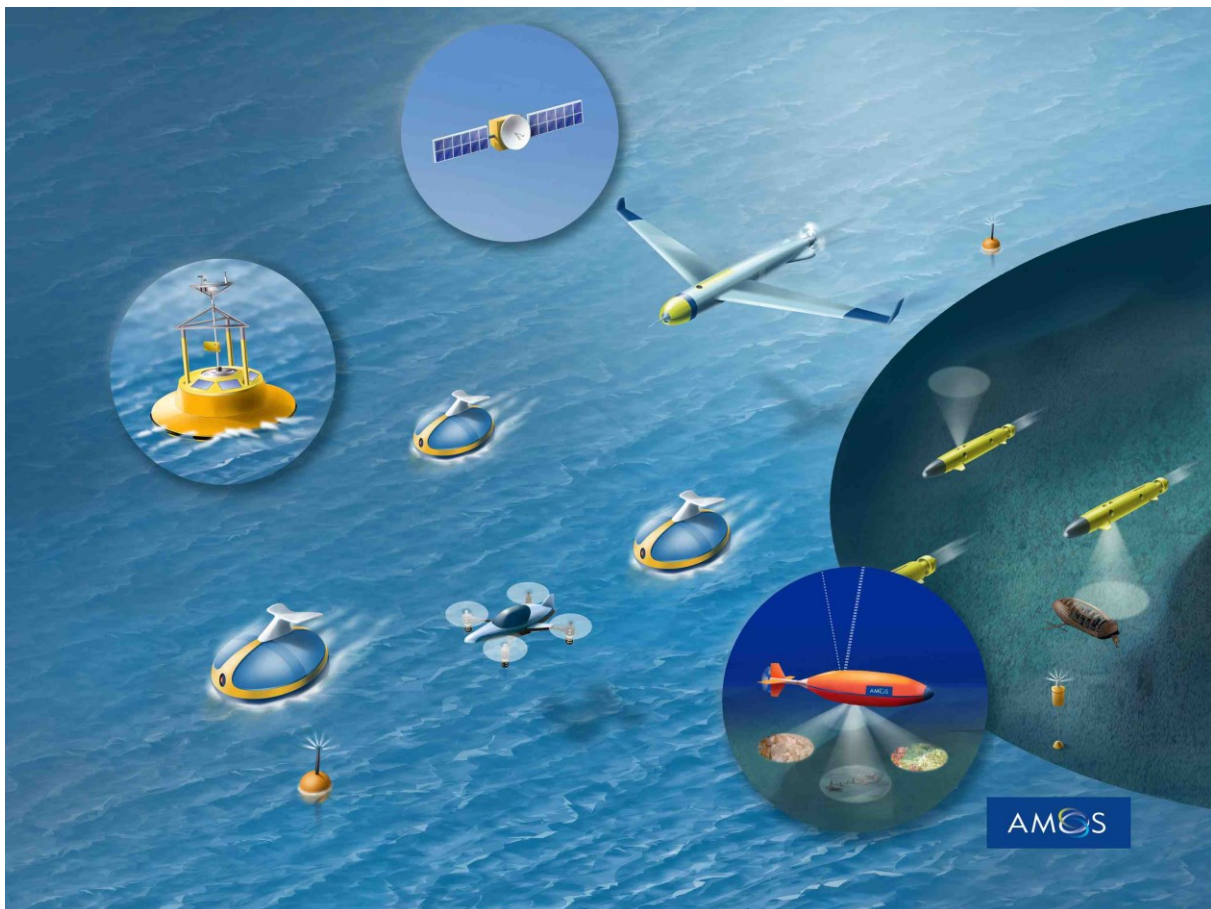
Figure 1.3: Multidimensional ocean observations, using multiple platforms (satellites, unmanned aerial vehicles (UAVs), drones, unmanned surface vehicles (USVs), AUVs, and buoy systems) covering a range of temporal and spatial scales. Bjarne Stenberg, NTNU (By perwork).

2000). This includes the combination of information from multiple platforms, sensors and data sources to form a multidimensional understanding of the nature and dynamics of algal blooms. Phytoplankton distributions and abundance are highly dynamic, indicating the need for studies covering different temporal and spatial resolutions (Dallolio et al., 2021; Grøtte et al., 2022; Johnsen et al., 2018). To retrieve useful information from a network of platforms, the observations made should be coordinated to observe the same area near-simultaneously for synoptic measurements (IOCCG, 2019). For validation of sensor data, fine-scale physical sampling is important to calibrate the measurements, however, the processing time is often high, making them harder to conduct (Fragoso et al., 2021). Here, local phenomena can help us understand the changes in the global environment (Dallolio et al., 2021; Grøtte et al., 2022).

Several studies have combined multiple autonomous platforms in an ocean sampling network and demonstrated an increase in observation quality beyond what each platform can achieve individually (Dallolio, 2020; Ferreira et al., 2019; Johnsen et al., 2018; Nilssen et al., 2015; Sousa et al., 2016). This applies well to the core value of NTNUs Centre for Autonomous Marine Operations and Systems (AMOS), as one of their main area of research is "technology for mapping and monitoring of the oceans" visualized in Figure 3.1 (NTNU AMOS, 2022).

1.5 Aim of study

This thesis is a part of a bigger research project looking into new sampling methods for studying algal blooms in coastal areas. The aim of this project was to study the annual spring bloom by combining different sampling methods with different spatial, spectral, and temporal resolutions. Using the concept of multidimensional ocean observations (IOCCG, 2000; NTNU AMOS, 2022), the interdisciplinary research group combined the use of satellites, aeroplanes, drones, unmanned surface vehicles (USVs), AUVs, physical sampling, and model prediction as a proof-of-concept. Combining all these platforms, sensors and methods can potentially provide a greater understanding of the phytoplankton spring bloom dynamics. However, this thesis mainly focuses on the use of AUVs and seawater samples as sampling methods, as a part of the AILARON plankton classification project.

The aim of this thesis was to do in situ detection of phytoplankton community using instrument-carrying robots combined with traditional seawater sampling for ground-truthing as a proof-of-concept. The role of KEVs and how they influence phytoplankton spring bloom dynamics outside the coast of Mid-Norway was also included. The thesis is split into four sub-goals, looking into different aspects of the phytoplankton spring bloom dynamics:

1. Study how KEVs can explain phytoplankton spring bloom dynamics by combining sensor data from an AUV and traditional seawater samples.
2. Use Chl *a* fluorescence data as a proxy for phytoplankton biomass, [Chl *a*], looking carefully into the variation between in situ and in vitro concentrations and distribution in the water column.
3. Use bio-optical techniques (spectral reflectance and chemotaxonomy) for information about pigment groups from water samples.
4. Compare the identification success of phytoplankton taxonomic groups by analysing images generated from the SilCam (deployed on an AUV) with preserved net samples in the microscope.

2 Materials and Methods

2.1 Study area

For this thesis, two different sampling sites, Mausund (M) and Hopavågen (H), were studied (see map in Figure 2.1). Different types of measurements were done for each sampling site according to the available equipment and study of interest (see Table 2.1). All the samples and measurements were collected during the spring (April and May) of 2021. Throughout this thesis, the three different fieldworks are referred to as: M1 (13.04.-14.04.21), M2 (20.04-21.04.21) and H (04.05-05.05.21).

2.1.1 Mausund, Frøya in Trøndelag

The study area in Sulfjorden south of Mausund (63°82'N 8°59'E) is located in the Froan archipelago, off the coast of Mid-Norway (Fragoso et al., 2021). The sampling took place on 13.04. 14.04, 20.04 and 21.04.21, where ten locations were used as physical sampling points in a 1km^2 sampling area.

The Mausund bank is shallow with many small islands and complex bathymetry (Fragoso et al., 2021). This area is considered a dynamic biological hotspot with high levels of primary productivity and biological diversity due to shallow irregular bathymetry, tidal mixing, wind, and internal waves. The regional economy benefits from the area's high productivity in the seafood and fishing industry targeting e.g. Saith (*Pollachius virens*) and Atlantic cod (*Gadus morhua*), large scallop (*Pecten maximus*), and edible crab (*Cancer pagurus*) (Fragoso et al., 2019a).

The circulation around Froan is dominated by hydrographical forcing, where the Norwegian Coastal Current (NCC) and the North Atlantic Current (NAC) are the dominant currents (Skagseth et al., 2011). The NCC is a surface current that flows northwards along the Norwegian coast, transporting freshwater runoffs from Norwegian fjords and brackish water from the Baltic Sea. Underneath the NCC, the NAC brings warm, saline, and nutrient-rich water along the continental shelf, reaching the surface through coastal upwelling (Fragoso et al., 2021). Two weeks prior to the first fieldwork there was a storm event at the Mausund bank. The period between the fieldworks M1 and M2 was dominated by sunny and calm conditions. Weather conditions for all the fieldworks are shown in Table 2.2.

Table 2.1: Overview of the methods and equipment used for each sampling date (dd.mm.yy). Environmental sensors include an oxygen optode, a conductivity, temperature, and depth (CDT) sensor and a fluorometer (Chl *a*).

Date	Physical sampling			LAUV	
	Nutrients	Filters	Net samples	Environmental sensors	SilCam
M1: 13.04.21	X	X	X	X	X
M1: 14.04.21	X	X		X	X
M2: 20.04.21	X	X	X	X	X
M2: 21.04.21	X	X		X	X
H: 04.05.21	X	X	X	X	X
H: 05.05.21	X	X	X	X	X
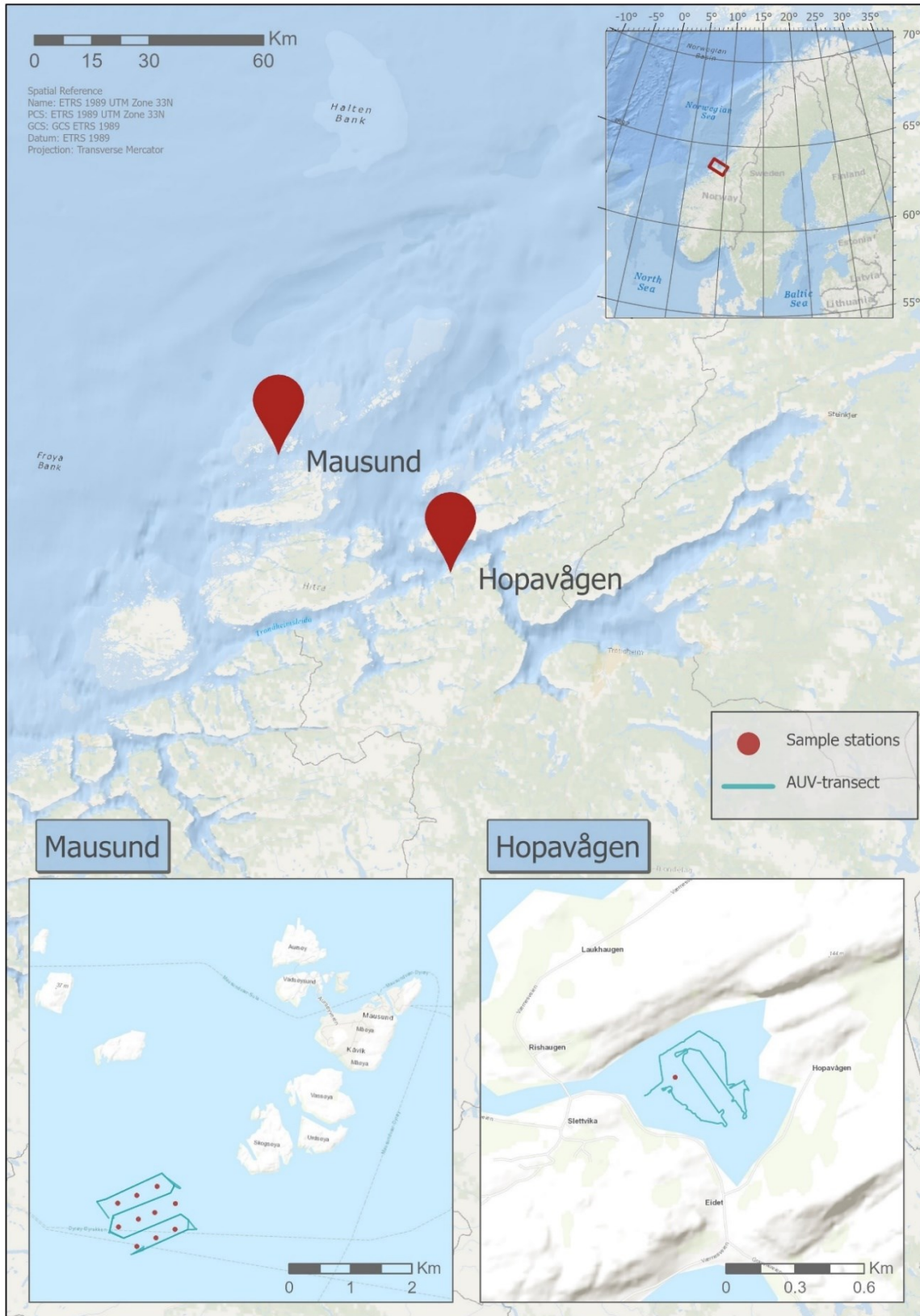
Figure 2.1: Map of sampling locations (red dots). Seawater samples and net samples were both sampled at Mausund (63°82'N 8°59'E) and in Hopavågen (63°35'N 9°32'E). The AUV-transect is an example of a transect run viewed from the surface at each location, several other different AUV-transects were performed at all locations on all dates. The map was made using the software ArcGIS pro (2022).

2.1.2 Hopavågen, Agdenes in Trøndelag

The second survey area was Hopavågen (63°35'N 9°32'E), a sheltered bay in Agdenes, Trøndelag. The area of the bay is approximately 370,000 m^2 with a maximum depth of 32 m and is connected to the NCC through a narrow tidal channel (Marion, 1996; Mogstad et al., 2019). The sampling took place on 04.05. and 05.05.21, where a buoy (63°59'N 9°54'E) located in the middle of the basin, was used as the sampling station, taking samples at different depths.

The hydrographic and biological conditions of Hopavågen are strongly affected by the shallow sill (underneath the bridge of the inlet) (Marion, 1996). This makes it an interesting area to study because organisms are pushed through the channel decreasing the biodiversity compared to areas around. The deep-water renewal is restricted due to the low turnover time of water masses, causing anoxic conditions below 25 m depth (Marion, 1996). This is caused by the fact that the tidal range is much smaller in Hopavågen than in the main fjord. Studies have been conducted in Hopavågen for more than 25 years, with a focus on plankton ecology, biodiversity, hydrography, nutrient dynamics, and benthic ecology (Mogstad et al., 2019).

Table 2.2: Weather, tidal and sea conditions for the different fieldwork dates. The weather information is based on data from Mausund and Hopavågen observation stations using average conditions for the time period (www.yr.no). The tidal data are retrieved from kartverket.no for Mausund and Ørland meteorological station, Trøndelag, and the "Sea condition" is from observed notes from during the fieldwork.

Date	Time (UTC+2)	Weather	Temperature (°C)	Wind (m/s)	Tide (cm)	Sea condition
13.04.21	09:42-13:13		2.7	8.4 (Some wind)*	118-215 (rising -top)	Small waves
14.04.21	08:55-09:12		5.1	8.0 (Some wind)*	69 (rising)	Calm sea
20.04.21	08:46-10:31		7.3	6.8 (Almost no wind)*	128-100 (falling)	No waves
21.04.21	08:42-9:08		4.0	7.5 (Wind)*	154 (falling)	Waves
04.05.21	12:21-14:51		8.5	4.5 (Varied wind)	77-96 (bottom-rising)**	Calm
05.05.21	10:11-11:35		8.0	9.3 (Wind)	173-116 (falling)**	Small waves

*Only average of all day is available, can therefore be a conflict of observed vs measured wind, the sampling is more sheltered.
**Delay and less variation inside Hopavågen compared to Ørland meteorological station, Trøndelag.

2.2 Field measurements (physical sampling)

Prior fieldwork, the bottles and buckets used for nutrient analysis were cleaned with hydrochloride (HCL) and deionized water, then rinsed with saltwater to avoid contamination (Barwell-Clarke & Whitney, 1996). All bottles and sampling containers were pre-marked and labelled with date, numbers, location, and contents.

2.2.1 Seawater sampling of phytoplankton, pigments and nutrients

Seawater samples (8 L) were taken at the surface using a bucket or a custom-made acrylic glass tube water sampler (1 m long, 6 L) when sampling from specific depths (Figure 2.2). The different depths sampled for the different locations are shown in Table 2.3. The seawater was filtered through a 200 μm filter to avoid zooplankton grazing of phytoplankton cells. Until filtration, within a maximum of 12 hours after collecting the seawater samples, they were kept shaded and cool in a container. The seawater samples were used for HPLC, measurement of in vitro Chl *a* fluorescence, in vivo spectral reflectance, and for nutrient (NO_3^- and PO_4^{3-}) analysis.

Table 2.3: Seawater samples taken from different depths and at different stations during all the fieldworks at Mausund (M1-M10) and Hopavågen (H). At Hopavågen there were taken two samples at each depth indicated by the "x2".

Date/Depth (m)	0	5	15	20
13.04.21	M2-M10		M2-M4, M6, M9	
14.04.21	M1, M3		M5	
20.04.21	M1-M7		M3-M4, M6	
21.04.21	M1-M7			
04.05.21	Hx2	Hx2	Hx2	Hx2
05.05.21	Hx2	Hx2	Hx2	Hx2

Figure 2.2: Annecken Nøland taking seawater samples from 15 m depth, Mausund, Frøya. Photo: Maren Thu
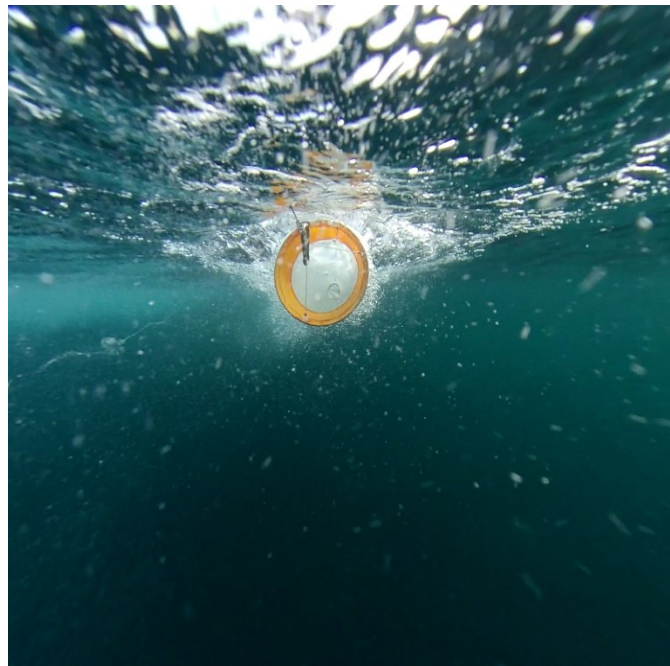
Figure 2.3: Horizontal sampling using a phytoplankton net at surface, Mausund, Frøya. Photo: Geir Johnsen

2.2.2 Net sampling

At Mausund (13.04 and 20.04.21), two net hauls were sampled vertically at the surface (< 5 m) by towing a plankton net (mesh size 20 µm) behind the boat for 10 minutes (Figure 2.3). For the 04.05. and 05.05.21 at Hopavågen, the net samples were taken vertically, sampling different transects of the water column by depth. On both days, there were taken two samples from the depths of 5, 10, and 15 meters, pulling the rope up at a speed of 30 cm s^{-1}. The net hauls were directly fixed with non-acid Lugol (neutral iodine solution) to a final concentration of 0.5%. Further, the samples were kept cool and in the dark for later phytoplankton identification in the microscope.

2.3 Light Autonomous Underwater Vehicle (L-AUV)

To be able to compare the data from the seawater samples and get additional information about the water column, the L-AUV Roald (manufactured by OceanScan – Marine Systems & Technology L.da, operated by Applied Underwater Robotics Laboratory, AUR-lab) was deployed in the same area. The vehicle is shown in Figure 2.4 and can operate down to 100 m at a speed from 0.5 to 2 m s^{-1}, with an endurance of 9 h full payload (NTNU AURLab, 2022; Sousa et al., 2012). The control architecture consists of three main entities: Unified Navigational Environment (DUNE) onboard software, inter-module communication (IMC) for message-based communication protocol, and Netputs command and control software, implemented as a toolchain (Pinto et al., 2012).

2.3.1 Mission Planning

Before each field day, the AUV transects were preprogrammed in Neptus, setting operational area, path, depth, and transect type. For the fieldworks at Mausund, several Yo-yo (the AUV undulates up and down the water column with a fixed angle and given depth range) and depth-specific transects were performed in a 1 km^2 operational area down to 40 m depth. Because of the unique hydrography in Hopavågen and the operational limits of the AUV, several elevator transects (the AUV moves gradually downward at a given distance around a fixed point) were performed around the buoy where the physical sampling took place. When covering a larger area of the bay, several Yo-yo and depth-specific transects were also performed.

2.3.2 L-AUV Sensors

The L-AUV was equipped with several orientational and environmental sensors giving information about the position of the vehicle and the environment (Sørensen et al., 2020). The Attitude Heading Reference System (AHRS) Microstrain 3DM-GX4-25 is a navigation device used to measure vehicle direction and orientation in the water (MicroStrain, 2015). The AUV also has an acoustic sensor, a Doppler Velocity Log (DVL) (Hz), that estimates velocity (Nortek DVL 1000-300m) relative to the sea bottom, used as a positioning system (Nortek, 2022). The AML X2change CTD (conductivity, temperature, and depth) sensor includes a conductivity, pressure (bar), and temperature (°C) sensor, all giving information about the ocean at different depths (AML Oceanographic, 2021). Another important sensor was the Andreaa Oxygen Optode 4831F which measures absolute oxygen concentration (µM) (Xylem, 2020). The vehicle was also equipped with a Turner Cyclops 7 fluorometer (µg L^{-1}) to measure Chlorophyll *a* (Turner Designs Inc, 2021).
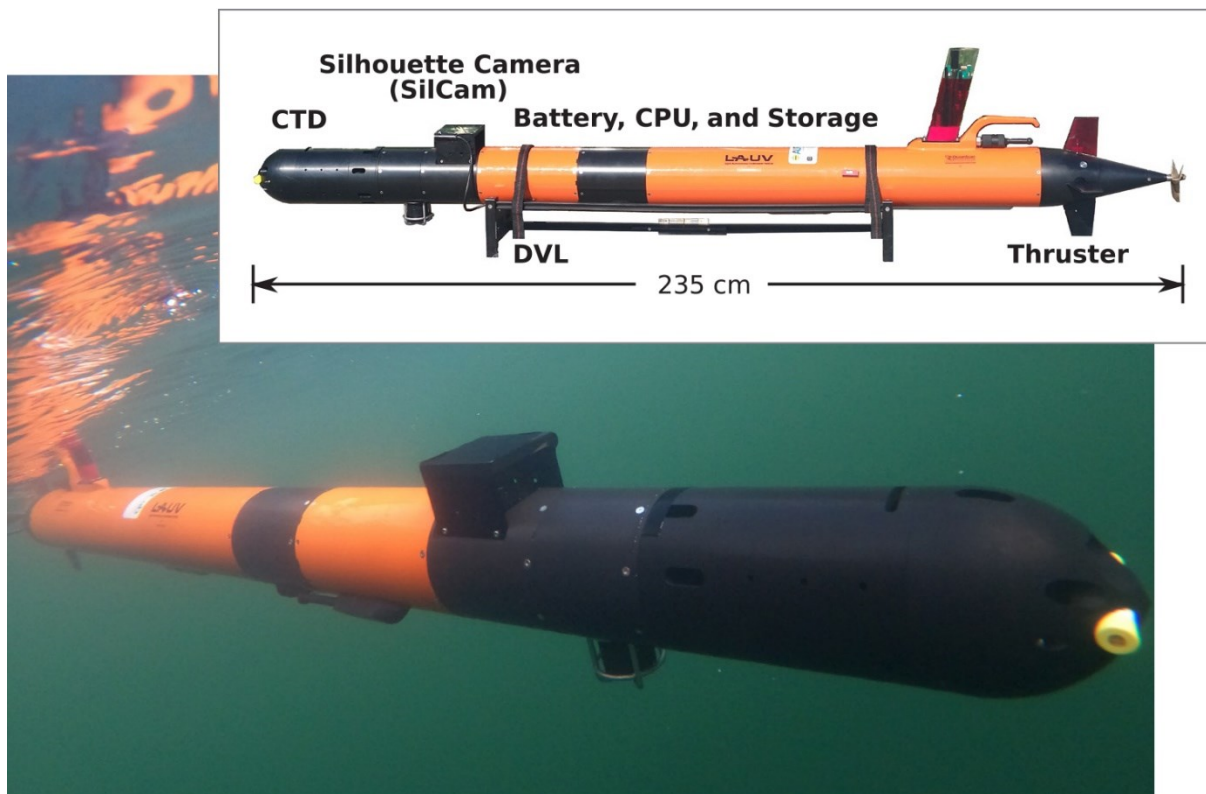
Figure 2.4: The L-AUV is shown navigating in Trondheimsfjorden, Norway. The vehicle has a length of 226 cm with an air weight of 36 kg, including components such as a silhouette camera (SilCam), a Doppler velocity log (DVL), and CTD sensor (Saad et al., 2020).

2.3.3 In situ imaging of plankton by L-AUV-SilCam

A SINTEF designed in situ SilCam (Davies et al., 2017) was integrated into the hull of the AUV. The SilCam is a particle imaging system that can capture objects in the size range of 100 µm to 12 mm (Fragoso et al., 2019a). The movement of the AUV makes water flow through a backlighted capture volume, where the SilCam capture images, and objects are directly recorded in colours for minimal processing. These pictures are similar to microscope images at a lower magnification (Fragoso et al., 2019a). The sample volume is 75.6 cm^3 (45 mm × 56 mm × 30 mm) and the pixel resolution of the image produced is 27.5 µm (Saad et al., 2020). In theory, the images from the SilCam system can be analysed to extract information on the abundance of particles present, such as diatom chains, fecal pellets, and copepods (Davies et al., 2017; Fragoso et al., 2019a; Saad et al., 2020).

2.4 Laboratory work

2.4.1 Filtration for nutrients, Chl *a* and $R(\lambda)$

The seawater samples collected in the field were filtrated through Whatman GF/F glass-fibre filters (25 mm in diameter, pore size 0.4 µm) using a vacuum pump with gentle pressure to avoid sequestered cells. The process happened within 12 hours of the collection of the seawater, commonly within 2-4 hours. For every seawater sample, three replicates were taken (n=3), using 1-2 L of seawater, depending on the concentration of particles in the seawater. Approximately 40 mL of the filtered seawater for the nutrient samples (NO_3^- and PO_4^{3-}) was collected in a test tube and immediately frozen.

The filtering units had water funnels above the filters. These were placed on top of a plastic grid (filter holder) in a plastic funnel, by using a tweezer. Before adding the seawater to the filtering units, the containers with the samples were mixed by upending them 10 times. The amount of seawater was adapted according to the colouration on the filters. Immediately after the filtration was completed, the filters were removed from the plastic holder and placed in a petri dish with the filtration side up. The petri dish was placed in aluminium foil and frozen. All the frozen samples were transported in freezing units to TBS for further analysis.

2.4.2 In vivo spectral reflectance $R(\lambda)$

Before the frozen filters were prepared for the HPLC pigment analysis the in vivo spectral reflectance ($R(\lambda)$) was measured. This was done to indicate spectral absorption of wavelengths for ground-truthing of drone based hyperspectral imaging. For the spectrometer analysis, a QE Pro scientific-grade spectrometer from Ocean Insight Inc. (Largo, USA) with a spectral resolution of 0.7 nm (using a 5 μm light entrance slit), and a spectral range of 347-1113 nm was used. The QR400-7-VIS-BX reflection probe (Ocean Insight Inc., USA) is connected to the spectrometer through an optical fibre bundle and used for all the measurements. A 20W HL-2000-HP high power tungsten halogen light source (Ocean Insight Inc., Largo, USA) provided light on the tip of the reflection probe. Using the software OceanView 1.5.2 (Ocean Insight Inc., USA) the spectrometer data (i.e. optical signatures) were recorded. To optimize the signal-to-noise ratio, both the integration time and the boxcar width were tuned. The integration time was set to 3,000 μs and the boxcar width was set to 3, where the boxcar smoothing averages adjacent pixels, reducing the optical resolution to increase the signal to noise ratio (Insight, 2020). To further smooth the spectral curves the scans-to-average was set to 10, which implies that 10 subsequent scans were averaged per measurement. All spectrometer measurements were recorded at an angle of 90° to the filter surface, at a 0.1 cm distance. The measurements were recorded in a room with no natural light, where the light from the lamps and the stray of light from the tungsten-halogen lamp were subtracted from the measurements using the OceanWiew's "Dark spectrum" function.

The spectrometer raw data were in the form of $L_u(\lambda)$, using a spectrally white reflectance standard plate for conversion into R(λ) (Eq.1). The WS-1 reflectance standard (Ocean Insigth Inc) is a Lambertian reflector made of polytetrafluoroethylene (PTFE) that reflects >98% of all incident light of all wavelengths (spectral range of 250-1500 nm). Since the filter with the algae was wet when frozen, wet clean filters in combination with a reflectance standard were used for R(λ) conversion. Prior and during to the algal spectrometer analysis, the in-water optical signature of the filters was measured 11 times. Based on these measurements, a mean optical signature (n=11) was assigned the "reference" filter ($L_{u\,ref}(\lambda)$). Since a perfectly white surface reflects all wavelengths 100%, the $L_u(\lambda)$ spectrum of a white reference ($L_{u\,ref}(\lambda)$) becomes identical to $L_{d\,OOI}(\lambda)$. With the assumption that the measured optical signature represented the actual optical signature of the reference filter, the R(λ) of filtered seawater (phytoplankton) could be calculated using the equation:

$$R(\lambda) = \frac{L_{u\,OOI}(\lambda)}{L_{u\,ref}(\lambda)} \times R_{PTFE}(\lambda)$$
Eq. 2

For the R$_{PTFE}(\lambda)$ the value is known ($\sim$0.98) for 400-700 nm. For each filter three measurements were performed at different spots on the filter, giving nine measurements for each seawater sample (n=3x3). Both the measurement data and the spectral measurements of the reference filters were exported from OceanView to Excel, converted

to CSV files and imported to the statistical software RStudio. Here raw data were converted into R(λ) by dividing the values by 100 and using Eq. 2. In RStudio the mean spectra for all samples were calculated including the standard deviation. To better compare the HPLC pigment absorption peaks and the R(λ) measurements, R(λ) was converted to absorbance by taking the negative logarithm of the R(λ).

2.4.3 HPLC pigment analysis

To retrieve chemotaxonomic information about the plankton community, the phytoplankton pigments were extracted from the filters. First, the filters were put in glass vials, added 1.6 mL methanol, and then shaken using a vortex mixer (to ensure that the whole filter was covered in methanol). Then pure nitrogen gas was blown into the vials to replace air avoiding oxidation of the pigments. The filters were extracted for 24 hours at -20°C. To avoid filter material and debris prior to the pigment analysis, the extracts were re-filtered using a 13 mm syringe filter (0.2 µm pore size, PTFE) (Rodríguez et al., 2006).

To analyse the pigments, the HPLC instrument, Hewlett Packard Agilent 1100 was used. The HPLC was equipped with a Waters Symmetry C8 (4,6x150 mm, 3,5 um pore size) column that separates the different pigments using time-based polarity and a diode array absorbance detector, using the method of Rodríguez et al (2006) with modifications from Zapata et al. (2000). This is referred to as an "HPLC system 2" in Roy et al. (2011), which is an internationally accepted standard. Before starting, a cleaning procedure as described in Rodríguez et al. (2006) was used. Several pigment extracts were placed on a cooling tray (5°C) and the HPLC was programmed by a connected computer to sample each vial. The HPLC drew 77 µL of extracts and mixed this with 23 µL of water before the samples moved to the water column which serves as the stationary phase. The mobile phase is a 50:25:25 mixture of methanol, acetonitrile, and aqueous pyridine (0.25 M) (Rodríguez et al., 2006).

The different pigments were identified based on retention time, and their corresponding absorbance spectra (at 1 nm spectral resolution at the interval 350-700 nm) were measured using the diode array detection. The detection limit was 0.001 µg L^{-1} for all pigments, and no pigment concentrations below this were reported. To calculate the concentration of the pigments, here denoted p, found through HPLC analysis Eq. 3 is used. Where the integrated value of the area under the sensor curve at 440 nm is denoted A. The volume filtered is denoted V_f and the extracted volume is denoted V_{ex}, both given in mL. Denoted Rf_p is the reference value for the pigments (p), this is found by calculation or calibration. The end concentration has the unit µg L^{-1}.

$$[p] = \frac{A*Rf_p*V_{ex}*1000}{77*V_f}$$ Eq. 3

2.4.4 In vitro Chlorophyll *a* fluorescence for [Chl *a*]

The fraction of the sample not used for HPLC analysis was used to measure in vitro Chlorophyll *a* fluorescence. The instrument used was a Turner Designs Trilogy fluorometer and the module used was the Chlorophyll *a* (Non-Acid) (485 nm excitation filter, 685/10 nm filter). The instrument was first calibrated with a 100% methanol vial used as the blank. To calculate the [Chl *a*] in the samples, Eq. 4 was used. The reading of the sample is denoted FL and the reading of the 100% methanol is denoted BL. The calibration factor (f) is set to 0.47, the extraction volume (E) is 1.6 mL and V is the filtered volume in L. The final concentration is given in µg Chl *a* L^{-1}.

$$[Chl\ a] = \frac{(FL-BL)*f*E}{V}$$

Eq. 4

2.4.5 Nutrients

Filtrated seawater samples were analysed for inorganic nitrogen (NO_3^- + NO_2^- ($\mu g\ L^{-1}$)) and phosphate (PO_4^{3-}, $\mu g\ L^{-1}$)) in the autoanalyzer (Flow Solution IV from O.I.Analytical), following the Norwegian Standard 4745:1991 and 6878:2004, respectively (NS., 1991; NS., 2004).

2.4.6 Microscopic identification of phytoplankton groups

From all the preserved net haul samples, five sub-samples were analysed using an inverted microscope (Lecia DM IRB). Different objectives (4x, 10x, 20x) were used to observe a range of major taxa (class to species level, all >20 μm). Mainly the 40x and 100x magnification were used to identify the larger and most dominant species. The dominant species were photographed using a SONY DFW-X700 Axiocam 105 colour connected to the inverted microscope. The pictures were then sorted into folders, where the best pictures were sorted by group and genus for a visual representation of the biodiversity. Phytoplankton were identified into groups and genus following Throndsen and Eikrem (2001) and Kraberg et al. (2010), with expertise help from Glaucia Moreira Fragoso. The pictures and schematic overviews were stored by AILARON as resources to be used for creating new models based on microscope pictures to improve the classification of particles from the SilCam.

2.5 Data processing

For all the data from the seawater samples with replicate measurements, the mean and standard deviation of the replicates were calculated. This includes the in vitro [Chl *a*] fluorescence, pigment samples for pigment-group specific chlorophylls and carotenoids from HPLC, in vivo spectral reflectance and nutrient concentrations. The absorbance spectra (Optical Density) of individual pigments from HPLC were compared to the internal HPLC pigment database. This was further verified by pigment reference spectra overview in Roy et al. (2011) to ensure that our HPLC isolated pigments were identified correctly and also to ensure the use of correct extinction coefficients for correct quantitative data.

2.5.1 Imaging processing (SilCam)

The SilCam time-series images (frame rate of 4 pictures s^{-1}) are fed into the deep learning image classification system. Classification of plankton and fecal pellets was obtained using a Deep Convolutional Neural Network. Here the classifier assigns a probability to each detected object showing how likely they are to belong to each class; objects assigned a probability between 50-95% were counted in a given class (Fragoso et al., 2019a; Saad et al., 2020). The analysis of SilCam data is performed using the workflow described in Davies et al. (2017) using PySilCam (github.com/emlynjdavies/PySilCam). More details of the imaging processing are described in Fragoso et al. (2019a) and Davies et al. (2017).

The processed and classified pictures, containing classified particles at a given depth range, were studied trying to identify shapes and groups of phytoplankton species. The model is based on algorithms trained on simulated and classified data sets, containing misclassified particles. To improve the training data and increase the classification success, the software Robowflow was used to manually classify particles from field data. This data set was then used to train a new model.

2.5.2 Statistical analysis

AUV data (temperature (°C), Chl *a* (µg L^{-1}), oxygen (µM), salinity, depth (m), and navigation data) was retrieved from Neptus and processed using the statistical software RStudio. GJSON data was also used to display the AUV transect on a map using ArcGIS pro. The AUV data were also resampled per date per depth to be used in the PCA analysis and for linear regression models. This was done by filtering a one-meter interval from +/- 0.5 meters for all samples below 0 meters, to get a mean estimate of the concentration of the given value. Since there is a lot of noise in the data at surface, the surface samples were resampled using the interval (0.2-1.2 m). The resampling of the data makes them relative and this needs to be taken into consideration. For the in situ [Chl *a*] values used in the AUV plot, the data has been filtered for noise in the upper layer, removing noise from the turning point where bubbles influence the fluorescence measurements.

To test for significance of the variables in the seawater sampling data set and in in situ Chl *a*, T-tests were performed on the data set using the statistical software R. Assumed normality (Shapiro test), linear models (lm) were run to test for significance and variance between fieldworks (M1, M2, M3) and [Chl *a*], [NO$_3^-$] and [PO$_4^{3-}$]. Then an ANOVA (one-way and two-way, a test of variance) was used to test if there were any statistical differences between the means of the dates and fieldworks. R^2 and p−values were used to determine if the model is a good fit. Linear regression in the linear models was used to investigate the linear relationship between the variables.

To analyse the effects of gradients (KEV) on the spring phytoplankton biomass and community structure, a principal component analysis (PCA) was performed. The "prcomp" function from the built-in stats package was used to perform the analysis. All the variables were scaled since the PCA is a variance maximizing exercise. The analyses were thus performed on correlation matrices. PCA results were visualized in biplots (Gabriel, 1971) using the "ggbiplot" function from the ggbiplot package available from GitHub (GitHub Inc., USA). To quantify the relative contribution (%) of all variables to the variance explained by principal components (PCs) 1 and 2 the "facto_summarize" function from the factoextra package (GitHub) was used.

3 Results

The following section describes the major findings, presented with the focus on comparing the state of the spring bloom for the three different fieldworks (M1, M2, H) based on biological factors and KEVs. The two first fieldworks (M1, M2) were sampled at the same location (exposed coastal area) allowing for direct comparison. However, the last fieldwork was sampled at a different location (sheltered bay) not allowing for direct comparison, describing a different type of environment.

3.1 Chlorophyll *a* concentration – phytoplankton biomass

3.1.1 Satellite [Chl *a*] estimates

The distribution of the phytoplankton spring bloom shown from satellite images during the sampling period from April and May of 2021 indicates an increased [Chl *a*] throughout the spring. There was a gradual increase in phytoplankton biomass from A to C (13.04. – 05.05.21) shown in Figure 3.1. Sentinel satellite data give a high spatial resolution of the area of interest showing the development of [Chl *a*] at the ocean surface, indicating the state of the phytoplankton spring bloom.
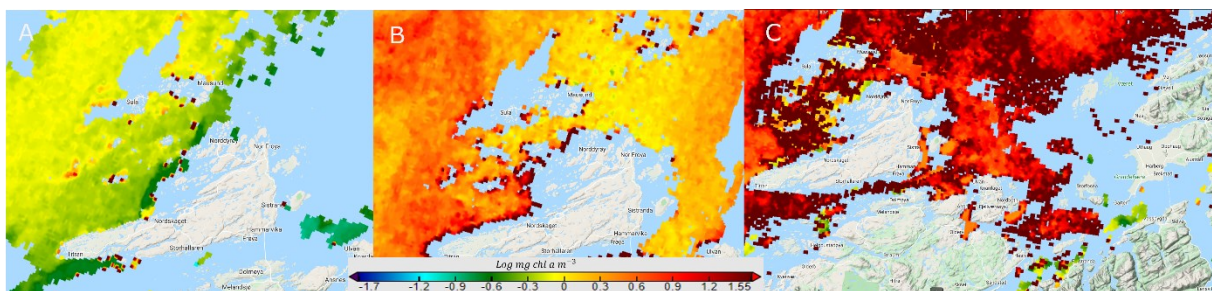
Figure 3.1: Remotely sensed sea surface algal bloom indicated by [Chl *a*] from the time period of the fieldworks of spring 2021, covering the area of interest (Mausund and Hopavågen). Figure A is from M1 (13.04.-14.04.21), figure B is from M2 (20.04.-21.04.21) and figure C is from H (04.05.-05.05.21). The phytoplankton biomass (colour bar in log mg Chl *a* m^{-3}=log µg Chl a L^{-1}=10 $^{µg\ Chl\ a\ L^{-1}}$), showed an increase over the duration of the spring season, images A to C. The images are retrieved from oceanDataLab using a 3-day sampling combination from the OLCI Chlorophyll *a* from the Sentinel-3A satellite (ESA, 2022)).

3.1.2 In vitro [Chl *a*] fluorecence

The map in Figure 3.2 shows the sampling stations used at Mausund, coloured according to mean in vitro [Chl *a*] (µg L^{-1}) (n=3) at the surface on 13.04. and 20.04.21. A lower [Chl *a*] was observed on 13.04. compared to on 20.04.21. On 20.04.21, there was a greater variance in the [Chl *a*] between the sampled locations. The [Chl *a*] was between 0-1 µgL^{-1} on 13.04. and between 1-2.5 µgL^{-1} on 20.04.21.

Figure 3.2: Map of sampling stations (M1-M10) coloured as a function of in vitro [Chl *a*] (μg L^{-1}) at Mausund (63°82'N 8°59'E). The sampling dates 13.04. and 20.04.21 are used to present the surface (0 m) mean (n=3) [Chl *a*] for M1 and M2. The map was made using the software ArcGIS pro (2022).
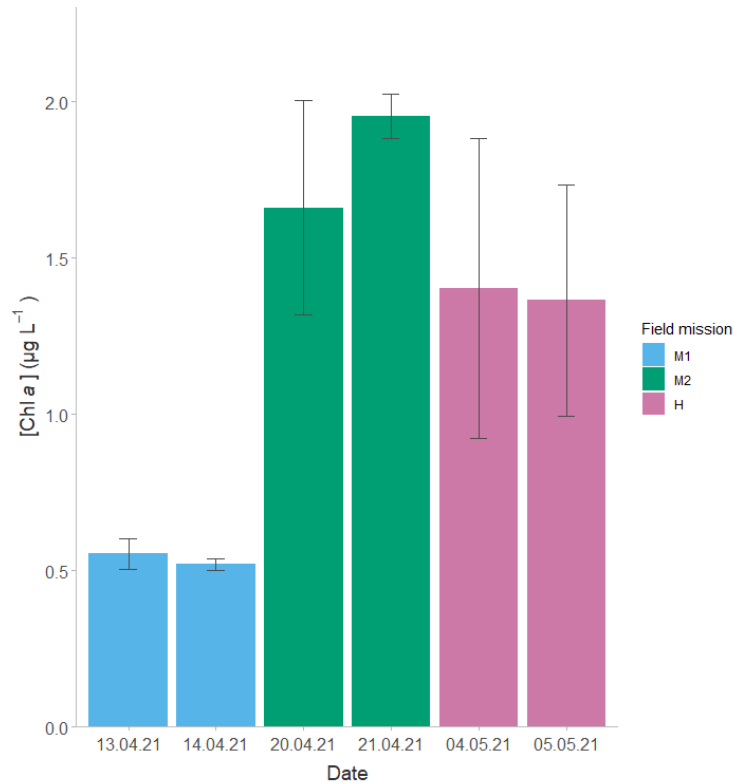
Figure 3.3: The plot shows the mean in vitro [Chl *a*] (µg L^{-1}) and standard deviation for each sampling date, where each fieldwork (M1, M2, H) is grouped by colour. In vitro [Chl *a*] was measured by filtering seawater and then using a Turner Designs fluorometer. Each sample has (n=3) replicates, and each date has (n=3 to 15) samples.

Figure 3.3 shows the in vitro [Chl *a*] (µg L^{-1}) for each date, where each fieldwork (M1, M2, H) is grouped by colour. Each sample has (n=3) replicates, and each date has (n=3 to 15) samples. A more detailed plot is shown in Appendix A (Figure 0.1) where the depth variation (0-20 m) was also accounted for. There were found to be a significant [Chl a] difference between the three different fieldworks, and between 20.04. and 21.04.21. The lowest in vitro [Chl *a*] was found on 14.04, with a concentration of 0.553 µg L^{-1} +/- 0.047. The highest value was found on 21.04.21 with a concentration of 1.951 µg L^{-1} +/- 0.071. All the mean [Chl *a*] are found in Appendix A (Table 0.1).

3.1.3 In situ and in vitro [Chl *a*]

Figure 3.4 shows the difference between the Chl a measured with AUV and seawater samples. The blue dots represent the [Chl *a*] in vitro fluorescence measurements and the green dots are sampling points from the AUV, coloured by in situ [Chl *a*] concentration. A-B show the results for the first fieldwork (M1), C-D for the second fieldwork (M2) and E-F for the last fieldwork (H). Both fieldwork M1 and M2 had [Chl *a*] values with correlation between the in situ and in vitro concentrations. However, for the last fieldwork, there was a great variation between the two measurements. For M1 the [Chl *a*] was relative homogenous throughout the sampled water column of 40 m (Plot A-B), and for M2 a stratification layer was starting to form (Plot C-D). For H rapid changes in [Chl *a*] was observed around 15 m indicating layering in the water column (Plot E-F).
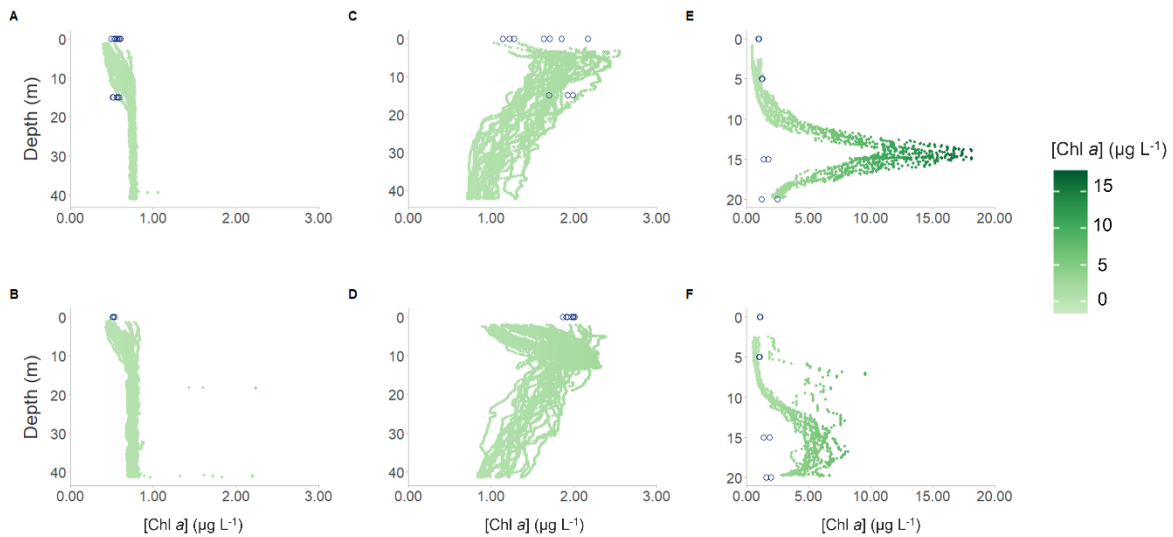
Figure 3.4: Plot of in situ and in vitro [Chl *a*] for all six field days, [Chl *a*] (µg L^{-1}) measured in situ using a cyclops turner 7 fluorometer, and measured in vitro by filtering seawater and then measure using a Turner Designs fluorometer. The blue dots represent the [Chl *a*] in vitro fluorescence measurements and the green dots are sampling points from the AUV, coloured by [Chl *a*] concentration. A-B show the results for the first fieldwork (M1: 13.04.-14.04.21), C-D for the second fieldwork (M2: 20.04.-21.04.21) and E-F for the last fieldwork (H:04.05.-05.05.21).

The relationship between the in vitro and in situ Chl *a* measurement, and the vitro fluorescence [Chl *a*] measurements and the HPLC [Chl *a*] measurements was tested using linear models. The AUV data was resampled from the mean of a specific depth, only showing estimates. All models are statistically significant. As shown in Table 3.1 there was a relative good R^2 value (0.7421) for the in vitro and in situ data for the Mausund (M1, M2) samples. However, the in vitro and in situ measurement for Hopavågen or the whole data set had a low linear relationship. For all the in vitro measurements, looking at lm for fluorescence and HPLC measurements, the R^2 was relatively high, indicating a linear relationship (R^2=0.88).

Table 3.1: Results from testing linear relationship between [Chl *a*] in situ, in vitro fluorescence and in HPLC measurements. The tests was performed on the whole data set and for the location Mausund and Hopavågen, including the p and R^2 values.

Model (lm)	R^2	p-value
In situ [Chl *a*] ~ in vitro [Chl *a*]	0.1137	< 0.001
Mausund: In situ [Chl *a*] ~ in vitro [Chl *a*]	0.7421	< 0.001
Hopavågen: In situ [Chl *a*] ~ in vitro [Chl *a*]	0.1849	0.002
HPLC [Chl *a*] ~ in vitro [Chl *a*]	0.8721	< 0.001
Mausund: HPLC [Chl *a*] ~ in vitro [Chl *a*]	0.8799	< 0.001
Hopavågen: HPLC [Chl *a*] ~ in vitro [Chl *a*]	0.8819	< 0.001

3.2 Spectral characteristics and pigment composition

3.2.1 Bio-optical signatures

The verification of bio-optical signatures is to be used in concert with mini-satellites, drones, USVs and AUVs. When equipped with optical sensors such as Chl *a* sensors and hyperspectral imagers, these can be used for detection, mapping, and monitoring of algal blooms at the surface and in deeper water masses. The spectral reflectance signature shown in Figure 3.5 was measured from filters containing algae from the seawater samples. All spectrometer analyses were done using a QE Pro scientific-grade spectrometer with a spectral resolution of 0.7 nm looking at the spectral range of 350-750 nm. Because the in vivo reflectance analysis was carried out under highly controlled conditions, the spectra $R(\lambda)$ from the QE Pro spectrometer were considered true spectra of the algae in the ocean. Inspecting the "red-peak" between 650-700 nm, the Chl *a* absorbance peak (Johnsen et al., 2011), the maximum peak was found at 674.4 nm. This represents the absorbance maximum for diatoms in the red part of the spectrum, indicating a dominance of this group (Johnsen & Sakshaug, 2007). The different absorbance peaks is further discussed according to previous studies in section 4.4.
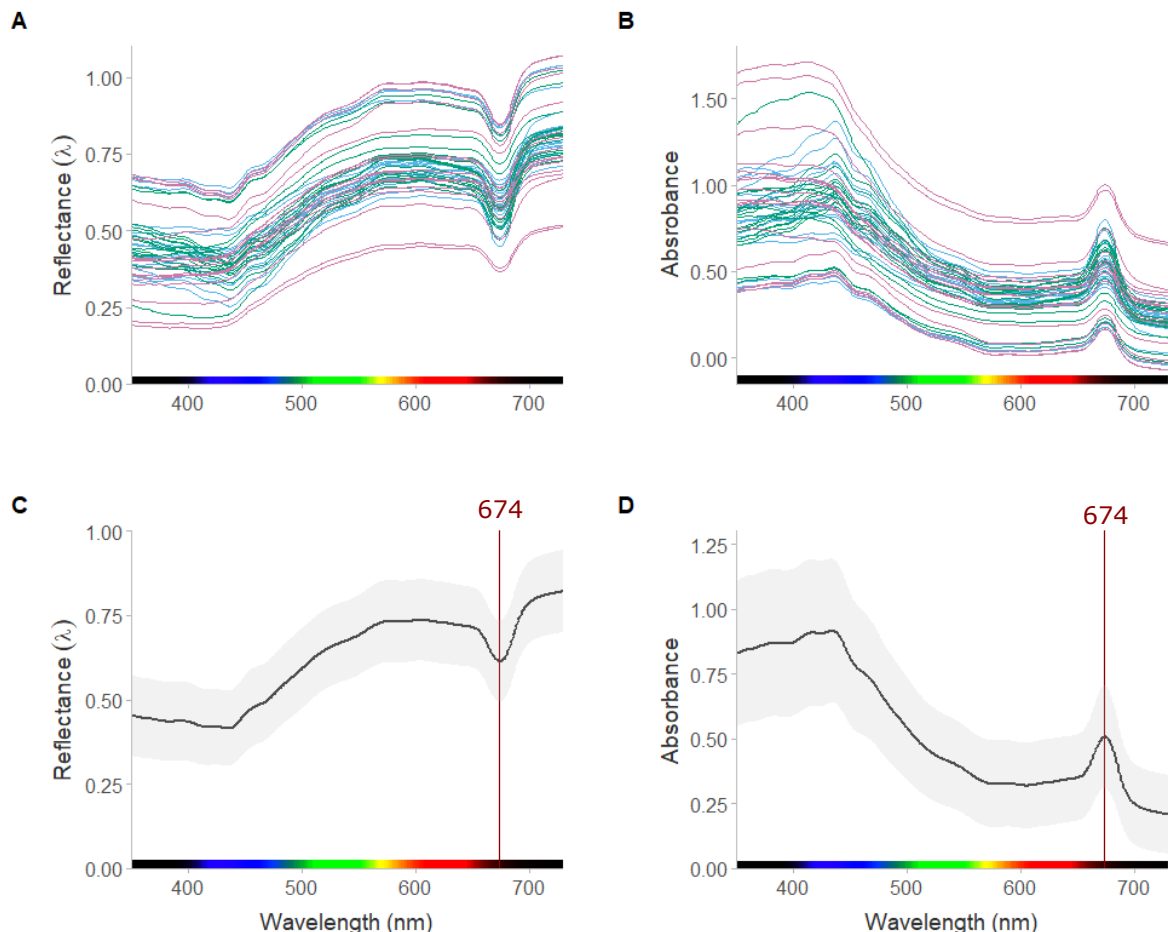
Figure 3.5: A) Mean in vivo reflectance ($R(\lambda)$) spectra (n = 3*3) of living phytoplankton cells (n=51). B) -log(A) showing the absorbance of each seawater sample. C and D are the mean reflectance ($R(\lambda)$) and absorbance of A and B accordingly. The grey shaded area represents the standard deviation. The red line in C and D represents the "in vivo red-peak of Chl *a* absorption" at 674 nm.

3.2.2 HPLC - Pigment composition

Pigments can be used as indicators for the differentiation of phytoplankton pigment groups present in the ocean e.g. during the course of a spring bloom scenario. Figure 3.6 shows the concentration (µg L^{-1}) of the LHP and PPC found during all the fieldworks retrieved using HPLC. The LHP found were chlorophylls *a*, *b*, *c$_1$* and *c$_2$*, Fucoxanthin, and Peridinin. The two PPC present in sufficient amounts to be detected were Diatoxanthin and Diadinoxanthin. By using the chemotaxonomy information from Table 1.1, pigments can be set as biomarkers for different functional groups. Peridinin, a biomarker for dinoflagellates, was found during the second fieldwork (M2), but not during the first (M1) and third (H) fieldworks. Fucoxanthin is for this thesis used as a biomarker for diatoms, showing a gradual increase throughout the three fieldworks. More Chl *b*, *a* bioindicator of Chlorophyceae, was found during the second fieldwork (M2) than for the two other fieldworks. High Chl *c$_{1+2}$* was found during both M2 and H, a common pigment for many functional groups. The M2 fieldwork had a heterogenic distribution of pigments with several different pigment groups present. The last fieldwork (H) was dominated by diatoms (peridinin), but other groups were also present (seen from microscopic analysis).
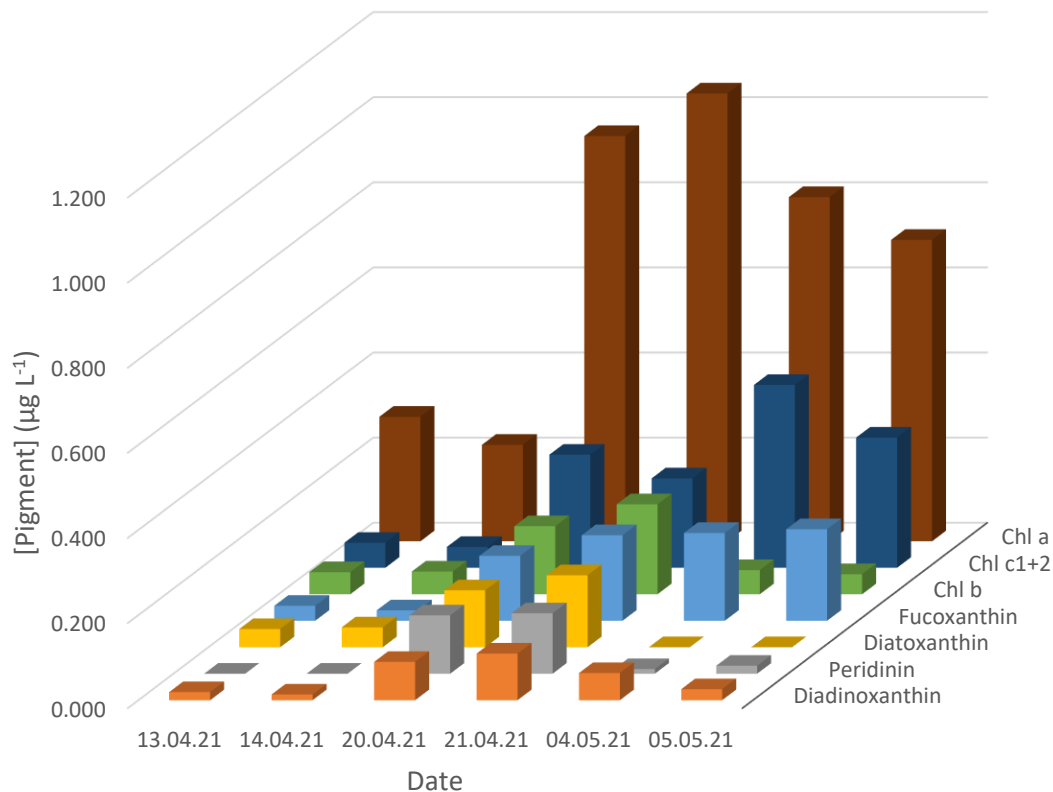
Figure 3.6: Results from HPLC analysis of phytoplankton pigment concentrations (µg L^{-1}) in seawater samples from the three fieldworks (M1 (13.04-14.04.21), M2 (20.04-21.04.21), H (04.05.-05.05.21)). The LHP found were chlorophylls *a*, *b*, *c$_1$* and *c$_2$*, Fucoxanthin, and Peridinin. The two PPC present in sufficient amounts to be detected were Diatoxanthin and Diadinoxanthin. Peridinin is used as a biomarker for dinoflagellates, Fucoxanthin is used as a biomarker for diatoms and Chl *b* is used as a biomarker for Chlorophyceae.

3.3 Nutrients

Figure 3.7 shows the in vitro [Chl a], [NO_3^-] and [PO_4^{3-}] for each date, where each fieldwork (M1, M2, H) is grouped by colour. Each sample has (n=3) replicates, and each date has (n=3 to 15) samples. More detailed plots are shown in Appendix B (Figure 0.2-0.3), where the depth variation (0-20 m) was also accounted for. Alle mean nutrient values are found in Appendix B (Table 0.2). There was a significant difference in both nutrient concentrations between the three different fieldworks, and both nutrients decreased throughout the spring period. The highest [NO_3^-] is given at 6.0 µM+/- 0.1 on 14.04. and the lowest is given on 04.05.21 at 0.30 µM +/-0.09. The highest [PO_4^{3-}] is given at 0.53 µM +/- 0.01 on 14.04. and the lowest is given on 04.05.21 at 0.030 µM +/- 0.02.
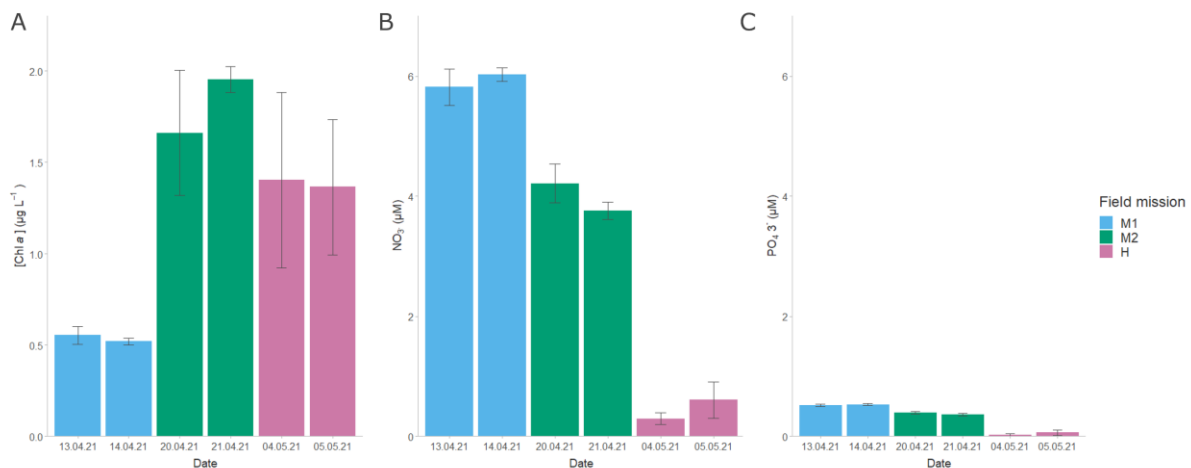
Figure 3.7: The plot shows the mean concentrations of A: in vitro Chl a (µg L^{-1}), B: nitrate ((NO_3^- (µM)) and C: phosphate (PO_4^{3-} (µM)), and standard deviation for each sampling date, where each fieldwork (M1, M2, H) is grouped by colour. In vitro [Chl a] was measured by filtering seawater and then using a Turner Designs fluorometer, and nutrients were measured using an autoanalyzer according to Norwegian standards. Each sample has (n=3) replicates, and each date has (n=3 to 15) samples.

The in vitro [Chl a] is displayed together with the nutrients to look at the correlation and relationship between the nutrient concentration (µg L^{-1}) and in vitro [Chl a]. All the models are shown in Table 0.3 (Appendix B). For the Mausund data, there was a linear relationship between the [Chl a] and both [NO_3^-] (p<0.001, R^2=0.83) and [PO_4^{3-}] (p<0.001, R^2=0.84).

3.4 KEV – AUV sensor data

Since phytoplankton drift with currents, the KEVs highly influence and give valuable information about the plankton distribution. All the KEV data were collected from different sensors on the AUV, where A-B show the results for the first fieldwork (M1), C-D for the second fieldwork (M2) and E-F for the last fieldwork (H).

3.4.1 Temperature

The temperature was retrieved from the CTD sensor on the AUV, the results are shown in Figure 3.8, plotted by depth. The temperature range for all the fieldworks was between 5-7°C. M1 had a stable temperature throughout the water column, and then for M2 a stratification layer was starting to form around 20 m depth. For the H fieldwork, there were observed two rapid changes in temperature forming two distinct water layers, one around 5-10 meters and one below 18 meters.
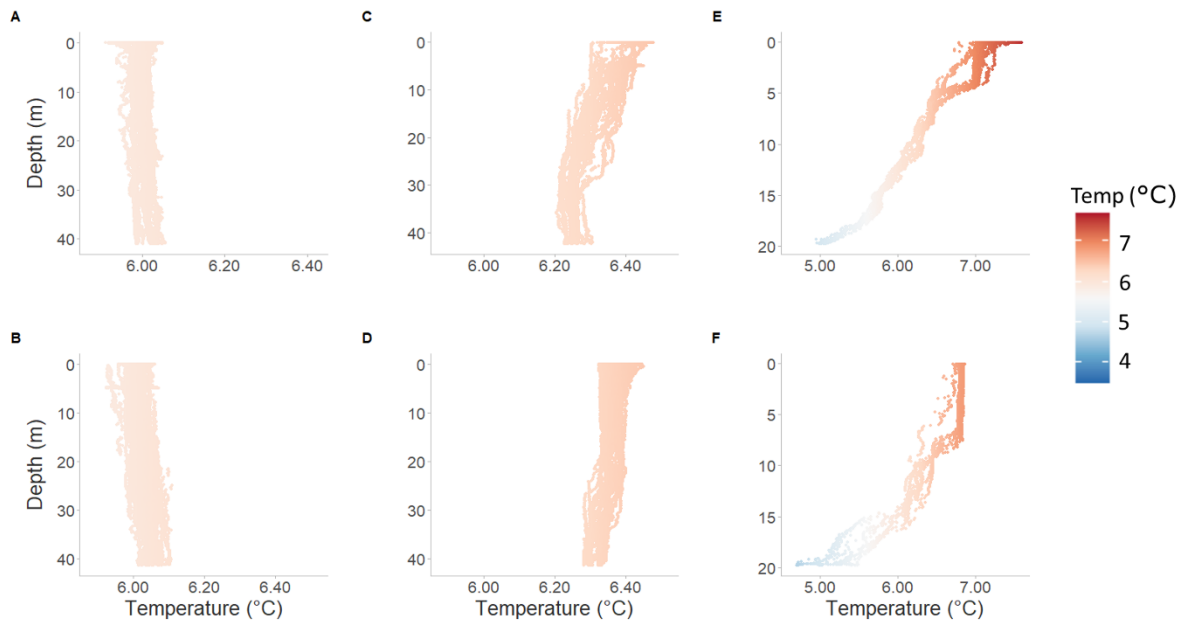
Figure 3.8: Plot of vertical temperature profiles (°C) for all six field days, measured using a CTD mounted on the L-AUV. The temperature sampling points are coloured by temperature. A-B show the results for the first fieldwork (M1: 13.04.-14.04.21), C-D for the second fieldwork (M2: 20.04.-21.04.21) and E-F for the last fieldwork (H:04.05.-05.05.21).

3.4.2 Salinity

The salinity was retrieved from the CTD sensor on the AUV, the results are shown in Figure 3.9, plotted by depth. The salinity range for all the fieldworks was between 31.5-33.7. M1 showed a stable salinity of around 33.6 throughout the water column. For M2, the starting of a stratification layer was formed around 20 m depth, and for the H fieldwork, some variations in the values with a gradual increase from below 10 meters were observed.
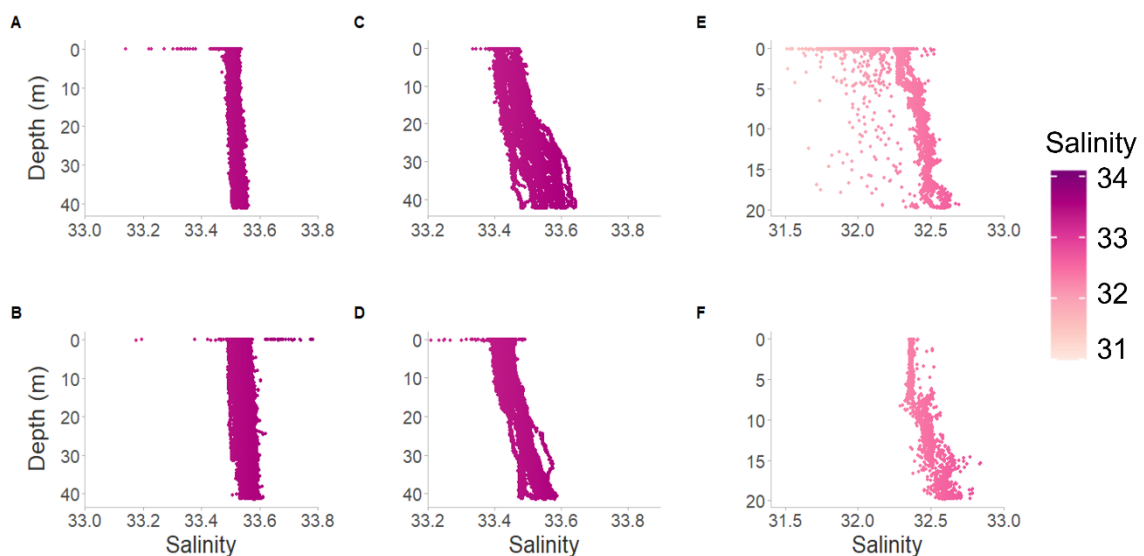
Figure 3.9: Plot of salinity for all six field days, measured using a CTD mounted on the L-AUV. The salinity sampling points are coloured by salinity. A-B show the results for the first fieldwork (M1: 13.04.-14.04.21), C-D for the second fieldwork (M2: 20.04.-21.04.21) and E-F for the last fieldwork (H:04.05.-05.05.21).

3.4.3 Dissolved Oxygen

An increase in dissolved oxygen indicates production from phytoplankton, as O_2 is a product of photosynthesis. The dissolved oxygen (µM) concentration, $[O_2]$, was retrieved from the oxygen optode sensor on the AUV, the results are shown in Figure 3.10, plotted by depth. The $[O_2]$ range for all the fieldworks was between 284-400 µM. M1 showed a stable $[O_2]$ around 284-288 throughout the water column while for M2 there was observed an increase $[O_2]$ from 40 m to surface (0 m). For the H fieldwork, there were some variations where the first day (Plot E) had an outlier with values up to 400 µM. The opposite $[O_2]$ trend was observed for the next day (Plot F) with overall lower concentrations and a decrease in $[O_2]$ from 10 m to 20 m.
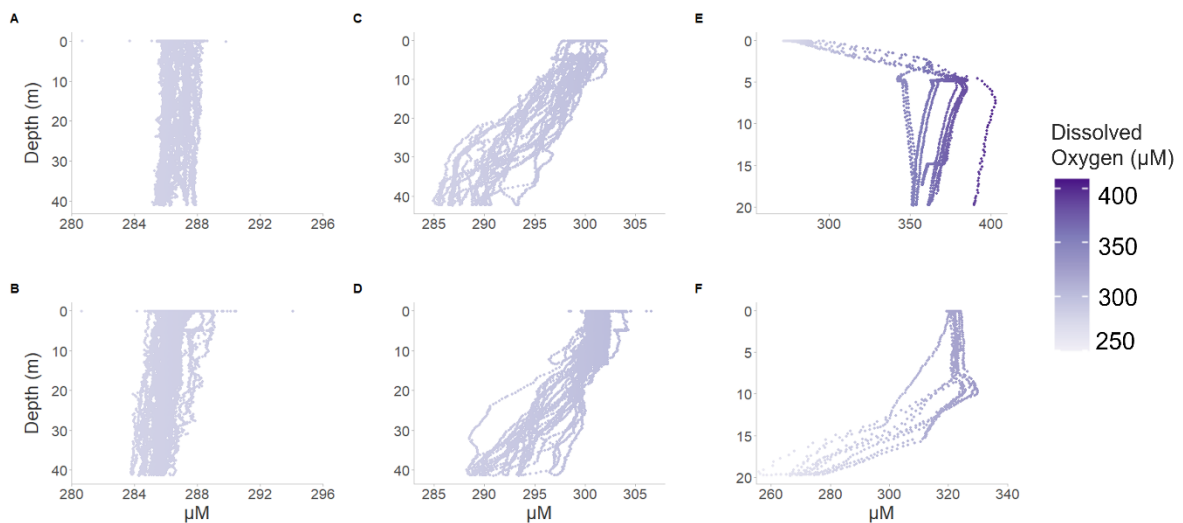
Figure 3.10: Plot of $[O_2]$ (µM) for all six field days, measured using an oxygen optode mounted on the L-AUV. The oxygen sampling points are coloured by $[O_2]$. A-B show the results for the first fieldwork (M1: 13.04.-14.04.21), C-D for the second fieldwork (M2: 20.04.-21.04.21) and E-F for the last fieldwork (H:04.05.-05.05.21).

3.5 Principle component analysis (PCA)

Since there are many variables influencing the spring bloom dynamics, a principal component analysis (PCA) was a useful technique for visualising and identifying similarities, correlations and grouping of individuals and variables in the data. As variables, both bio-optical (pigments) and KEVs, were implemented in the model. For simplification, pigments were used as a proxy for phytoplankton functional groups, where; Fucoxanthin = diatoms, Chl *b* = Chlorophyceae and Peridinin = dinoflagellates. For the KEVs nutrients (nitrate and phosphate), dissolved oxygen, salinity and temperature were included as variables.

Principle components (PC) are the underlying structure in the data, and the first PC (PC1) is the straight line that shows the most variance in the data. Since the data set has 8 variables, it also has 8 dimensions. From the overall summary of the PCA shown in Table 0.4 (Appendix C), PC1 explain 48.67% of the variance, PC2 explains 27.02% of the variance and PC3 explains 14.50% of the variance of the data. In total the three first PC described 90.1% of the variance of the data, which means that by focusing on three dimensions, only <10% of the variance of the data is lost. To determine the number of PC to be considered, eigenvalues need to be inspected (standard deviation in Table 0.4).
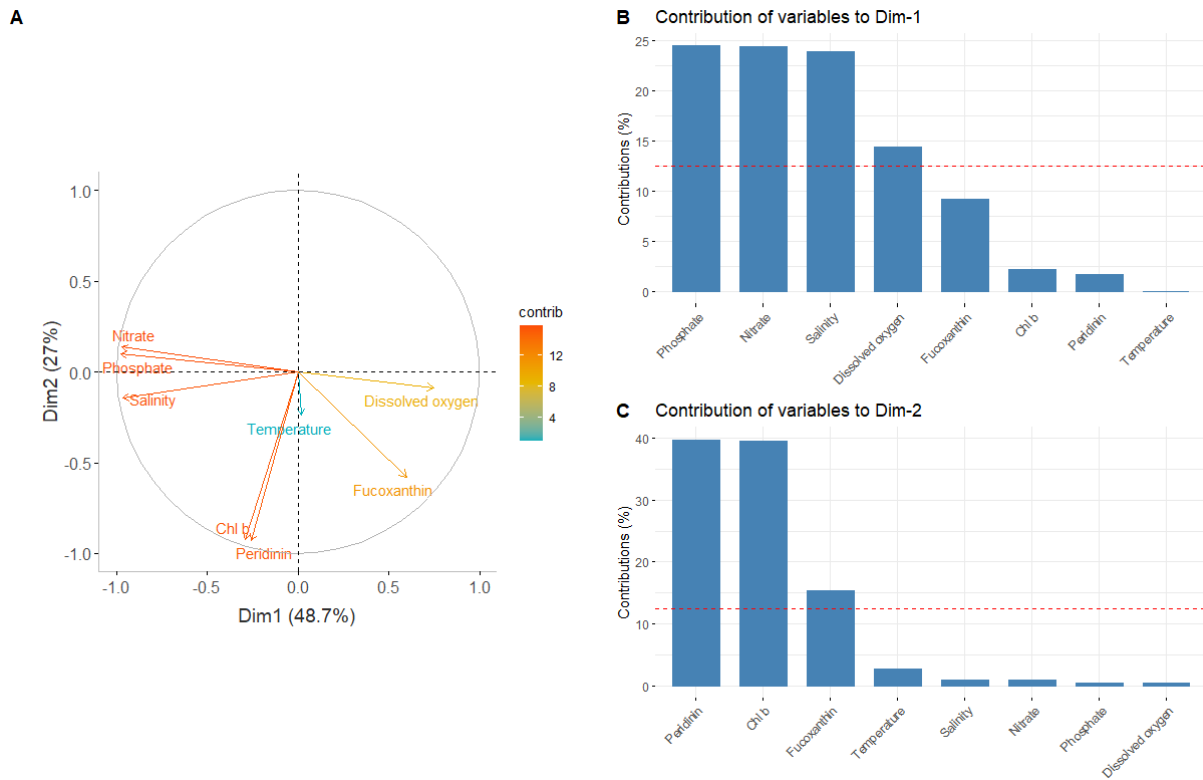
Figure 3.11: Results of the principal component analysis (PCA) of variables influencing the phytoplankton spring bloom and functional group distribution. Panel A shows a plot of variables contributing to PC1-2. Arrows point in the direction of correlation and contribution for PC1 and PC2 and are coloured according to their total contribution to both dimensions. Panels B and C show relative contributions (%) of the variables to PCs 1 and 2. Red dashed lines represent expected contributions if contributions were uniform.

Eigenvalue > 1 was used as a cutoff, explaining why only PC1-PC3 were used. The percentage of explained variance is also visualized in Figure 0.4 (Appendix C).

In Figure 0.5 (Appendix C), the contribution of the loadings of individual samples are represented in a PCA plot, where the individuals most far away from the centre [0,0] contribute most to the PC1-2. The figure showed a form of clustering. The focus was to look at the contribution of the different variables and how they correlate to each other in PC1-2 (visualized in Figure 3.11). Plot B shows that phosphate, nitrate, salinity and dissolved oxygen all contributed to PC1 to a relatively high degree. In Pot A arrows are coloured according to contribution and direction explains correlation. For PC2 (Plot C), peridinin, Chl *b* and fucoxanthin contributed the most to the dimension. Temperature has a short arrow and did not contribute to explaining the variance of the two first dimensions.

The summary of the correlation for each PC, Cos2 and contribution for each variable for PC1-PC3 is presented in Table 3.2. The PC1 column and Plot A in Figure 3.11 provide information on the correlation of the different variables. For PC1 the angle between the variables nitrate, phosphate and salinity are low, indicating correlation, these variables were highly negative correlated opposite to dissolved oxygen which was positively correlated to PC1. For PC2 the variables Chl *b* and peridinin was highly negatively correlated with a low angle showing a high correlation between the two variables. For PC1-PC2 all the variables contributed to the variation relative similar except dissolved oxygen, which only has a 7.8 % contribution in total. The contribution of each variable for each PC is visually presented in Figure 0.6 (Appendix C).

Table 3.2: Results from the principal component analysis (PCA) of variables influencing the phytoplankton spring bloom and functional group distribution. The correlation of each variable for the PC is given from PC1-PC3, including Cos2 and the contribution for the model looking at PC1-PC3 which explains over 90% of the variance in the data.

Variables	PC1	PC2	PC3	cos2	Contribution
Phosphate	-0.975	0.0981	-0.0729	0.966	13.399
Nitrate	-0.973	0.136	-0.0637	0.970	13.448
Salinity	-0.962	-0.142	-0.1408	0.967	13.407
Temperature	0.0196	-0.239	0.957	0.973	13.493
Dissolved oxygen	0.747	-0.088	-0.000435	0.567	7.858
Peridinin	-0.255	-0.927	0.0416	0.927	12.849
Chl b	-0.292	-0.924	0.00349	0.939	13.022
Fucoxanthin	0.597	-0.577	-0.461	0.903	12.520
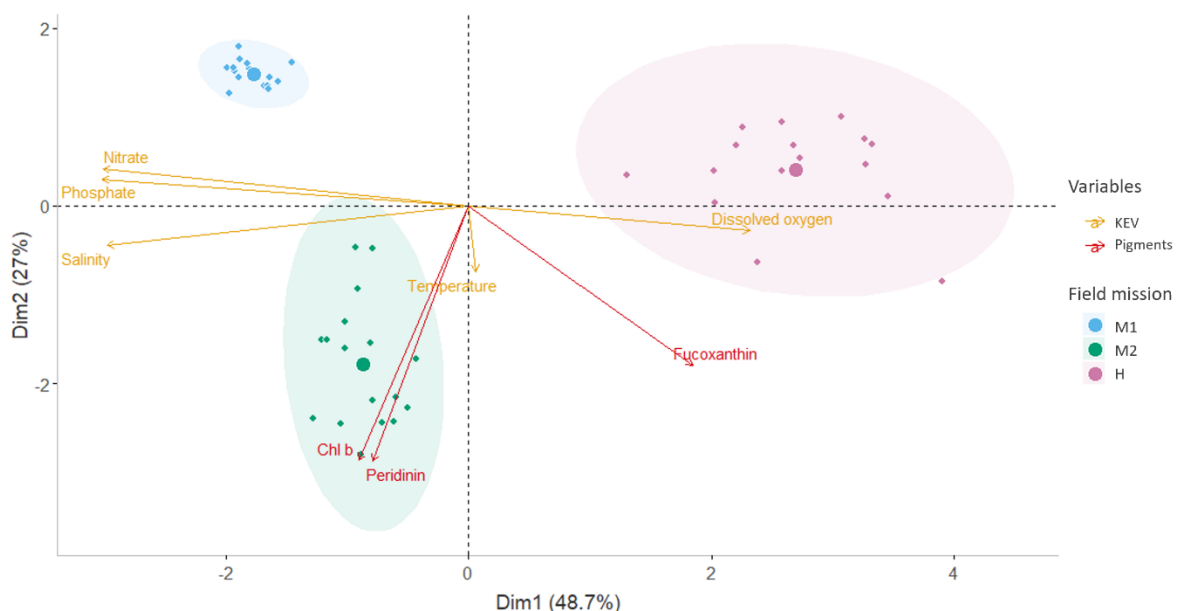
Figure 3.12: Results of the principal component analysis (PCA) visualizing PC1 and PC2. The analysis included samples (n=51) from all three fieldworks, and variables from HPLC analysis, AUV-sensors, and nutrient analysis of seawater samples. The figure shows a biplot of the PCA results. Points represent principal component (PC) scores (individual mean samples (n=3)), ellipses represent group-specific 95% confidence intervals of the three different fieldworks (M1, M2, H) and coloured arrows represent the different variables coloured by pigments and KEVs. Arrows point in the direction of correlation and contribution for PC1 and PC2 and are coloured according to their total contribution to both dimensions.

In Figure 3.12 both the contribution of the individuals and the variables were plotted together. The individuals are clustered by fieldwork, and the factors were separated into pigments and KEVs. Fucoxanthin was not correlated with the two other pigments, indicated by an almost 90-degree angle between the arrows.

3.6 Microscope analysis of phytoplankton

To study the phytoplankton biodiversity, a qualitative analysis of phytoplankton taxa was performed, by identification and imaging in the microscope. The phytoplankton size range included in this analysis was 20-200 µm. A full list of taxa present in the sample is given in Table 0.5 in Appendix D, where the most dominant taxa are marked.

For the Mausund fieldworks (M1, M2), only horizontal plankton net samples were analysed. Here species such as the dinoflagellates *Tripos tripos* and *Tripos fusus* were dominating in many of the samples. There was, however, a great abundance of diatoms in the samples dominated by large and typical spring bloom species such as *Coscinodiscus* sp. and *Thalossisoria* spp.. In addition, in several samples *Pleurosigma normanii* was also quite dominant. Some major other groups present were tintinnids and foraminifera which both are protozooplankton and green algae. At Hopavågen, the transects were performed using horizontal plankton net tows at the depth range 0-20 meters. The overall biodiversity was lower here compared to the fieldworks at Mausund. The samples were dominated by *Chaetoceros* spp. and *Parafavella* sp. (tintinnid), where the overall taxa composition was quite similar for all fieldworks, with some variations. Since this was not a quantitative analysis, the abundance of different species groups was not accounted for, only indicating the presence of species. However, combining microscopic images (Figure 3.13) and HPLC
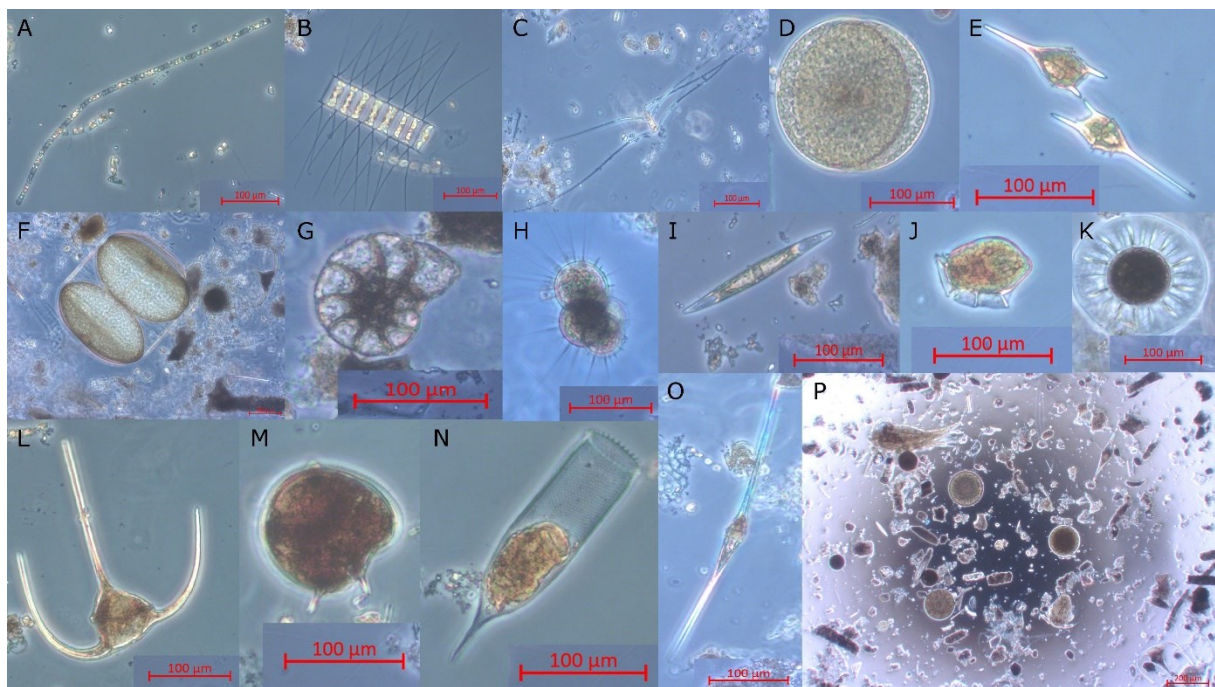
Figure 3.13: Major phytoplankton species from the spring bloom, species were photographed using a SONY DFW-X700 Axiocam 105 color connected to the inverted microscope: *Leptocylindrus danicus* (A), *Chaetoceros decipiens* (B), *Chaetoceros cf. convolutes* (C), *Coscinodiscus* sp. (D), *Tripos furca* (E), *Coscinodiscus* sp. (F), Foraminifera (G)*, *Globigerina bulloides* (H)*, *Pleurosigma normanii* (I), *Dinophysis acuminata* (J), *Pterosperma* sp. (K), *Tripos tripos* (L), *Protoperidinium* spp. (M), *Parafavella* sp. (N)*, *Tripos fusus* (O), Overview of organisms and particles in the microscope (P). Full detailed species biodiversity in Table 0.5 in Appendix D. *Protozooplankton: heterotrophic organisms that have no ability to do photosynthesis.

pigment composition, provides a better understanding of the phytoplankton groups dominating the water masses during the sampling period.

3.7 SilCam classification

For automatic identification of phytoplankton in situ, the SilCam was mounted on the L-AUV. The SilCam classification failed to identify and correctly classify "diatom chains" using the PySilCam approach with a pixel resolution of 27.5 µm. This was identified by looking at the montages created for the class "diatom chains" where all organisms identified were copepods, concluding that the algorithm did not work to classify the field data sampled using this setup. As an alternative approach, the field data containing potential organisms were selected and classified manually using the software Roboflow. The idea was to use this classification to train a new model using deep learning and then use the algorithm to automatically classify the field data. Some examples of manually classified *Coscinodiscus sp.* (with uncertainty if the object is phytoplankton) are shown in Figure 3.14. Further information regarding optical image resolution and results from SilCam are discussed in Nøland (2022).
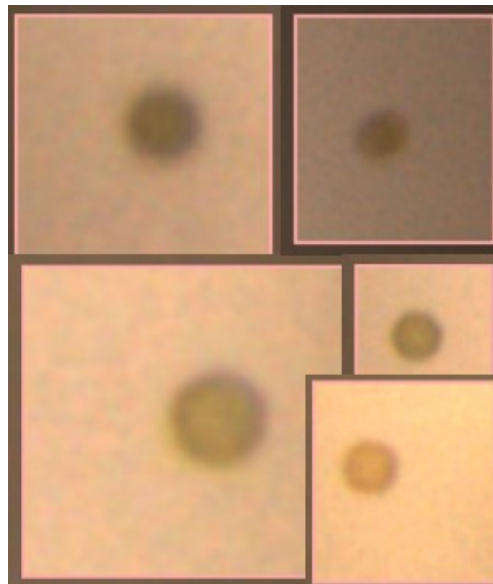
Figure 3.14: Examples of manually classified *Coscinodiscus sp.*, imaged with SilCam and retrieved from the classification software Roboflow.

4 Discussion

The main aim of this thesis was to use new technology and methods to study the phytoplankton spring bloom in coastal areas, as a proof-of-concept. Data provided in the results were obtained simultaneously from two different platforms: an L-AUV equipped with environmental sensors and analyses from seawater samples. Since the algal bloom mapping at Mausund also included the use of satellites, aeroplanes, and drones, all equipped with HI, the in vivo spectral reflectance and pigment composition will also be discussed in relation to these platforms. The use of multidimensional ocean observations (observational pyramid), where different instruments and platforms are used to study a common area at the same time, is a relatively new field of study and monitoring approach (Grøtte et al., 2022). A discussion of how to best combine and use this approach is valuable for future research highlighting information, knowledge and experience that is important to optimize the spectral, spatial, and temporal sampling resolution of the data.

4.1 State of phytoplankton spring bloom

Covering the main aim and sub-goal (1): Study how KEVs can explain phytoplankton spring bloom dynamics by combining sensor data from AUV and physical seawater samples, this first section investigates the state of the spring bloom and discuss the main findings. Given that there is a significant difference in [Chl *a*] and [nutrient] between all three fieldworks (M1, M2, H) these will be discussed separately as they all represent different states of the bloom. The pre-bloom, bloom and post-bloom phases are all discussed according to KEV data, weather conditions, [Chl *a*], [nutrient] (NO_3^- and PO_4^{3-}) and zooplankton grazing.

Since there are many variables influencing the spring bloom dynamics, the PCA results easily visualised and identified similarities, correlations and grouping of individuals and variables in the data set. Variables such as nitrate, phosphate and salinity are correlated and contribute to explaining the variation in the analysis. All the three different fieldworks are clustered together, indicating that they are similar and creating a grouping in the data set. This supports the decision of comparing and looking at the different fieldworks as groups. The analysis also states that the concentration of diatoms is not correlated with the concentration of dinoflagellates and Chlorophyceae, supporting the findings of diatoms in all microscopic samples, and them being the dominant phytoplankton pigment group and algal class. Figure 3.11 explains that diatoms (fucoxanthin as a proxy) were found where there were low nutrient concentrations. This is caused by two main reasons, first, because the diatom bloom grew and used the nutrients and second because of freshwater (since the bloom happened after the freshwater input from snowmelt) (Erga et al., 2012; Silva et al., 2021). The correlation between fucoxanthin and dissolved oxygen indicates that an increase in diatom biomass results in increased production of oxygen (Gökçe, 2021; Rahlff et al., 2019). According to the PCA analysis, the temperature is not correlated with the other variables, nor contributes to explaining the variation in the data set for the first two principal components. It is important to again point out that all the statistics performed on the AUV data were done from resampling the mean of each depth interval, which is not optimal but done to compare them to the seawater samples.

4.1.1 Mausund 13.04.-14.04.21 (M1)

The Mausund bank is considered a dynamic biological hotspot, with many small islands and complex bathymetry leading to high levels of primary productivity and biological diversity due to tidal mixing, wind, and internal waves (Fragoso et al., 2021). Two weeks prior to

the first fieldwork the area was exposed to storm events (extreme wind conditions) resulting in low light conditions and mixing of the water column. This can be seen in the temperature, salinity and Chl a profiles sampled by the AUV, where the MLD is below 40 m and low in vitro [Chl a] with the mean values of 0.55 and 0.52 µg L^{-1}, respectively. The [NO_3^-], with mean values of 5.8 and 6.0 µM, is "medium" in relation to the deepwater concentration of 10 µM (i.e winter concentrations, values of annual max [NO_3^-] before the bloom period) (Forbord et al., 2021). Earlier studies have shown much lower [NO_3^-] in May, and according to Fragoso et al. (2019a) the value of 2 µM at Mausund, Frøya, indicates low concentration for phytoplankton growth.

Even though nutrients are present, the ocean was at M1 in a pre-bloom phase. Supported by the Sverdrup hypothesis (Sverdrup, 1953), claiming that when phytoplankton are in low abundance and uniformly distributed within the ocean mixed layer, they will not bloom. He further states that a bloom will not occur until the ocean warms and stratifies in spring, as observed for the wate column at Mausund (Brody & Lozier, 2015). This is also seen from the qualitative microscopic analysis and pigment concentration; where the qualitative observations of phytoplankton present are low, and the pigment concentration is low. The benthic species *Pleurosigma normanii* (Belt et al., 2000) was observed both in M1 and M2, suggesting that the storm might have re-inserted this species to the surface.

4.1.2 Mausund 20.04.-21.04.21 (M2)

Between M1 and M2, the weather conditions were calm and sunny, which are known conditions to trigger phytoplankton photosynthesis and growth (Assmy & Smetacek, 2009; Fragoso et al., 2019b). The water column has started to stratify at the upper 20 m, which can be seen in both the salinity (Figure 3.9) and temperature (Figure 3.8) profiles from the AUV. When stratification occurs, the phytoplankton MLD shoals, keeping the phytoplankton in the euphotic zone and allowing them to be more exposed to light, which in turn, increases the production (Silva et al., 2021). The [Chl a] from both the in situ and in vitro measurements had increased to mean values of 1.66 and 1.95 µg L^{-1} for the two sampling days, respectively. There were a significant difference between the [Chl a] concentration between the two days, which might indicate that the bloom was in the starting phase and that the phytoplankton biomass was increasing. To say more about the development of the bloom, the area should have been revisited throughout the spring. However, the satellite images from Figure 3.1 indicated higher [Chl a] in the area for the 04.05. and 05.05.21, supporting the assumptions of further bloom development. Looking at the in situ Chl a measurements, it seems like the phytoplankton concentration was highest just above the stratification layer, around 15 m depth, which might indicate a sub-surface bloom, not visible using aerial remote sensing (Richardson et al., 2000).

Comparing the nutrient concentrations from the first and second fieldworks, there was a significant reduction in both [NO_3^-] and [PO_4^{3-}]. At the same time, there was an increased oxygen production with the highest concentrations near the surface. Both these factors support increased production and phytoplankton growth (Gökçe, 2021). Microscope and stereoscope analysis performed showd fecal pellets present in the water column, this is used as an indication of zooplankton grazing (Cyr & Pace, 1992). This is potentially a major source of phytoplankton mortality, altering both the biomass and composition of communities (Cyr & Pace, 1992), defined as a limiting factor influencing the rate of phytoplankton growth and bloom development. The combination of zooplankton grazing and vertical mixing by wind due to stormy conditions has the potential to prolong the

bloom, not creating a high Chl *a* maximum, but rather creating a succession of smaller peaks until nutrients are exhausted (Assmy & Smetacek, 2009).

4.1.3 Hopavågen 04.05.-05.05.21 (H)

The last fieldwork took place at Hopavågen, which is a sheltered bay where hydrographic and biological conditions are strongly affected by the shallow sill (underneath the bridge of inlet) (Marion, 1996; Mogstad et al., 2019). This makes it an interesting area to study because organisms from the coastal current are pushed through the channel decreasing the biodiversity inside the bay compared to areas around (Marion, 1996). The contrast from the areas surrounding can be exemplified by comparing the satellite estimation (Figure 3.1) and the observed surface in vitro [Chl *a*]. Satellite estimations indicated a much higher [Chl *a*] than those observed in Hopavågen. From this, estimations of in vitro [Chl *a*] would also be expected to be higher for H than for the M2 fieldwork, however, these concentrations are lower, with the mean values of 1.40 and 1.36 µg L^{-1} accordingly. The special hydrography and limited NO_3^- input from the inlet due to restricted deepwater renewal (Marion, 1996) can explain the variations between the high surface [Chl *a*] observed by satellite for the area outside Hopavågen (indicating bloom conditions) and the low surface [Chl *a*] inside. For more correct comparison, measurements of the water column should have been sampled in Trondheim's fjord and at Mausund to verify the [Chl *a*], as satellite Chl *a* estimations are based on algorithm calculations (Stock & Subramaniam, 2020). The use of remote sensing for phytoplankton studies will be discussed in more detail in section 4.4.1.

Looking at the in situ Chl *a* data from the AUV, the Chl *a* maximum was observed at around 15 m for both dates. This is defined as a sub-surface bloom, which occurs when persistent upper water column stratification concentrates phytoplankton in the bottom of the thermocline to better use nutrients available and adapt to light conditions (Silsbe & Malkin, 2016). Phytoplankton moving down the water column during a post-bloom phase is also shown in other studies such as in Rodríguez et al. (2010). Further the low [NO_3^-] (0.3 and 0.6 µM) support the conclusion that the state of the bloom is in a post-bloom phase. NO_3^- is consumed by phytoplankton for growth earlier in spring resulting in depleted values in Hopavågen in May (limiting values <1 µM) (Fragoso et al., 2018; Rumyantseva et al., 2019). *Chaetoceros* spp. being dominant for the H fieldwork contradicts with Volent et al. (2011), stating that a decline in the number of diatoms characterize a post-bloom.

4.2 In vitro versus in situ Chl *a* fluorescence

Sub-goal (2) for this thesis was to use Chl *a* fluorescence data as a proxy for phytoplankton biomass, [Chl *a*], looking at the variation between in situ and in vitro concentrations. Moving towards more efficient detection of [Chl *a*] using in situ fluorometric measurements as a proxy of phytoplankton biomass, interpretation of sensor data needs to be done with caution. The linear models indicate varied linearity and composability of in vitro and in situ [Chl *a*] between the fieldworks. As shown in Table 3.1 there is a relatively good linear relationship (R^2 = 0.7421) for the in situ and in vitro [Chl *a*] for the Mausund (M1, M2) data. However, the in vitro and in situ measurement for both Hopavågen and the whole data set has a low linear relationship. This indicates that for the first two fieldworks, the [Chl *a*] for the in situ and in vitro measurements align well. The overall low relationship is a great example of why we need to compare and analyse data from different sensor and measurement types with caution discussed both in Johnsen et al. (2018) and Fragoso et al. (2021).

The difference between in situ and in vitro estimations of [Chl a] may be due to sub-surface patchiness of phytoplankton biomass, non-photochemical quenching (NPQ) and the layering of water masses (Johnsen et al., 2018). When comparing in situ and in vitro [Chl a] – based fluorometry the effect of photosynthetic quenching (PQ) and NQP needs to be consider. NPQ is a mechanism where cells exposed to high light levels give off excess energy as heat, due to light absorption of PPC resulting in a reduction in Chl a fluorescence emitted from living cells during well-lit daytime hours (Huot & Babin, 2010; Johnsen et al., 2018; Roesler et al., 2017). The in situ concentration for fieldwork H showed [Chl a] up to 18 µg L^{-1}, which is according to Roy et al. (2011) classified as high-density bloom. In contrast, the corresponding in vitro [Chl a] ranges from 0.9 µg L^{-1} to 2.5 µg L^{-1}, values that are 8 times lower than the in situ measurements. The in situ Chl a values are of high uncertainty and need to be treated with caution and further discussed in section 4.3. The AUV survey indicated a patchy distribution with Chl a maximum of around 15 m, and lower concentrations at the surface and below 15 m. The temperature measurements show two rapid changes in temperature forming two distinct water layers, one around 5-10 meters and one below 18 meters. Such layering can trap high biomass of phytoplankton below the rapid temperature shift, resulting in higher concentrations at that depth interval (Richardson et al., 2000). The discrepancy between the in situ and in vitro measurements at Hopavågen can also be explained by the variation in spatial and temporal resolutions, where seawater samples give a snapshot of the exact moment where it is sampled, and the AUV sample a larger volume and area. A thin layer of high phytoplankton biomass is easily missed by blind point samples of the water.

4.3 The use of L-AUV to sample KEV data in the water column

Considering the findings discussed in sections 4.1 and 4.2 there is a need for looking into the sampling method to fully explain sub-goals (1) and (2). For this thesis, the L-AUV was used for autonomous mapping of the spatial heterogeneity of KEVs in the water column. Compared to traditional seawater sampling the vehicle covers a substantially larger sampling area and provides a broad and more extensive perspective of the pelagic activity. The complexity of conducting phytoplankton ecological studies and combining data from different platforms are both shown in the results in this thesis and commented on by Fossum et al. (2019) and Ryan et al. (2010). One of the advantages of using an AUV is the ability to map the entire water column, following a pre-planned mission. This makes it possible to map the patchy distribution and sub-surface blooms. They occur when persistent upper water column stratification concentrates phytoplankton in the bottom of the thermocline to better use light and nutrients (Silsbe & Malkin, 2016) as seen for the Hopavågen fieldworks.

Even though the AUV has shown to perform well in areas that are hard to reach, as under the sea ice (Johnsen et al., 2018), in shallow and small areas such as Hopavågen there is an increased risk of collision, limiting exploration in areas close to shore or bottom. The largest source of sampling uncertainty comes from the effects of currents (speed and direction), which makes the observations time-dependent. Therefore, keeping the AUV in the "same water masses" can effectively be done by limiting the survey area to sub km size (Fossum et al., 2019), an approach used for collecting data for this thesis. The AUV increases the temporal and spatial sampling resolution, however since the water masses (i.e. phytoplankton) are constantly in motion, the use of adaptive sampling, both tested in Fossum et al. (2019) and as a separate part of the Mausund fieldwork has shown promising results. This introduces a level of autonomy where the AUV thinks and learns by itself,

adapting to the surrounding dynamic environment, and making decisions based on information received during the mission (onboard processing) such as detection of Chl *a* hotspots (Fiorelli et al., 2006; Saad et al., 2020).

There is a need to investigate how to operate the vehicle according to best practices for sampling data when environmental sensors are applied, where the amount of different sensors complicates the operation further. According to the technical specifications of the oxygen optode (Xylem, 2020) the response time is set to 8 seconds. Since the response time of the sensors is not instantaneous and dependent on the flow regime of the platform (Bittig et al., 2018) there is a need for studying optimal sampling procedures according to speed, response time, temperature and salinity using the L-AUV. For all the fieldworks except the one for 04.05.21, all the oxygen measurements show similar trends as for the other KEVs data. The strange $[O_2]$ pattern is most likely due to a method or sensor error, however, the rapid change in temperature resulting in water layer stratification in combination with lag in response time can have influenced the observed consentrations. Another explanation can be that the $[O_2]$ in water masses is dependent on the consumption from different organisms, and therefore resulting in a time delay compared to fluorescence measurements of [Chl *a*] used as a proxy for phytoplankton biomass (Gökçe, 2021).

Another known problem is that Chl *a* fluorometer measurements are influenced by the effect of scattering from bubbles at the surface when the AUV turns during a Yo-yo transect (Suggett et al., 2010). To remove the effect of bubbles from the surface, the Chl *a* data sampled by the AUV were filtered, potentially removing valuable information about the surface [Chl *a*]. The values from the in situ measurements are necessary not true, and the high values at Hopavågen are most likely due to overestimated sensor calibration, however, the trend of the data was most likely correct. A thin layer Chl *a* maximum (around 15 m depth) was observed in Hopavågen, indicating that the rapid change in concentration might influence the measurement accuracy, as the mixed layer measurements from Mausund matched the in vitro [Chl *a*]. To optimize the accuracy of the sensor measurements, correct calibration routines are crucial (Bittig et al., 2018; Suggett et al., 2010).

4.4 Use of bio-optical approches to study phytoplankton functional groups

Considering climate change, HABs, ecosystem management and aquaculture industry there is a need to improve the quality of remote sensing information and the efficiency of phytoplankton monitoring (Asch et al., 2019; Dallolio et al., 2021; Lewandowska & Sommer, 2010; Pettersson & Pozdnyakov, 2012). Simple and efficient ways to detect functional groups, toxic algal indicator pigments, spectral signatures, and species present in the water column are highly valued (Benfield et al., 2007; Johnsen et al., 2009; Kulk et al., 2020). The data can provide information about functioning, health, and trends in the phytoplankton community. This section will discuss the use of different bio-optical approaches that can contribute to enhancing the study of phytoplankton at different spectral and spatial resolutions.

4.4.1 In vivo spectral reflectance and pigment composition

This section discuss sub-goal (3): Use bio-optical techniques (spectral reflectance and chemotaxonomy) for information about pigment groups from seawater samples, and connected the data in relation to remote sensing. Different groups of phytoplankton play

different ecological and biochemical roles in the ocean during the spring bloom. Pigments can be used as phytoplankton group pigment indicators, were diatoms can be indicated by fucoxanthin, dinoflagellates by peridinin and Chlorophyceae by Chl *b* (Roy et al., 2011). These simplifications are necessary to be able to distinguish between different phytoplankton pigment groups using optical remote sensing. Determination of phytoplankton community composition using satellite remote sensing is expected to improve in the near future (Bracher et al., 2017; Stock & Subramaniam, 2020) and initial studies have suggested a strong potential for hyperspectral ocean colour mapping (Dierssen et al., 2020; Sadeghi et al., 2012). Moving from global and open ocean algorithms to more local algorithms to study optical complex coastal waters, will improve the accuracy of the observed phytoplankton community estimations (IOCCG, 2000; Roy et al., 2011; Stock & Subramaniam, 2020; Volent et al., 2011).

The in vivo reflectance analysis was carried out under highly controlled conditions, therefore $R(\lambda)$ spectra from the QE Pro spectrometer were considered the true in vivo reflectance spectra of the algae in the ocean. Compared to the vast amount of satellites using multispectral bands, looking at band rations to determine ocean colour constituents from the signals (Borfecchia et al., 2019; Chusnah & Chu, 2022; Tilstone et al., 2021), the spectrometer measurements were performed with the high spectral resolution of 0.7 nm. Since the spectral reflectance is measured on filtered seawater samples there is no effect of total suspended matter, colour dissolved matters, apparent optical properties or water itself. The signal is purely from microscopic algae (and potentially some zooplankton <200µm). As a part of the development and increased use of hyperspectral sensors on satellites, planes, and drones (Dierssen et al., 2020), the true algae spectra can serve as the reference spectra when searching for useful signals and spectral signatures in processed remote sensing signals.

Since the spectral resolution is high for the in vivo measurement, it is possible to look at pigment reflectance dips (inverse of pigment absorbance peaks) affecting the signature.
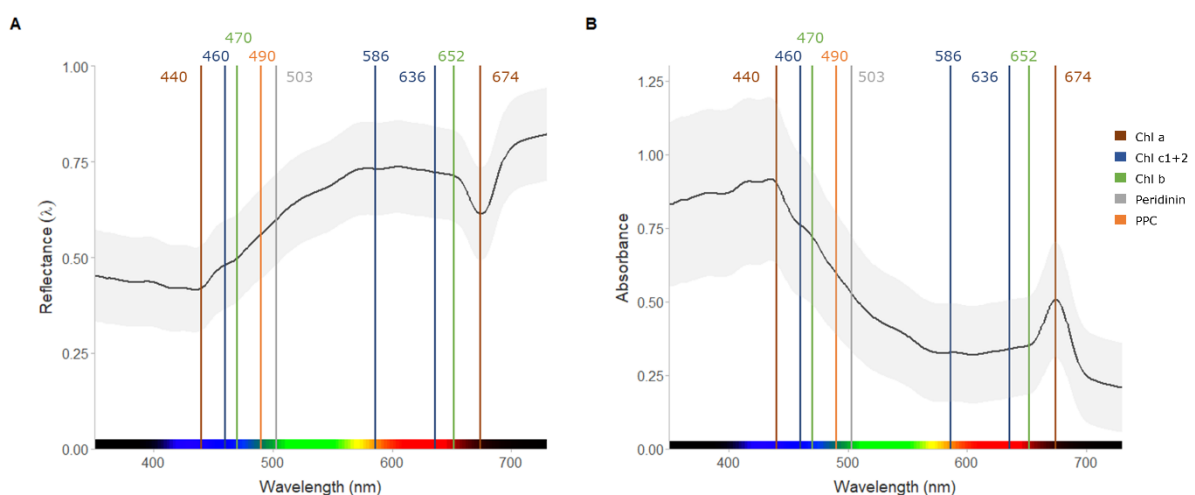
When comparing spectral signatures of individual pigments (measured using HPLC) with in

Figure 4.1: A) Mean in vivo reflectance ($R(\lambda)$) of living phytoplankton cells. B) -log(A) showing the mean absorbance. The gray shaded area represents the standard deviation of mean values (black line). Vertical lines represent modelled in vivo absorbance maxima of the pigments Chlorophyll *a* (Chl *a*; (Bidigare et al., 1990; Johnsen et al., 1994a)), Chlorophyll c_1+c_2 (Chl c_{1+2};(Bidigare et al., 1990; Johnsen, et al., 1994a; Johnsen et al., 1994b), Chlorophyll b (Chl *b*;(Bidigare et al., 1990)), Peridinin ((Johnsen et al., 1994a) and photoprotective carotenoids (PPC;(Bidigare et al., 1990; Johnsen et al., 1994a).

vivo spectral reflectance, the spectral shifts need to be considered (Hunter et al., 2008; Roy et al., 2011). This spectral shift happens when pigments are extracted from cells using organic solvents, then a breakage between the pigment and protein bonds occurs, changing the bio-optical characteristics of the spectral absorption coefficient. In addition, different types of organic solvents have different effects on the blue to red ratios of Chl *a* as an example (Johnsen et al., 1994a). This is also observed when inspecting the "red-peak" of Chl *a* between 650-700 nm (Johnsen & Sakshaug, 2007), where the maximum peak is detected at 674.4 nm. This peak occurs since 75% of the cellular Chl *a* in diatoms are bonded to the major light-harvesting complex of PSII. The dominance of diatoms is supported by the pigment extraction (HPLC) where Fucoxanthin (diatom indicator pigment) was highly present and further supported by microscope analysis showing the dominance of C*oscinodiscus* sp. and C*haetoceros* spp., which both are diatoms.

Even though Chl *a* is the pigment used as a proxy for phytoplankton biomass the other pigments are also of interest (IOCCG, 2000). A high amount of PPC such as diadinoxanthin and diatoxanthin indicates high-light acclimated cells indicating a fast growth rate (Rodríguez et al., 2006). Explaining major in vivo absorbance peaks (reflectance dips), modelled in vivo pigment peaks (Bidigare et al., 1990; Johnsen et al., 1994a; Johnsen et al., 1994b) of observed pigments are shown for the mean algae reflectance/absorbance spectra in Figure 4.1. Not surprisingly, the two biggest absorbance/reflectance peaks are explained by the 440 nm and 674 nm Chl *a* absorbance peak, as this was the dominating pigment for all HPLC pigment extractions (Figure 3.6). The 460 nm and 586 nm Chl c_{1+2} absorbance peaks might explain two smaller peaks observed in the in vivo measurements, and the 470 nm Chl *b* peak, in addition, contributing to a shoulder in the spectra.

The measurement of spectral reflectance on filters was done as a pilot test to check if it was possible to retrieve any useful information from the results. The in vivo $R(\lambda)$ is very important for verification and calibration of satellites and aerial drones equipped with hyperspectral imager (HI). For future use, there is a lot more information that potentially can be obtained using this technique. For example, could the individual signatures be investigated, looking for variation between samples and fieldworks. If calculating the absorbance L^{-1} filtered seawater, there is a potential for using this technique to determine phytoplankton biomass.

4.4.2 Silcam

The last sub-goal of this thesis was (4): Compare the identification success of phytoplankton taxonomic groups by analysing images generated from the silhouette camera (deployed on an AUV) with preserved net samples in the microscope. The SilCam (pixel resolution of 27.5 μm) classification failed to identify and correctly classify "diatom chains" using the PySilCam, however, a few *Coscinodiscus* sp. was identified from a collection of fieldwork through manual classification. The classification is highly uncertain, and only includes an extremely small number of observed individuals compared to the total amount of SilCam data. This manual classification is time-consuming and not an effective way to identify organisms detected through the SilCam. If this classification succeed to identify more classes than the PySilCam (Davies et al., 2017) when trained on several new model algorithms using deep learning, there is potential for this method to highly reduce the processing time of plankton classification. On the other hand, the biodiversity resolution is highly limited compared to microscopic analysis. As of today, the SilCam used in this thesis is only able to image the largest centric diatoms, giving a wrong impression of the abundance of phytoplankton compared to [Chl *a*] and microscopic analysis, missing

biodiversity information. The use of microscopic analysis describes biodiversity with a higher accuracy. For future work, a suggested approach is to use microscopy pictures to train and develop new models and algorithms for classification. Then later test the new classification in the field, potentially also onboard processing (Saad et al., 2020), which is one of the end goals of AILARON.

Although the identification success of phytoplankton using this setup failed due to low spatial resolution, the larger organisms, such as zooplankton, had a much higher identification success as expected using the given pixel resolution of 27.5 μm. This is further discussed in Nøland (2022). The improved resolution is necessary if being able to detect and classify phytoplankton. An example of successful phytoplankton identification using SilCam was a survey performed at Runde, Norway (Fossum et al., 2019), deploying the SilCam using a winch at different stations. Here the SilCam systems imaged a particle size range spanning 28 μm to 4 cm in equivalent diameter (higher resolution than for the setup in this thesis) and were able to identify and quantify the dinoflagellate genus *Tripos* sp. One of the main challenges of using an AUV as a sampling platform, is the speed and form, creating a flow pressure that pushes away a large amount of water moving through the water column (Fossum et al., 2019; Sousa et al., 2012). However, to sample the entire water column this vehicle is most suitable, as an ROV is tethered and deployment vertically from a boat only gives a limited spatial resolution. Furthermore, by increasing the optical resolution the sampling volume is reduced leading to lower spatial resolution. SilCam being a state-of-the-art approach under development, there is a lot of potential for further research and improvement for use of this technology in algae bloom studies in the future.

4.5 Multidimensional ocean observations

Placing the results in a larger context, this section shows how the different results contribute to the multidimensional ocean observations and their potential use by other disciplines. The discussion has shown that obtaining reliable data about phytoplankton distribution and abundance with a high temporal, spatial and spectral resolution is challenging. For the research at Mausund, several platforms such as remote sensing technologies (satellites/hyperspectral imaging), UAVs, ASVs, and L-AUVs were used to observe the spring bloom event (NTNU AMOS, 2022). The result from this thesis serves as ground-truthing for all the data sampled by the different sensors. Where spectral reflectance and pigment composition can be connected to remote sensing using satellite, aerial vehicles and drones deployed with a hyperspectral imager. Here, the algae spectral signature can be used as a reference for spectra when they are using a higher spatial and lower spectral resolution on the other platforms. Remote sensing technology is limited to observing the upper water column, missing valuable information about plankton distribution in the deeper layers. By deploying an L-AUV a 3D picture of the water column can be mapped at a lower spatial and temporal resolution, detecting sub-surface Chl *a* maximum and other KEVs affecting the phytoplankton distribution. To validate and give more information about the plankton community dynamics than is possible to detect using these platforms, analysis in microscope and chemotaxonomy are also of value.

4.6 Challenges

Regarding challenges, it is important to be able to learn from and avoid them in the future, so some of the main challenges are highlighted here. Firstly, the study of marine ecosystems is highly affected by weather conditions, and as a storm event occurred for the planned fieldwork on 29.03.21, this fieldwork was cancelled and rescheduled. Because of

the storm, the USV also lost signal to the control centre and beached, luckily there were only minor damages to the vehicle and sensors. Also, platforms such as drones are also dependent on calm and dry weather conditions. The main survey was an interdisciplinary collaboration, which challenge the communication and understanding of limitations, knowledge, and possibilities of different topics of expertise. Secondly, this highlights the need for interdisciplinary collaboration, where new possibilities and development outside own expertise occurs. A consequence of being a part of a larger project is that your study is more dependent on data from other people, making it a bit more challenging to gather and prepare them in time. Due to data loss from a server, some of the SilCam results were lost and therefore not analysed properly. Combining several platforms measuring the same area at different spatial resolutions is a relatively new approach, which requires new methods for comparing the data.

There were taken a lot of seawater samples on the first day, as the seawater filtration and the lab work afterwards was very time consuming, this was reduced for the next fieldwork. If logistically possible the ideal scenario would be to sample time series to study the spring bloom. This thesis includes data from two different locations, making the comparison in time hard since the different locations varies in hydrographic characteristics influencing the ecosystems and therefore are not directly comparable.

5 Conclusion and future perspectives

5.1 Conclusion

The result from this thesis serves as ground-truthing for the data sampled by the different sensors and provides details about the phytoplankton community and how they are affected by KEVs. By combining information from the seawater samples, laboratory analysis and AUV sensors, the results suggest observation of three different bloom phases (pre-bloom, bloom and post-bloom) for the different fieldworks. Chemotaxonomy is an important tool for estimating the state of the bloom, pigment groups present, and indicating the light conditions in the water column and the corresponding light acclimation status in the phytoplankton cells. Where spectral reflectance and pigment composition can be connected to remote sensing from satellites, aerial vehicles and drones deployed with hyperspectral imagers. In vivo spectral reflectance can by use of the red absorption maxima (reflectance dip) (at 674 nm) detect that the water was dominated by diatoms, which is further supported by the pigment extraction analysis. The pilot study of measuring spectral reflectance on filters containing phytoplankton showed promising results and can be implemented as the "perfect" phytoplankton signature, connected to HI. The use of satellite remote sensing technology is restricted to studying the surface water, therefore this data needs to be connected to sub-surface surveys.

Using an AUV to collect information about Chl a distribution in the water column complements spatial coverage of the satellite remote sensing. The AUV detected several sub-surface [Chl a] maximum at around 15 meters, illustrating the increased quality of data collected by using multiple platforms. Interpretation of sensor data needs to be done with caution as seen from the high in situ [chl a] sampled by the fluorometer on the AUV, identifying the need of investigating how to operate the vehicle for optimal data quality. The difference between in situ and in vitro estimations of [Chl a] may be due to the patchy distribution of phytoplankton biomass, non-photochemical quenching (NPQ) and the layering of water masses. It is valuable to use different sampling methods to cover different spatial, temporal, and spectral resolutions, creating a greater understanding of the mechanisms and the dynamic processes that influence the phytoplankton spring bloom. Phytoplankton being microorganisms and at the same time forming mesoscale blooms (<37 0000 km^2), indicates the need for studies covering different temporal and spatial resolutions, where local phenomena can help us understand the changes in the global environment. However, no platform can collect data covering the entire phytoplankton dynamics, highlighting that knowledge of coverage in temporal, spatial and spectral resolution obtained by the platform and sensor is necessary. Interdisciplinary research provides valuable knowledge sharing, improving the understanding of limitations and possibilities of conducting algal bloom research. To improve efficiency and collect data of value, a common understanding of best practices should be conducted before executing the fieldwork.

5.2 Future perspectives

This thesis presents some ideas as small steps towards more efficient mapping and monitoring of phytoplankton spring blooms in coastal areas. Hence, further work would include an improvement of the work presented in this thesis, and research efforts aimed at bettering our understanding of phytoplankton spring bloom dynamics should be increased. Phytoplankton represent an ecologically important organism group (Assmy &

Smetacek, 2009; Fragoso et al., 2021; Kraberg et al., 2010; Lindemann & St. John, 2014; Throndsen et al., 2007), that may be vulnerable to environmental changes (Kuffner et al., 2008; Nelson, 2009; Porzio et al., 2011). Changes in the timing of the spring bloom alter the export of carbon to deeper water layers and the transfer of energy to higher trophic levels (Asch et al., 2019; Dezutter et al., 2019). Since these factors change with latitude, ocean depth and season, long term surveys and seasonal studies of phytoplankton community structure and fluctuations are crucial (Fragoso et al., 2019a; Johnsen et al., 2020; Volent et al., 2011). The Mausund fieldwork was also repeated this year (2022) making it interesting to compare the data findings from 2021 and 2022.

At the cost of a greatly increased operational complexity, additional assets such as another AUV and the introduction of adaptive sampling could be used to increase the spatial coverage capacity and sampling density (Fiorelli et al., 2006; Kemna, 2018; Saad et al., 2020). A new state-of-the-art research structure is the OceanLab being established in Trondheim, Norway, together with SINTEF and NTNU (Davies, 2022). This dynamic fieldlaboratory will provide time-series measurements from sensors on buoys and gliders, increasing the temporal resolution of plankton studies. This research structure encourages collaboration across research communities, and testing of solutions for autonomous operations and ocean ecosystem monitoring.

The launch of NTNUs own small satellite HYPerspectral Smallsat for Ocean observation (HYPSO-1) on the 13., aims to detect ocean colour events with characteristic spectra, in particular algal blooms, using HI. HYPSO-1 is equipped with a custom-built push-broom hyperspectral imager with wavelengths 387–801 nm at 3.33 nm bandpass will provide ocean colour data products with high spatial-spectral resolution (Grøtte et al., 2022). The spectral in vivo algae signature serves as a "ground-truth" and can be used in additional improvements, such as Artificial Intelligence (AI) and Machine Learning connected to remote sensing (Li et al., 2021). Computer programs can be taught to recognize significant algae spectra and potentially tell the difference between spectra from algae groups and other spectra from the ocean (Pyo et al., 2022). These concepts are highly interesting and relevant for mapping at large ocean scales. Measuring in vivo algae spectral reflectance is as of this year implemented as a part of the Primary Production course (AB-323 Light Climate and Primary Productivity in the Arctic) at Svalbard.

In general, there are endless possibilities for technological improvements to increase knowledge about algal blooms and how their abundance influences other organisms in the ecosystem. Each step contributes to ensuring more knowledge towards ecosystem management, aquaculture industry, and the effects of climate change. The new sampling methods have led to an explosion of ocean data, where it can be challenging to find, extract and treat the data needed. HUB Ocean is tackling this problem and is dedicated to sharing ocean data through an Ocean Data Platform which provides deep and contextualized insight for global industry leaders, researchers, and policymakers (HUB Ocean, 2022). Through previous development and the results of this thesis, optical approaches and multidimensional sampling using autonomous underwater vehicles have proven to provide a large potential for phytoplankton studies, a rapidly developing research area.

References

Asch, R. G., Stock, C. A. & Sarmiento, J. L. (2019). Climate change impacts on mismatches between phytoplankton blooms and fish spawning phenology. *Global Change Biology*, *25*(8), 2544-2559. https://doi.org/10.1111/gcb.14650

Assmy, P., Fernández-Méndez, M., Duarte, P., Meyer, A., Randelhoff, A., Mundy, C. J., Olsen, L. M., Kako, H. M., Bailey, A., Chierici, M., Cohen, L., Dougleris, A. P., Ehn, J. K., Fransson, A., Gerland, S., Hop, H., Hudson, S. R., Hughes, N., Itkin, P. & Granskog, M. A. (2017). Leads in Arctic pack ice enable early phytoplankton blooms below snow-covered sea ice. *Scientific Reports*, *7*(1), 40850. https://doi.org/10.1038/srep40850

Assmy, P. & Smetacek, V. (2009). Algal Blooms. In M. Schaechter (Ed.), *Encyclopedia of Microbiology (Third Edition)* (pp. 27-41). Academic Press. https://doi.org/10.1016/B978-012373944-5.00001-8

Barwell-Clarke, J. & Whitney, F. (1996). Institute of Ocean Sciences Nutrient Methods and Analysis. Can. Tech. Rep. Hydrogr. Ocean Sci. 182: vi + 43 p. https://www.researchgate.net/publication/246481736_Institute_of_Ocean_Scienc es_nutrient_methods_and_analysis

Behrenfeld, M. J. (2010). Abandoning Sverdrup's critical depth hypothesis on phytoplankton blooms. *Ecology*, *91*(4), 977-989. https://doi.org/10.1890/09-1207.1

Belt, S. T., Allard, G., Massé, G., Robert, J.-M. & Rowland, S. (2000). Important sedimentary sesterterpenoids from the diatom Pleurosigma intermedium. *Chemical Communications*(6), 501-502. https://doi.org/10.1039/A909670A

Benfield, M. C., Grosjean, P., Culverhouse, P. F., Irigoien, X., Sieracki, M. E., Lopez-Urrutia, A., Dam, H. G., Hu, Q., Davis, C. S., Hansen, A., Pilskaln, C. H., Reisman, E. M., Schultz, H., Utgoff., P. E. & Gorsky, G. (2007). RAPID: Research on Automated Plankton Identification. *Oceanography*, *20*(2), 172-187. http://www.jstor.org/stable/24860058

Bidigare, R., Ondrusek, M., Morrow, J. & Kiefer, D. (1990). *In-vivo absorption properties of algal pigments* (Vol. 1302). SPIE. https://doi.org/10.1117/12.21451

Bittig, H. C., Körtzinger, A., Neill, C., van Ooijen, E., Plant, J. N., Hahn, J., johnson, K. S., Yang, B. & Emerson, S. R. (2018). Oxygen Optode Sensors: Principle, Characterization, Calibration, and Application in the Ocean [Original Research]. *Frontiers in Marine Science*, *4*. https://doi.org/10.3389/fmars.2017.00429

Borfecchia, F., Micheli, C., Cibic, T., Pignatelli, V., De Cecco, L., Consalvi, N., Caroppo, C., Rubino, F., Di Poi, E., Kralj, M. & Del Negro, P. (2019). Multispectral data by the new generation of high-resolution satellite sensors for mapping phytoplankton blooms in the Mar Piccolo of Taranto (Ionian Sea, southern Italy). *European Journal of Remote Sensing*, *52*(1), 400-418. https://doi.org/10.1080/22797254.2019.1625726

Bracher, A., Bouman, H. A., Brewin, R. J. W., Bricaud, A., Brotas, V., Ciotti, A. M., Clemetson, L., Devred, E., Di Cicco, A., Dutkiewicz, S., Mountford, N. J. H., Hickman, A. E., Hieronymi, M., Hirata, T., Losa, S. N., Mouw, C. B., Organelli, E., Raitsos, D. E., Utiz, J., . . . Wolanin, A. (2017). Obtaining Phytoplankton Diversity from Ocean Color: A Scientific Roadmap for Future Development [Review]. *Frontiers in Marine Science*, *4*. https://doi.org/10.3389/fmars.2017.00055

Brody, S. R. & Lozier, M. S. (2015). Characterizing upper-ocean mixing and its effect on the spring phytoplankton bloom with in situ data. *ICES Journal of Marine Science*, *72*(6), 1961-1970. https://doi.org/10.1093/icesjms/fsv006

Broms, C. & Melle, W. (2007). Seasonal development of Calanus finmarchicus in relation to phytoplankton bloom dynamics in the Norwegian Sea. *Deep Sea Research Part II: Topical Studies in Oceanography*, *54*(23), 2760-2775. https://doi.org/10.1016/j.dsr2.2007.08.021

Brunet, C., Johnsen, G., Lavaud, J. & Roy, S. (2011). Pigments and photoacclimation processes. S. Roy, C. A. Llewellyn, E. S. Egeland & G. Johnsen (Red), Ohytoplankton pigments: Characterization, Chemotaxonomy and Applications in Oceanography (pp. 445-471). Cambridge. https://doi.org/10.1017/CBO9780511732263.017

Cavicchioli, R., Ripple, W. J., Timmis, K. N., Azam, F., Bakken, L. R., Baylis, M., Behrenfeld, M. J., Boetius, A., Boyd, P. W., Classen, A. T., Crowther, T. W., Danovaro, R., Foreman, C. M., Huisman, J., Hutchins, D. A., Jansson, J. K., Karl, D. M., Koskella, B., Welch, D. B. M., . . . Webster, N. S. (2019). Scientists' warning to humanity: microorganisms and climate change. *Nature Reviews Microbiology*, *17*(9), 569-586. https://doi.org/10.1038/s41579-019-0222-5

Chiswell, S. M. (2011). Annual cycles and spring blooms in phytoplankton: don't abandon Sverdrup completely. *Marine Ecology Progress Series*, *443*, 39-50. http://dx.doi.org/10.3354/meps09453

Chiswell, S. M., Calil, P. H. R. & Boyd, P. W. (2015). Spring blooms and annual cycles of phytoplankton: a unified perspective. *Journal of Plankton Research*, *37*(3), 500-508. https://doi.org/10.1093/plankt/fbv021

Chusnah, W. N. & Chu, H.-J. (2022). Estimating chlorophyll-a concentrations in tropical reservoirs from band-ratio machine learning models. *Remote Sensing Applications: Society and Environment*, *25*, 100678. https://doi.org/10.1016/j.rsase.2021.100678

Cohen, J. H., Berge, J., Moline, M. A., Johnsen, G. & Zolich, A. P. (2020). Light in the Polar Night. In J. Berge, G. Johnsen, & J. H. Cohen (Eds.), *POLAR NIGHT Marine Ecology: Life and Light in the Dead of Night* (pp. 37-66). Springer International Publishing. https://doi.org/10.1007/978-3-030-33208-2_3

Cyr, H. & Pace, M. L. (1992). Grazing by zooplankton and its relationship to community structure. *Canadian Journal of Fisheries and Aquatic Sciences*, *49*(7), 1455-1465. https://doi.org/10.1139/f92-160

Dallolio, A. (2020, 12. October). The AutoNaut - Wave Propelled Unmanned Surface Vessel. *NTNU AutoNaut Documentation Wiki*. https://autonaut.itk.ntnu.no/doku.php

Dallolio, A., Quintana-Diaz, G., Honoré-Livermore, E., Garrett, J. L., Birkeland, R. & Johansen, T. A. (2021). A satellite-usv system for persistent observation of mesoscale oceanographic phenomena [Article]. *Remote Sensing*, *13*(16), Article 3229. https://doi.org/10.3390/rs13163229

Davies, E. (2022, 01. May). *OceanLab Observatory, Trondheim, Norway*. https://oceanlabobservatory.no/

Davies, E. J., Brandvik, P. J., Leirvik, F. & Nepstad, R. (2017). The use of wide-band transmittance imaging to size and classify suspended particulate matter in seawater. *Marine Pollution Bulletin*, *115*(1), 105-114. https://doi.org/10.1016/j.marpolbul.2016.11.063

Dezutter, T., Lalande, C., Dufresne, C., Darnis, G. & Fortier, L. (2019). Mismatch between microalgae and herbivorous copepods due to the record sea ice minimum extent of 2012 and the late sea ice break-up of 2013 in the Beaufort Sea. *Progress in Oceanography*, *173*, 66-77. https://doi.org/10.1016/j.pocean.2019.02.008

Dierssen, H., Bracher, A., Brando, V., Loisel, H. & Ruddick, K. (2020). Data needs for hyperspectral detection of algal diversity across the globe. *Oceanography*, *33*(1), 74-79. https://doi.org/10.5670/oceanog.2020.111

Dierssen, H. M. & Randolph, K. (2013). Remote Sensing of Ocean Color. In J. Orcutt (Ed.), *Earth System Monitoring: Selected Entries from the Encyclopedia of Sustainability Science and Technology* (pp. 439-472). Springer New York. https://doi.org/10.1007/978-1-4614-5684-1_18

Erga, S. R., Ssebiyonga, N., Frette, Ø., Hamre, B., Aure, J., Strand, Ø. & Strohmeier, T. (2012). Dynamics of phytoplankton distribution and photosynthetic capacity in a western Norwegian fjord during coastal upwelling: Effects on optical properties.

Estuarine, Coastal and Shelf Science, *97*, 91-103.
https://doi.org/10.1016/j.ecss.2011.11.034

ESA. (2022, 30. March). *OceanDataLab*. OLCI Chlorophyll_a Sentinel-3A satellite.
https://ovl.oceandatalab.com/

Falkowski, P. (2012). Ocean Science: The power of plankton. *Nature*, *483*(7387), S17-S20. https://doi.org/10.1038/483S17a

Falkowski, P. G., Barber, R. T. & Smetacek, V. (1998). Biogeochemical Controls and Feedbacks on Ocean Primary Production. *Science*, *281*(5374), 200-206.
https://doi.org/10.1126/science.281.5374.200

Falkowski, P. G. & Raven, J. A. (2013). *Aquatic Photosynthesis: (Second Edition)*.
Princeton University Press. https://doi.org/doi:10.1515/9781400849727

Fehling, J., Davidson, K., Bolch, C. J. S., Brand, T. D. & Narayanaswamy, B. E. (2012).
The Relationship between Phytoplankton Distribution and Water Column
Characteristics in North West European Shelf Sea Waters. *PLOS ONE*, *7*(3),
e34098. https://doi.org/10.1371/journal.pone.0034098

Ferreira, A. S., Costa, M., Py, F., Pinto, J., Silva, M. A., Nimmo-Smith, A., Johansen, T. A., Sousa, B. & Rajan, K. (2019). Advancing multi-vehicle deployments in
oceanographic field experiments. *Autonomous Robots*, *43*(6), 1555-1574.
https://doi.org/10.1007/s10514-018-9810-x

Fiorelli, E., Leonard, N. E., Bhatta, P., Paley, D. A., Bachmayer, R. & Fratantoni, D. M.
(2006). Multi-AUV control and adaptive sampling in Monterey Bay. *IEEE journal of
oceanic engineering*, *31*(4), 935-948. https://doi.org/10.1109/JOE.2006.880429

Forbord, S., Etter, S. A., Broch, O. J., Dahlen, V. R. & Olsen, Y. (2021). Initial short-term
nitrate uptake in juvenile, cultivated Saccharina latissima (Phaeophyceae) of
variable nutritional state. *Aquatic Botany*, *168*, 103306.
https://doi.org/10.1016/j.aquabot.2020.103306

Fossum, T. O., Eidsvik, J., Ellingsen, I., Alver, M. O., Fragoso, G. M., Johnsen, G.,
Mendes, R., Ludvigsen, M. & Rajan, K. (2018). Information-driven robotic
sampling in the coastal ocean. *Journal of Field Robotics*, *35*(7), 1101-1121.
https://doi.org/10.1002/rob.21805

Fossum, T. O., Fragoso, G. M., Davies, E. J., Ullgren, J. E., Mendes, R., Johnsen, G.,
Ellingsen, I., Eidsvik, J., Ludvigsen, M. & Rajan, K. (2019). Toward adaptive
robotic sampling of phytoplankton in the coastal ocean. *Science Robotics*, *4*(27),
eaav3041. https://doi.org/10.1126/scirobotics.aav3041

Fragoso, G. M., Davies, E. J., Ellingsen, I., Chauton, M. S., Fossum, T., Ludvigsen, M.,
Steinhovden, K. B., Rajaqn, K. & Johnsen, G. (2019a). Physical controls on
phytoplankton size structure, photophysiology and suspended particles in a
Norwegian biological hotspot. *Progress in Oceanography*, *175*, 284-299.
https://doi.org/10.1016/j.pocean.2019.05.001

Fragoso, G. M., Johnsen, G., Chauton, M. S., Cottier, F. & Ellingsen, I. (2021).
Phytoplankton community succession and dynamics using optical approaches.
Continental Shelf Research, *213*, 104322.
https://doi.org/10.1016/j.csr.2020.104322

Fragoso, G. M., Poulton, A. J., Pratt, N. J., Johnsen, G., & Purdie, D. A. (2019b). Trait-based analysis of subpolar North Atlantic phytoplankton and plastidic ciliate
communities using automated flow cytometer. *Limnology and Oceanography*,
64(4), 1763-1778. https://doi.org/10.1002/lno.11189

Fragoso, G. M., Poulton, A. J., Yashayaev, I. M., Head, E. J. H., Johnsen, G. & Purdie, D.
A. (2018). Diatom Biogeography From the Labrador Sea Revealed Through a
Trait-Based Approach [Original Research]. *Frontiers in Marine Science*, *5*(297).
https://doi.org/10.3389/fmars.2018.00297

Gabriel, K. R. (1971). The Biplot Graphic Display of Matrices with Application to Principal
Component Analysis. *Biometrika*, *58*(3), 453-467.
https://doi.org/10.2307/2334381

Gollop, A. M., Raitsos, D. E., Edwards, M. & Attrill M. J. (2007). Spatial patterns of
diatom and dinoflagellate seasonal cycles in the NE Atlantic Ocean. *Marine Ecology
Progress Series*, 339, 301-306. https://doi.org/10.3354/meps339301

Gökçe, A. (2021). A mathematical study for chaotic dynamics of dissolved oxygen-phytoplankton interactions under environmental driving factors and time lag. *Chaos, Solitons & Fractals*, *151*, 111268. https://doi.org/10.1016/j.chaos.2021.111268

Greve, W., Reiners, F., Nast, J. & Hoffmann, S. (2004). Helgoland Roads meso- and macrozooplankton time-series 1974 to 2004: lessons from 30 years of single spot, high frequency sampling at the only off-shore island of the North Sea. *Helgoland Marine Research*, *58*(4), 274-288. https://doi.org/10.1007/s10152-004-0191-5

Grøtte, M. E., Birkeland, R., Honoré-Livermore, E., Bakken, S., Garrett, J. L., Prentice, E. F., Sigernes, S., Orlandic, M., Gravdahl, J. T. & Johansen, T. A. (2022). Ocean Color Hyperspectral Remote Sensing With High Resolution and Low Latency—The HYPSO-1 CubeSat Work. *IEEE Transactions on Geoscience and Remote Sensing*, *60*, 1-19. https://doi.org/10.1109/TGRS.2021.3080175

Gutiérrez-Rodríguez, A., Latasa, M., Estrada, M., Vidal, M. & Marrasé, C. (2010). Carbon fluxes through major phytoplankton groups during the spring bloom and post-bloom in the Northwestern Mediterranean Sea. *Deep Sea Research Part I: Oceanographic Research Papers*, *57*(4), 486-500. https://doi.org/10.1016/j.dsr.2009.12.013

HUB Ocean, H. (2022, 03. May). *HUB Ocean - Center for the Fourth Industrial Revolution* https://www.hubocean.earth/

Huisman, J., van Oostveen, P. & Weissing, F. J. (1999). Critical depth and critical turbulence: two different mechanisms for the development of phytoplankton blooms. *Limnology and Oceanography*, *44*(7), 1781-1787. https://doi.org/10.4319/lo.1999.44.7.1781

Hunter, P. D., Tyler, A. N., Présing, M., Kovács, A. W. & Preston, T. (2008). Spectral discrimination of phytoplankton colour groups: The effect of suspended particulate matter and sensor spectral resolution. *Remote Sensing of Environment*, *112*(4), 1527-1544. https://doi.org/10.1016/j.rse.2007.08.003

Huot, Y. & Babin, M. (2010). Overview of Fluorescence Protocols: Theory, Basic Concepts, and Practice. In D. J. Suggett, O. Prášil, & M. A. Borowitzka (Eds.), *Chlorophyll a Fluorescence in Aquatic Sciences: Methods and Applications* (pp. 31-74). Springer Netherlands. https://doi.org/10.1007/978-90-481-9268-7_3

Turner Design Inc. (2021). *CYCLOPS-7FSubmersible Sensors* http://docs.turnerdesigns.com/t2/doc/brochures/S-0209.pdf

Insight, O. (2020). *Glossary: Boxar Smoothing*. Retrieved 18.02.2022 from https://www.oceaninsight.com/support/knowledge-hub/glossary/#bad-pixel

IOCCG (2000) Remote Sensing of Ocean Colour in Coastal, and Other Optically-Complex,Waters, (ed. S. Sathyendranath). Dartmouth, NS, Canada, International Ocean-Colour Coordinating Group (IOCCG), 140pp. (Reports of the International Ocean-Colour Coordinating Group, No. 3) http://dx.doi.org/10.25607/OBP-95

IOCCG (2019) Uncertainties in Ocean Colour Remote Sensing. (ed. Mélin F.) Dartmouth, NS, Canada, International Ocean-Colour Coordinating Group (IOCCG), 164pp. (Reports of the International Ocean-Colour Coordinating Group, No. 18) http://dx.doi.org/10.25607/OBP-696

Irigoien, X., Flynn, K. J. & Harris, R. P. (2005). Phytoplankton blooms: a 'loophole' in microzooplankton grazing impact? *Journal of Plankton Research*, *27*(4), 313-321. https://doi.org/10.1093/plankt/fbi011

Johnsen, G., Leu, E. & Gradinger, R. (2020). Chapter 4: Marine Micro- and Macroalgae in the Polar Night. In *Polar Night Marine Ecology - Life and light in the dead of the night* (pp. 67-112). Springer. https://doi.org/10.1007/978-3-030-33208-2_4

Johnsen, G., Moline, M., Pettersson, L., Pinckney, J., Pozdnyakov, D., Egeland, E. & Schofield, O. (2011). Optical monitoring of phytoplankton bloom pigment signatures. *Phytoplankton pigments: Updates on Characterization, Chemotaxonomy and Applications in Oceanography. Cambridge University Press, Cambridge*, 538-581. https://doi.org/10.1017/CBO9780511732263.020

Johnsen, G., Nelson, N. B., Jovine, R. V. & Prezelin, B. B. (1994a). dinoflagellates, Prorocentrum minimum and Heterocapsa pygmaea. *Marine Ecology Progress Series*, *114*, 245-258.

Johnsen, G., Norli, M., Moline, M., Robbins, I., von Quillfeldt, C., Sørensen, K., Cottier, F. & Berge, J. (2018). The advective origin of an under-ice spring bloom in the Arctic Ocean using multiple observational platforms. *Polar Biology*, *41*(6), 1197-1216. https://doi.org/10.1007/s00300-018-2278-5

Johnsen, G. & Sakshaug, E. (2007). Biooptical characteristics of PSII and PSI in 33 species (13 pigment groups) of marine phytoplankton, and the relevance for pulse-amplitude-modulated and fast-repetition-rate fluorometry1. *Journal of Phycology*, *43*(6), 1236-1251. https://doi.org/10.1111/j.1529-8817.2007.00422.x

Johnsen, G., Samset, O., Granskog, L. & Sakshaug, E. (1994b). In vivo absorption characteristics in 10 classes of bloom-forming phytoplankton: taconomic characteristics and responses to photoadaptation by means of discriminant and HPLC analysis. *Marine Ecology Progress Series*, 149-157. https://www.jstor.org/stable/24842895

Johnsen, G., Volent, Z., Dierssen, H., Pettersen, R., Van Ardelan, M., Søreide, F., Fearns, M., Ludvigsen, M. & Moline, M. (2013). Underwater hyperspectral imagery to create biogeochemical maps of seafloor properties. In *Subsea optics and imaging* (pp. 508-540e). Elsevier. https://doi.org/10.1533/9780857093523.3.508

Johnsen, G., Volent, Z., Sakshaug, E., Sigernes, F. & Petterson, L. (2009). Remote sensing in the Barent Sea. In *Ecosystem Barents Sea* (pp. 139-166). Tapir Academic Press.

Jonsson, P. R., Pavia, H. & Toth, G. (2009). Formation of harmful algal blooms cannot be explained by allelopathic interactions. *Proceedings of the National Academy of Sciences*, *106*(27), 11177-11182. https://doi.org/doi:10.1073/pnas.0900964106

Kaiser, M. J., Attrill, M. J., Jennings, S., Thomas, D. N., Barnes, D. K. A., Brieley, A. S., Hiddink, J. G., Kaartokallio, H., Polunin, N. V. C. & Raffaelli, D. G. (2011). Primary production processes. In *Marine ecology: processes, systems, and impact* (2nd ed., pp. 33-88). Oxford University Press.

Karlson, B., Andersen, P., Arneborg, L., Cembella, A., Eikrem, W., John, U., West, J. J., Klemm, K., Kobos, J., Lehtinen, S., Lundholm, N., Mazur-Marzec, H., Naustvoll, L., Poelman, M., Provoost, P., De Rijcke, M. & Suikkanen, S. (2021). Harmful algal blooms and their effects in coastal seas of Northern Europe. *Harmful Algae*, *102*, 101989. https://doi.org/10.1016/j.hal.2021.101989

Kemna, S. (2018). *Multi-robot strategies for adaptive sampling with autonomous underwater vehicles* University of Southern California].

Klais, R., Tamminen, T., Kremp, A., Spilling, K. & Olli, K. (2011). Decadal-Scale Changes of Dinoflagellates and Diatoms in the Anomalous Baltic Sea Spring Bloom. *PLOS ONE*, *6*(6), e21567. https://doi.org/10.1371/journal.pone.0021567

Klausmeier, C. A., Litchman, E. & Levin, S. A. (2004). Phytoplankton growth and stoichiometry under multiple nutrient limitation. *Limnology and Oceanography*, *49*(4part2), 1463-1470. https://doi.org/10.4319/lo.2004.49.4_part_2.1463

Kraberg, A., Baumann, M. & Dürselen, C.-D. (2010). Coastal phytoplankton. *Photo guide for northern European seas. Handbooks of Marine Flora and Fauna. Verlag Dr. Friedrich Pfeil, München*.

Krizhevsky, A., Sutskever, I. & Hinton, G. E. (2012). Imagenet classification with deep convolutional neural networks. *Advances in neural information processing systems*, *25*. https://papers.nips.cc/paper/2012/hash/c399862d3b9d6b76c8436e924a68c45b-Abstract.html

Kulk, G., Platt, T., Dingle, J., Jackson, T., Jönsson, B. F., Bouman, H. A., Babin, M., Brewin, R. J., Doblin, M., Estrada, M., Figueiras, F. G., Furuya, K., Gonzàlez-Benitez, N., Gudfinnsson, H. G., Gudmundsson, K., Huang, B., Isada, T., Kovac, Z., Lutz, V. A., . . . Sathyendranath, S. (2020). Primary Production, an Index of Climate Change in the Ocean: Satellite-Based Estimates over Two Decades. *Remote Sensing*, *12*(5), 826. https://www.mdpi.com/2072-4292/12/5/826

Larsen, A., Flaten, G. A. F., Sandaa, R.-A., Castberg, T., Thyrhaug, R., Erga, S. R., Jacquet, S. & Bratbak, G. (2004). Spring phytoplankton bloom dynamics in Norwegian coastal waters: Microbial community succession and diversity. *Limnology and Oceanography*, *49*(1), 180-190. https://doi.org/10.4319/lo.2004.49.1.0180

Lewandowska, A. & Sommer, U. (2010). Climate change and the spring bloom: a mesocosm study on the influence of light and temperature on phytoplankton and mesozooplankton. *Marine Ecology Progress Series*, *405*, 101-111. https://doi.org/10.3354/meps08520

Li, Y., Zhou, Q., Zhang, Y., Li, J. & Shi, K. (2021). Research Trends in the Remote Sensing of Phytoplankton Blooms: Results from Bibliometrics. *Remote Sensing*, *13*(21), 4414. https://doi.org/10.3390/rs13214414

Lindemann, C. & St. John, M. A. (2014). A seasonal diary of phytoplankton in the North Atlantic [Perspective]. *Frontiers in Marine Science*, *1*. https://doi.org/10.3389/fmars.2014.00037

Ludvigsen, M. & Sørensen, A. J. (2016). Towards integrated autonomous underwater operations for ocean mapping and monitoring. *Annual Reviews in Control*, *42*, 145-157. https://doi.org/10.1016/j.arcontrol.2016.09.013

Marion, P. v. (1996). *Ecological studies in Hopavågen, a landlocked bay at Agdenes, Sør-Trøndelag, Norway*. NTNU Vitenskapsmuseet.

McCulloch, W. S. & Pitts, W. (1943). A logical calculus of the ideas immanent in nervous activity. *The bulletin of mathematical biophysics*, *5*(4), 115-133. https://doi.org/10.1007/BF02478259

MicroStrain, L. (2015). 3DM-GX4-25™ Attitute Heading Reference System User Manual. In. http://files.microstrain.com/3DM-GX4-25_User_Manual_(8500-0047).pdf

Mogstad, A. A. & Johnsen, G. (2017). Spectral characteristics of coralline algae: a multi-instrumental approach, with emphasis on underwater hyperspectral imaging. *Applied Optics*, *56*(36), 9957-9975. https://doi.org/10.1364/AO.56.009957

Mogstad, A. A., Johnsen, G. & Ludvigsen, M. (2019). Shallow-Water Habitat Mapping using Underwater Hyperspectral Imaging from an Unmanned Surface Vehicle: A Pilot Study. *Remote Sensing*, *11*(6), 685. https://doi.org/10.3390/rs11060685

Nilssen, I., Ødegård, Ø., Sørensen, A. J., Johnsen, G., Moline, M. A. & Berge, J. (2015). Integrated environmental mapping and monitoring, a methodological approach to optimise knowledge gathering and sampling strategy. *Marine Pollution Bulletin*, *96*(1), 374-383. https://doi.org/10.1016/j.marpolbul.2015.04.045

Nortek. (2022). *DVL1000 - 300 m* Retrieved 02.02.2022 from https://www.nortekgroup.com/products/dvl-1000-300m

NS4745 (1991), Vannundersøkelse - bestemmelse av summen av nitritt- og nitrat-nitrogen, Tech- nical Report 2, Standard Norge. Alternative title: Water analysis - Determination of the sum of nitrite nitrogen and nitrate nitrogen, ICS 13.060.50 - Undersøkelse av kjemikaler i vann.

NS-EN ISO 6878 (2004), Vannundersøkelse - bestemmelse av fosfor - spektrometrisk metode med ammoniummolybdat, Technical Report 1, Standard Norge. Alternative title: Water quality - Determination of phosphorus - Ammonium molybdate spectrometric method, ICS 13.060.50 - Undersøkelse av kjemikaler i vann.

NTNU AMOS. (2022). *NTNU AMOS: Annual Report 2021*. NTNU. https://www.ntnu.edu/documents/20587845/621664524/NTNU_AMOS_2021_Scr.pdf/a925fcbd-c90f-9e4d-5a5b-27dd41003e57?t=1648810597413

NTNU AURLab. (2022, 7. February). *LAUV Roald*. https://www.ntnu.edu/aur-lab/lauv-roald

Nøland, A. (2022). *Autonomous Underwater Vehicle (AUV) based study of zooplankton communities, using a silhouette camera and artificial intelligence* [Master thesis] NTNU. [Unpublished]

Oceanographic, A. (2021, 12. December). *x2change Sensors*. https://amloceanographic.com/shop-all/x2change-sensors.html

Pettersson, L. H., & Pozdnyakov, D. (2012). *Monitoring of harmful algal blooms*. Springer Science & Business Media.

Pinto, J., Calado, P., Braga, J., Dias, P., Martins, R., Marques, E. & Sousa, J. B. (2012). Implementation of a Control Architecture for Networked Vehicle Systems. *IFAC Proceedings Volumes*, *45*(5), 100-105. https://doi.org/https://doi.org/10.3182/20120410-3-PT-4028.00018

Pyo, J., Hong, S. M., Jang, J., Park, S., Park, J., Noh, J. H. & Cho, K. H. (2022). Drone-borne sensing of major and accessory pigments in algae using deep learning modeling. *GIScience & Remote Sensing*, *59*(1), 310-332. https://doi.org/10.3182/20120410-3-PT-4028.00018

Rahlff, J., Stolle, C., Giebel, H.-A., Ribas-Ribas, M., Damgaard, L. R. & Wurl, O. (2019). Oxygen Profiles Across the Sea-Surface Microlayer—Effects of Diffusion and Biological Activity [Original Research]. *Frontiers in Marine Science*, *6*. https://doi.org/10.3389/fmars.2019.00011

Richardson, K., Visser, A. W. & Pedersen, F. B. (2000). Subsurface phytoplankton blooms fuel pelagic production in the North Sea. *Journal of Plankton Research*, *22*(9), 1663-1671. https://doi.org/10.1093/plankt/22.9.1663

Rodríguez, F., Chauton, M., Johnsen, G., Andresen, K., Olsen, L. & M, Z. (2006). Photoacclimation in phytoplankton: Implications for biomass estimates, pigment functionality and chemotaxonomy. *Marine Biology*, *148*, 963-971. https://doi.org/10.1007/s00227-005-0138-7

Roesler, C., Uitz, J., Claustre, H., Boss, E., Xing, X., Organelli, E., Briggs, N., Bricaud, A., Schmechtig, C., Poeau, A., D'Ortenzio, F., Ras, J., Drapeau, S., Haëntjens, N. & Barbieux, M. (2017). Recommendations for obtaining unbiased chlorophyll estimates from in situ chlorophyll fluorometers: A global analysis of WET Labs ECO sensors. *Limnology and Oceanography: Methods*, *15*(6), 572-585. https://doi.org/https://doi.org/10.1002/lom3.10185

Roy, S., Llewellyn, C. A., Egeland, E. S. & Johnsen, G. (2011). *Phytoplankton Pigments: Characterization, Chemotaxonomy and Applications in Oceanography*. Cambridge: Cambridge University Press. https://doi.org/10.1017/CBO9780511732263

Rumyantseva, A., Henson, S., Martin, A., Thompson, A. F., Damerell, G. M., Kaiser, J. & Heywood, K. J. (2019). Phytoplankton spring bloom initiation: The impact of atmospheric forcing and light in the temperate North Atlantic Ocean. *Progress in Oceanography*, *178*, 102202. https://doi.org/10.1016/j.pocean.2019.102202

Ryan, J. P., McManus, M. A. & Sullivan, J. M. (2010). Interacting physical, chemical and biological forcing of phytoplankton thin-layer variability in Monterey Bay, California. *Continental Shelf Research*, *30*(1), 7-16. https://doi.org/10.1016/j.csr.2009.10.017

Saad, A., Stahl, A., Våge, A., Davies, E., Nordam, T., Aberle, N., Ludvigsen, M., Johnsen, G., Sousa, J. & Rajan, K. (2020). Advancing Ocean Observation with an AI-Driven Mobile Robotic Explorer. *Oceanography*, *33*, 50-59. https://doi.org/10.5670/oceanog.2020.307

Sadeghi, A., Dinter, T., Vountas, M., Taylor, B. B., Altenburg-Soppa, M., Peeken, I. & Bracher, A. (2012). Improvement to the PhytoDOAS method for identification of coccolithophores using hyper-spectral satellite data. *Ocean Sci.*, *8*(6), 1055-1070. https://doi.org/10.5194/os-8-1055-2012

Sakshaug, E., Johnsen, G. H. & Kovacs, K. M. (2009). *Ecosystem Barents Sea*. Tapir Academic.

Sakshaug, E. & Myklestad, S. (1973). Studies on the phytoplankton ecology of the trondheimsfjord. III. Dynamics of phytoplankton blooms in relation to environmental factors, bioassay experiments and parameters for the physiological state of the populations. *Journal of Experimental Marine Biology and Ecology*, *11*(2), 157-188. https://doi.org/10.1016/0022-0981(73)90053-1

Silsbe, G. & Malkin, S. (2016). Where Light and Nutrients Collide: The Global Distribution and Activity of Subsurface Chlorophyll Maximum Layers. In (pp. 141-152). https://doi.org/10.1007/978-3-319-30259-1_12

Silva, E., Counillon, F., Brajard, J., Korosov, A., Pettersson, L. H., Samuelsen, A. & Keenlyside, N. (2021). Twenty-One Years of Phytoplankton Bloom Phenology in the Barents, Norwegian, and North Seas [Original Research]. *Frontiers in Marine Science*, *8*. https://doi.org/10.3389/fmars.2021.746327

Skagseth, Ø., Drinkwater, K. F., & Terrile, E. (2011). Wind- and buoyancy-induced transport of the Norwegian Coastal Current in the Barents Sea. *Journal of Geophysical Research: Oceans*, *116*(C8). https://doi.org/10.1029/2011JC006996

Sørensen, A.J., Ludvigsen, M., Norgren, P., Ødegård, Ø. & Cottier, F. (2020). Sensor-Carrying Platforms. In: Berge, J., Johnsen, G., Cohen, J. (eds) POLAR NIGHT Marine Ecology. Advances in Polar Ecology, vol 4. Springer, Cham. https://doi.org/10.1007/978-3-030-33208-2_9

Sousa, A., Madureira, L., Coelho, J., Pinto, J., Pereira, J., Borges Sousa, J. & Dias, P. (2012). LAUV: The Man-Portable Autonomous Underwater Vehicle. *IFAC Proceedings Volumes*, *45*(5), 268-274. https://doi.org/10.3182/20120410-3-PT-4028.00045

Sousa, L. L., Lopez-Castejon, F., Gilabert, J., Relvas, P., Couto, A., Queiroz, N., Caldas, R., Dias, P. S., Dias, H., Faria, M., Ferreira, F., Ferreira, A. S., Fortuna, J., Gomes, R. J., Lourerio, B., Martins, R., Neiva, j., Oliveira, M. & Rajan, K. (2016). Integrated monitoring of Mola mola behaviour in space and time. *PLOS ONE*, *11*(8), e0160404. https://doi.org/10.1371/journal.pone.0160404

Stock, A. & Subramaniam, A. (2020). Accuracy of Empirical Satellite Algorithms for Mapping Phytoplankton Diagnostic Pigments in the Open Ocean: A Supervised Learning Perspective [Original Research]. *Frontiers in Marine Science*, *7*. https://doi.org/10.3389/fmars.2020.00599

Suggett, D. J., Prášil, O., & Borowitzka, M. A. (2010). Chlorophyll a fluorescence in aquatic sciences: methods and applications (Vol. 4). Dordrecht: Springer.

Sverdrup, H. (1953). On conditions for the vernal blooming of phytoplankton. *J. Cons. Int. Explor. Mer*, *18*(3), 287-295.

Throndsen, J., & Eikrem, W. (2001). *Marine mikroalger i farger*. Almater.

Throndsen, J., Hasle, G. R., & Tangen, K. (2007). *Phytoplankton of Norwegian coastal waters*. Almater.

Tilman, D., Kilham, S. S., & Kilham, P. (1982). Phytoplankton community ecology: the role of limiting nutrients. *Annual review of Ecology and Systematics*, *13*(1), 349-372.

Tilstone, G. H., Pardo, S., Dall'Olmo, G., Brewin, R. J. W., Nencioli, F., Dessailly, D., Kwiatkowska, E., Casal, T. & Donlon, C. (2021). Performance of Ocean Colour Chlorophyll a algorithms for Sentinel-3 OLCI, MODIS-Aqua and Suomi-VIIRS in open-ocean waters of the Atlantic. *Remote Sensing of Environment*, *260*, 112444. https://doi.org/10.1016/j.rse.2021.112444

Volent, Z., Johnsen, G., Hovland, E., Folkestad, A., Olsen, L., Tangen, K. & Sorensen, K. (2011). Improved monitoring of phytoplankton bloom dynamics in a Norwegian fjord by integrating satellite data, pigment analysis, and Ferrybox data with a coastal observation network. *Journal of Applied Remote Sensing*, *5*(1), 053561. https://doi.org/10.1117/1.3658032

Winder, M. & Sommer, U. (2012). Phytoplankton response to a changing climate. *Hydrobiologia*, *698*(1), 5-16. https://doi.org/10.1007/s10750-012-1149-2

Xylem (2020). *Oxygen Optode 4831/4831F*. A. d. i. As. https://www.aanderaa.com/media/pdfs/d403_aanderaa_oxygen_sensor_4831_4831f.pdf

Zapata, M., Rodríguez, F. & Garrido, J. (2000). Separation of chlorophylls and carotenoids from marine phytoplankton: A new HPLC method using a reversed phase C8 column and pyridine-containing mobile phases. *Mar. Ecol. Prog. Ser.*, *195*, 29-45. https://doi.org/10.3354/meps195029

Appendix A: In vitro [Chl *a*]

Figure 0.1: The plot shows in vitro [Chl *a*] (µg L^{-1}) for all samples (n=51) at each day as a mean of replicates (n=3). The samples are coloured by date and shaped by depth.

Table 0.1: Shows the mean in vitro [Chl *a*] (µg L^{-1}) and standard deviation for each sampling date. In vitro [Chl *a*] measured by filtering seawater and then using a Turner Designs fluorometer. Each sample has (n=3) replicates, and each date has (n=3-15) samples.

Date	Mean Chl a	Sd	Field
13.04.21	0.5537778	0.04773454	M1
14.04.21	0.5200000	0.01936492	M1
20.04.21	1.6606667	0.34365112	M2
21.04.21	1.9519048	0.07124739	M2
04.05.21	1.4033333	0.48007850	H
05.05.21	1.3641667	0.36819084	H

Appendix B: NO_3^- and PO_4^{3-}

Figure 0.2: The plot shows in vitro $[NO_3^-]$ (µM) for all samples (n=51) at each day as a mean of replicates (n=3). The samples are coloured by date and shaped by depth.
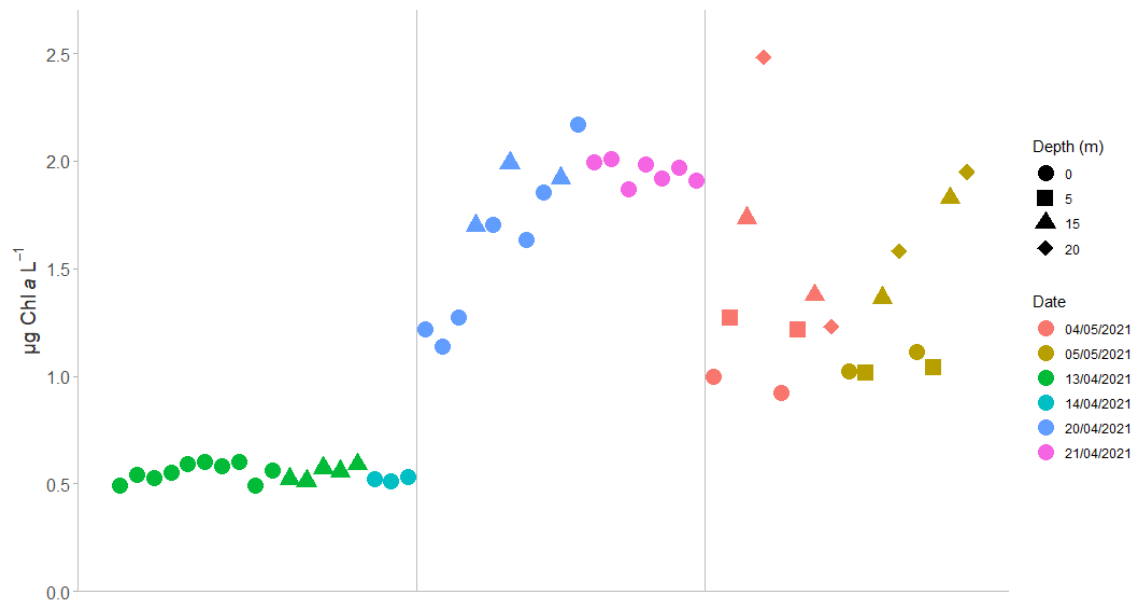

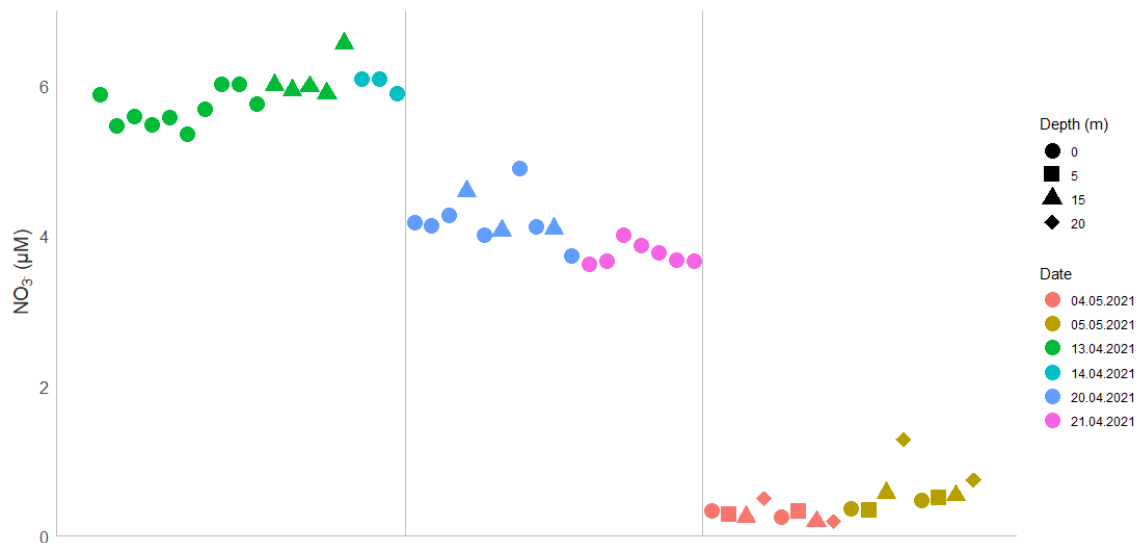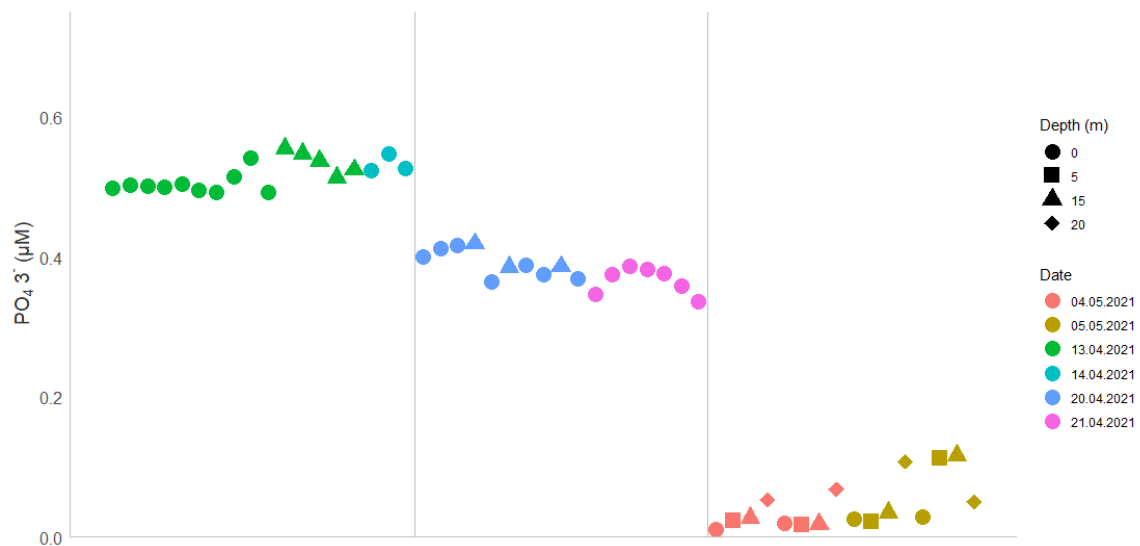**Figure 0.3:** The plot shows in vitro $[PO_4^{3-}]$ (µM) for all samples (n=51) at each day as a mean of replicates (n=3). The samples are coloured by date and shaped by depth.

Table 0.2: Shows the mean in vitro nutrients [NO_3^-] (μM) and [PO_4^{3-}] (μM) and standard deviation for each sampling date. In vitro [nutrient] measured by filtering seawater and then using an autoanalyzer. Each sample has (n=3) replicates, and each date has (n=3-15) samples.

Date	Mean [NO_3^-]	SD NO_3^-	Mean Phospate	SD Phospahte	Field
13.04.21	5.817	0.3055	0.5146	0.02116	M1
14.04.21	6.026	0.1099	0.5327	0.01268	M1
20.04.21	4.211	0.3243	0.3916	0.01962	M2
21.04.21	3.756	0.1418	0.3661	0.01926	M2
04.05.21	0.2972	0.09978	0.03008	0.02028	H
05.05.21	0.6076	0.3027	0.06250	0.04337	H

Table 0.3: Testing the linear relationship between [Chl *a*] in vitro fluorescence and nutrients (NO_3^- and PO_4^{3-}) measurments. The tests are performed on the whole data set, for each date and the location Mausud and Hopvågen, including the p and R^2 values.

Model (lm)	R^2	p-value
Nitrate~chla	0.2125	2.024e-09*
Mausund: Nitrate~chla	0.8372	< 2.2e-16*
Mausund1: Nitrate~chla	0.000157	0.9284
Mausund2: Nitrate~chla	0.1973	0.001094*
Hopavågen: Nitrate~chla	0.113	0.01948*
Phosphate~chla	0.1699	1.192e-07*
Mausund: Phosphate~chla	0.8411	< 2.2e-16*
Mausund1: Phosphate~chla	0.03528	0.1738
Mausund2: Phosphate~chla	0.1828	0.001752*
Hopavågen: Phosphate~chla	0.0414	0.1654

Appendix C: PCA

Table 0.4: Results of the overall summary of the PCA. Including all dimensions (PC1-PC8), their standard deviation (Eigenvalues), proportion of variance and cumulative proportion.

	PC1	PC2	PC3	PC4	PC5	PC6	PC7	PC8
Standard deviation	1.9732	1.4703	1.0770	0.72106	0.39236	0.30556	0.11149	0.07132
Proportion of variance	0.4867	0.2702	0.1450	0.06499	0.01924	0.01167	0.00155	0.00064
Cumulative proportion	0.4867	0.7569	0.9019	0.96690	0.98614	0.99781	0.99936	1.00000
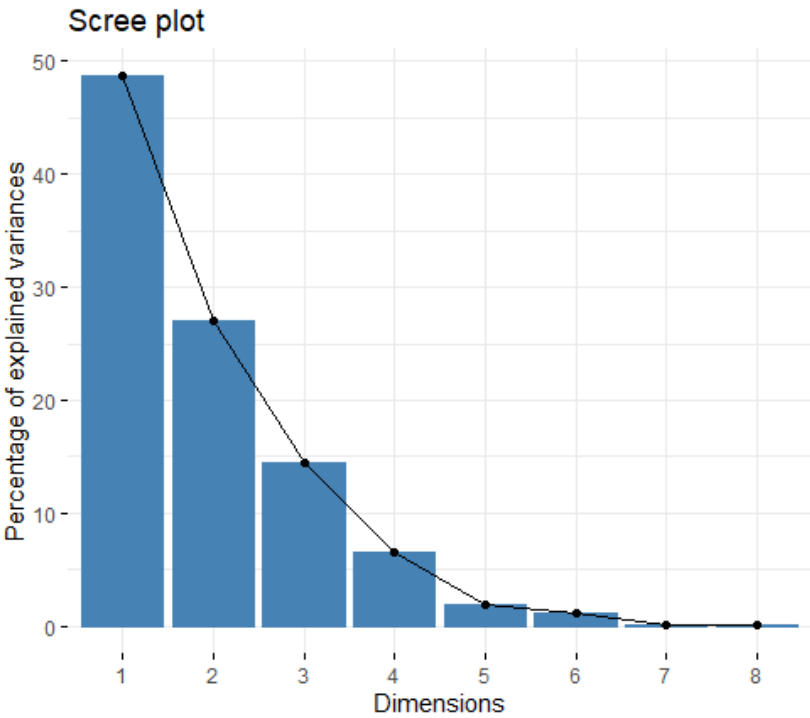
Figure 0.4: Scree plot showing the percentage of explained variance for each dimension, both as a bar plot and line plot.
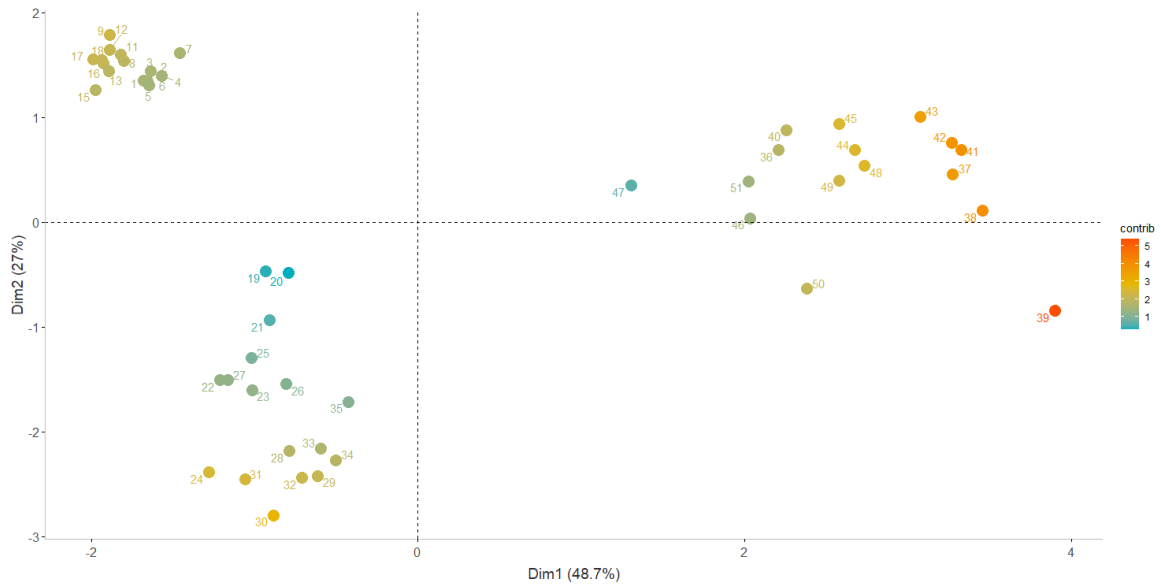
Figure 0.5: Shows the contribution of the loadings of individual samples represented in a PCA plot, where the individuals most far away from the centre [0,0] contribute most to the PC1-2.
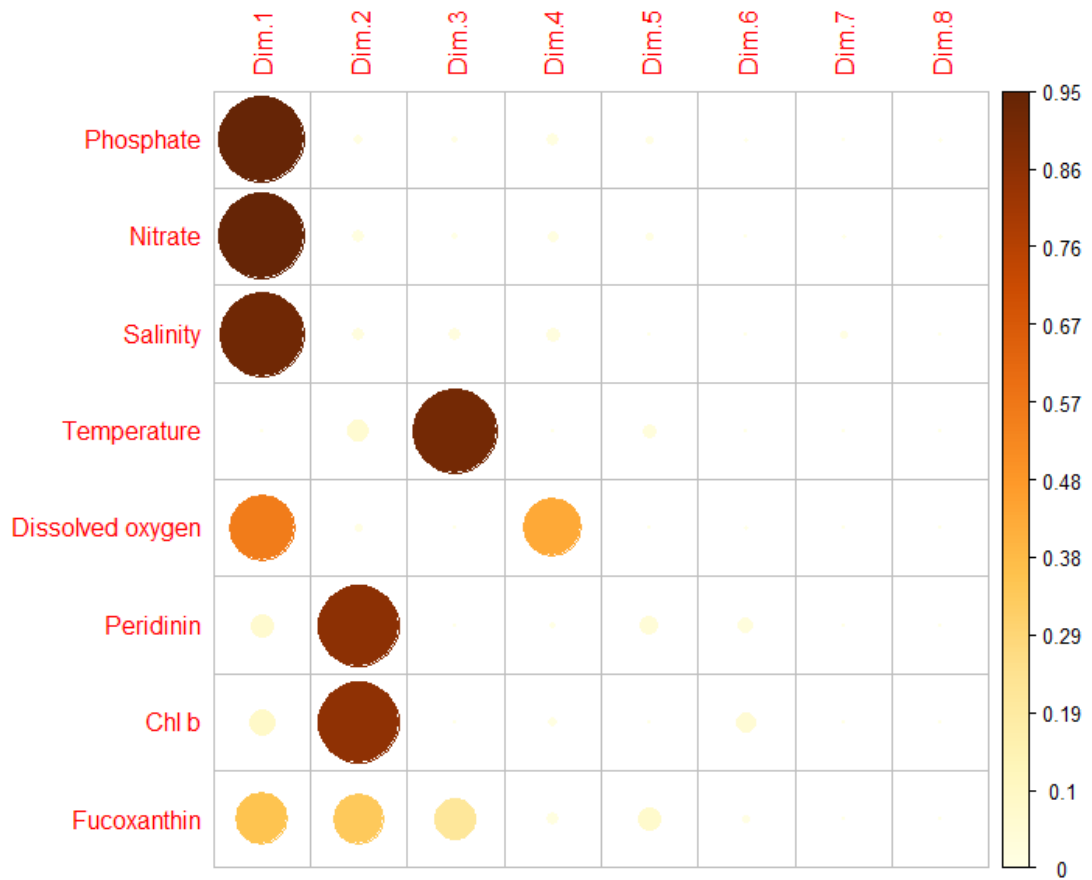
Figure 0.6: The contribution of each variable for each PC is visually presented, where the variable is coloured according to contribution of explaining the variance in the given PC.

Appendix D: Species list from microscope analysis

Table 0.1: Qualitative analysis of phytoplankton taxa in inverted microscope from net samples collected at depth (0-20m) and fixated by lugol in field. For every sample there have been looked through 5 replicates (n=5). The x marks presence of that taxa in the sample, and the D marks dominant, meaning they are highly represented in the sample from a subjective point of view. For each sample several images were saved, and some taxa are shown in Figure 3.13.

|		Mausund		Hopavågen													
	Sampling date	13.04.21	20.04.21	04.05.21								05.05.21					
Group	Taxa/Depth	0	0	0	0	5	10	15	5	10	15	5	10	15	5	10	15
Dinoflagellates	*Dinophysis acuminata (acuta, norvegica, rotundata)*	x	x	x	x	x	x	x	x	x	x	x	x	x	x	x	x
	Diplopsalis spp.		x														
	Protoperidinium depressum	x	x	x	x	x	x	x	x	x	x	x	x	x	x	x	x
	P. pellucidum	x				x											
	Protoperidinium spp.	x	x	x	x	x	x	x	x	x	x	x	x	x	x	x	x
	Prorocentrum spp.	x	x	x	x	x	x	x	x	x	x	x	x	x	x	x	x
	Tripos furca	x	x	x	x	x	x	x	x	x	x			x			x
	T. fusus	D	x	x	x	D	x	x	x	x	x	x	x	x	x	x	x
	T. horridum	x	x	x	x	x	x	x	x	x	x	x	x	x	x	x	x
	T. lineatum									x							
	T. longipes	x		x	x				x	x	x		x	x			
	T. macroceros	x	x	x	x					x			x	x			x
	T. tripos	D	x	x	D	D	x	x	x	x	x	x	x	x	x	x	x
Diatoms	*Cerataulina pelagica*				x					x			x				x
	Chaetoceros Borealis						x			x			x	x	x		x
	C. cf. *convolutus*					x	x	x	x	x			x				
	C. danicus	x		x	x	x	x			x	x	x	x	x	x	x	x
	C. debilis	x			x	x	x	x	x	x	x	x	x	x	x	x	x
	C. decipiens	x	x	x	x	x	x	x	x	x	x	x	x	x	x	x	x
	C. densus			x	x	x	x	x	x	x	x	x	x	x	x	x	x
	C. eibenii			x	x					x			x	x	x		x

		1	2	3	4	5	6	7	8	9	10	11	12	13	14	15	16
	C. laciniosus								x				x	x	x	x	x
	Chaetoceros spp.	x	x	x	D	x	D	D	D	D	D	D	D	D	D	D	D
	Coscinodiscus sp.	D	D	x	D	D		x		x							
	Cylindrotheca closterium			x	x			x								x	
	Dactyliosolen fragilissimus	x	x	x	x			x			x		x	x		x	x
	Fragilariopsis sp.	x	x	x	x			x	x	x		x	x	x	x	x	x
	Guinardia delicatula	x	x	x	x			x	x	x	x	x	x	x	x	x	x
	Leptocylindrus danicus	x	x	x	x	x	x	x	x	x	x	x	x	x	x	x	x
	Licmophora sp.	x	x	x	x	x	x		x	x		x	x	x	x	x	x
	Navicula/Diploneis sp.	x	x	x	x			x							x	x	x
	Odontella sp.	x	x														
	Rhizosolenia sp.	x	x	x	x	x	x	x	x	x	x	x	x	x	x	x	x
	Pleurosigma normanii	x	D	x	D	x	x	x	x	x	x	x	x	x	x	x	x
	Pseudo-nitzschia spp.	x	x	x		x	x	x	x	x	x	x	x	x	x	x	x
	Skeletonema costatum	x		x				x									
	Striatella unipunctata	x	x					x				x					
	Thalassionema nitzschioides	x	x	x	x	x	x	x	x	x	x	x	x	x	x	x	x
	Thalassiosira spp.	x	x	x	x	x		x		x	x	x	x	x	x	x	
	Pennate diatom	x	x	x	x		x	x		x	x	x	x	x	x	x	x
Chrysophyceae	*Meringosphaera* sp.	x	x												x		
Silicoflagellates	*Dictyocha speculum*	x	x	x	x	x									x		
Tintinnids	*Parafavella* sp.	x	x	x	x	x	D	D	D	D	D	x	x	x	x	x	x
Green algae	*Pterosperma* sp.	x		x	x	x	x			x	x	x				x	
Foraminifera	Foraminifera	x	x	x	x										x		
	Globigerina bulloides	x												x		x	

XVII